PRECIPITATION PROFILES FOR THE TOTAL RADAR COVERAGE

by

P.M. Hamilton, M.Sc.

A thesis submitted to the Faculty of Graduate Studies and Research in partial fulfilment of the requirements for the degree of Doctor of Philosophy.

Department of Meteorology,
McGill University,
Montreal.

July 1964

SUMMARY

Vertical profiles of the total precipitation in the area scanned by a radar have been obtained for the first time. Profiles for summer shower situations commonly show an accumulation of precipitation aloft, at a height which is observed to increase with the available energy of convection. This observation has been combined with calculations by other researchers to give a three-fold relation between mean updraught speed, height of accumulation and energy of convection. Profiles for continuous rain are quite distinct from those of showers, generally showing the greatest amount of precipitation at the base of the storm. Profiles form a useful digest of the radar data for the synoptic meteorologist. The essential data can be reduced to a small array of digits, which are economically transmitted and readily interpreted to give insight into the precipitation pattern and the accompanying convection.

ACKNOWLEDGEMENTS

It is a pleasure to acknowledge the considerable advice and encouragement of Professors K.L.S. Gunn and J.S. Marshall during their supervision of this work.

I am grateful to Dr. M. Wein, especially for his substantial contribution to the development of the equipment which recorded the necessary radar data. Technical assistance in operating the equipment was provided by Mr. M. Claasen and Mr. P. Seidenfuss.

Extensive analysis and computations have largely been carried out by Mrs. Joy Johnson, Mrs. Jennifer Niebyl, Miss Eugenia Schkurat and Miss Jean Taylor. I am most grateful for their indispensable assistance.

Many of the drawings have been drafted by Miss Ursula Seidenfuss. The photography was undertaken by Mr. R. Bartley.

The work reported in this thesis has greatly depended on the availability of the sophisticated McGill Radar. Therefore, I would like gratefully to acknowledge the contributions over the years of the many members of the Stormy Weather Group to the development of this Radar.

The research was sponsored largely by the U.S.A.F., Geophysics Research Directorate, Air Force Cambridge Research Laboratories, Office of Aerospace Research, under Contract AF 19(628)-249. The radar is operated under a grant from the National Research Council of Canada.

Much of the supporting meteorological information in this study was provided by the office of the Meteorological Service of Canada at Montreal International Airport.

I wish to thank my wife for typing the thesis. She also drafted some of the figures and improved the text in many places.

TABLE OF CONTENTS

1. INTRODUCTION

1.1 Precipitation Measurements by Radar

When the practicability of radar was being considered at the beginning of World War II, one question that assumed great importance was the magnitude of the absorption and scattering effects to be expected in the atmosphere. Accordingly, Ryde (1946) undertook a detailed theoretical investigation of the attenuation and reflections of radar waves by various meteorological phenomena. Amongst other things, his work showed that, with appropriate information about the relation of raindrop-size to rainfall intensity, one should be able to estimate rainfall rates from the intensity of radar echoes in storms. Soon after the war, Marshall et al. (1947) were able to establish that it was indeed possible to make useful radar measurements of rainfall intensity. Since that time a great many other workers have studied the relationship between radar echo intensity and rainfall rate, and it is now apparent that radar determinations of rainfall rate are generally accurate to within a factor 2. This limit is imposed by the statistical nature of the relation between the raindrop size distributions and the rainfall intensity.

Radar was soon employed to analyse precipitation patterns in the horizontal (Maynard, 1945) and in the vertical (Byers and Coons, 1947; and Langille and Gunn, 1948). It was instrumental in establishing the nature of the precipitation processes in both stratiform and convective clouds. It is now an indispensable tool for research into cloud physics, mesometeorology and synoptic meteorology.

1.2 Weather Radar Displays

With radar it is possible to measure at least five parameters of a precipitation pattern. These are the three dimensions of space, the precipitation intensity and time. There are thus many possible forms in which to display the pattern. In the most commonly used radar indicators the precipitation pattern in some plane is normally displayed on the face of a cathode ray tube. In the plan-position indicator (PPI) the plane is horizontal and in the range-height indicator (RHI) it is vertical. It is possible to produce maps on these displays in which precipitation intensities are indicated in shades of grey, and this is done in displays developed at McGill University (Legg, 1960).

Thus, four of the five dimensions of a precipitation pattern can be recorded, and another dimension of space is needed to complete the specification. If the basic display is the RHI then maps are required at various bearings, and if it is the PPI then it is convenient to produce maps at various constant altitudes (CAPPI). A method for producing such constant altitude precipitation maps has also been devised at McGill University (East and Dore, 1957).

Marshall and Gunn (1961) have described the present mode of operation of the McGill radar. Briefly, constant altitude maps out to range 120 n mi are produced at each of six altitudes every 7.5 minutes. The maps display the precipitation intensities in seven shades of grey with successive boundaries at 0.1, 0.4, 1.6, 6.4, 25, 100 and 400 mm hr^{-1}.

Although the maps are basically comprised of distinct shades, in practice there are rarely sharp boundaries between the consecutive shades. This may be ascribed to the rapidly fluctuating nature of the radar echoes from precipitation. It has been found that some form of densitometry is necessary if accurate measurements are required. Thus, the McGill Group has further developed equipment which automatically densitometers the grey-scale CAPPI maps (Wein, 1964). The maps finally appear in well-defined grey shades on a facsimile record, and it is now possible to measure rainfall rates by inspection.

1.3 Vertical Profiles of the Total Precipitation

The process by which the stepped grey-scale maps are produced includes a stage in which the photographic negative of the original map is completely scanned. Canadian Aviation Electronics of Montreal, in developing the McGill technique, have recently taken advantage of the opportunity that this affords of analyzing the whole radar map (Ballantyne, 1964). The analysis proceeds by measuring the total area of each of the grey shades, and the results of the analysis follow each map on the facsimile record. Given the area of precipitation of each intensity, it is possible to calculate such things as the total flux of precipitation at any height, including the lowest one which is of great interest to the hydrologist.

In anticipation of the development of these methods for the ready analysis of grey-scale maps, and because of the fruitful research possibilities, Professor J.S. Marshall initiated the research which is reported here. The automatic methods of analysis mentioned above were perfected only in the last few months, and it was necessary to develop other methods during the course of the research. A full account of the actual technique employed appears in Chapter 6 of this work. The equipment served well in the accumulation of records for more than 1000 hours of precipitation, but it has almost certainly been used for the last time.

With complete information on the distribution of precipitation with intensity at each height, it is natural to look at the vertical distribution of precipitation. One way of doing this is by means of profiles, and that is the way that has been adopted in this study. Fig. 1.1 gives

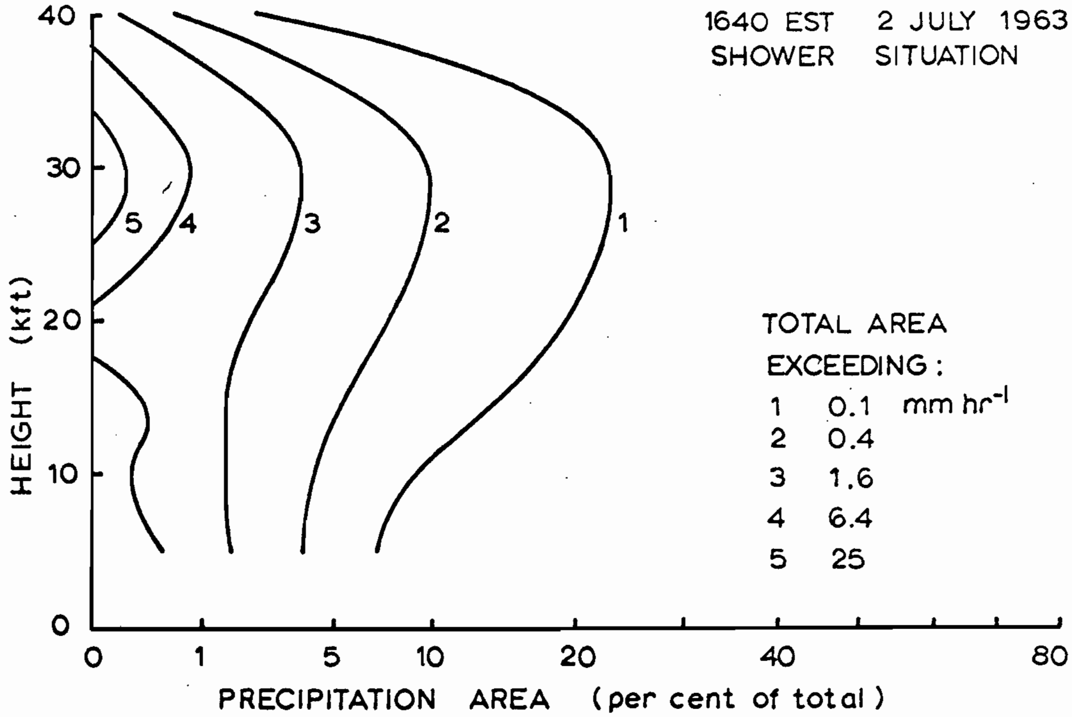

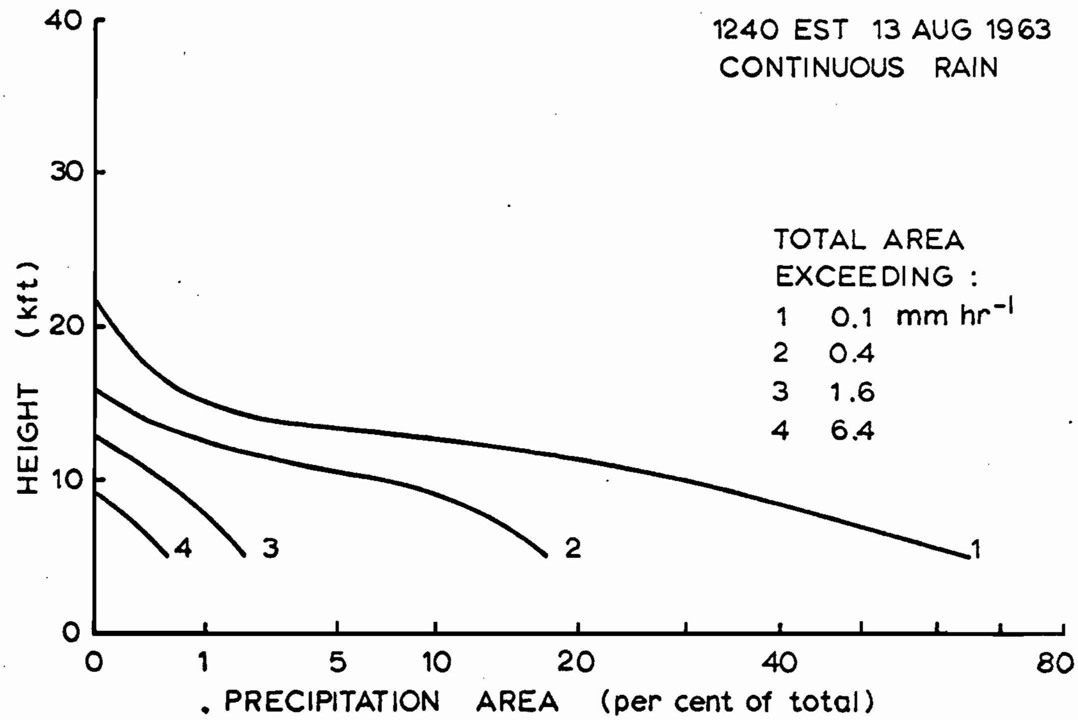

Fig. 1.1. Vertical profiles of the total area of precipitation exceeding each of the intensities indicated.

examples of the kind of profiles that have been drawn. The upper example is for an instant during the most exciting thunderstorm of the summer of 1963. The outer curve shows the total area of precipitation exceeding the radar threshold of 0.1 mm hr^{-1} as a function of height. The next curve shows all the precipitation exceeding 0.4 mm hr^{-1}, that is with grey-shade one omitted. Succeeding curves are each for a rainfall rate a factor four greater than the previous one. Thus, in the example, there is a little precipitation greater than 25 mm hr^{-1} at 30 kft. The lower example is from an occasion of continuous precipitation. The vertical extent of the precipitation is considerably less and its area at the lower levels greater than in the other example. Also the most intense precipitation is just over 6.4 mm hr^{-1} and occurs at 5 kft. Mention should be made about the scale of area: it is a scale of square roots, which is appropriate to the wide range of significant areas, as well as having other advantages.

Profiles of the kind illustrated in Fig. 1.1, together with profiles of additional quantities, have proved to be a most convenient method of displaying the essential features of the distribution of precipitation in the vertical. It is hoped that the present study will establish their value in both research and operations.

1.4 Profiles in Relation to Storm Structure

The great difference between the two examples of Fig. 1.1 is that in the shower situation there is a great accumulation of precipitation aloft at 30 kft, whereas in the continuous rain the precipitation is growing continually throughout its descent. The accumulation of great quantities of rain aloft in the strong updraughts of convective storms was suspected by

Marshall et al. (1947) and soon confirmed by Langille and Gunn (1948). Bowen (1950) also observed accumulations aloft in showers and was able to explain them in terms of the trajectories of growing droplets. Perhaps this point should be emphasized: the accumulations are often almost in a state of dynamic equilibrium, with precipitation arriving and departing at about the same rates.

There were many other observations that precipitation first formed and then developed at some point high in a shower cloud. Notable amongst these was an extensive study by Battan (1953), whose observations were later to be incorporated into calculations by East (1957). East gave a realistic treatment of the growth of droplets in updraughts, which showed that the height of precipitation formation would increase with the updraught speed. Kessler (1961), in considering the development of precipitation in a model convective cell, also found that accumulations developed aloft at a height which increased with the updraught speed. Meanwhile, Donaldson (1961b) had observed radar reflectivity maxima in the cores of thunderstorms at a height which increased with the severity of the storm. Thus the existence and cause of the accumulations aloft were fairly well established.

In the present work it has been found that the accumulations aloft in individual showers are sufficiently intense and persistent that they are also observed in profiles of the total precipitation from many showers. The height of formation of the accumulations has been found to increase with the amount of energy available for convection, as judged from a tephigram plot of the upper air sounding. The work of East (1957) and Kessler (1961) has also been used as a basis for relating the height of the accumulations to a mean updraught speed. In this way a threefold relation has been developed between the height of the accumulation, the updraught speed and the available energy of convection. This threefold relation is shown to be useful in studying the energy budgets of convective storms.

Considerable effort has been devoted to the study of shower profiles, and the study of continuous rain profiles has consequently been rather neglected. At first sight they show remarkably little variation in form from situation to situation, but close study would undoubtedly reveal features at present unexpected.

1.5 Profiles for the Synoptic Meteorologist

Perhaps the greatest virtue of radar is that it can scan the entire atmosphere within range every few minutes. It is able to detect all the significant precipitation and keeps it constantly under surveillance. However, the synoptic meteorologist cannot digest more than a small fraction of the available data, and so he must be provided with a suitable brief summary. Vertical profiles of the total precipitation form such a summary.

It will be shown that the essential features of a profile can be expressed in just a few digits. These few digits can be both readily transmitted on teletype circuits and readily interpreted by the synoptic meteorologist. For a modest investment of effort, the forecaster is able to study the main features of the three-dimensional precipitation pattern over an entire continent.

Profiles emphasize what is perhaps the most important dimension to the meteorologist, the vertical. From the vertical structure, as summarized in profiles, it is possible to tell whether the precipitation is stratiform or is in the form of showers. If it is in the form of showers it is possible to estimate the general intensity of convection, and to watch its trend with time. Showers embedded in areas of continuous rain can also be detected, and their development continually monitored.

In this study, attention has been devoted more to the qualitative aspects of profiles than to the quantitative. Precipitation is an important element of the atmosphere. Not only is it produced by dynamical processes within the atmosphere, but it also modifies the processes themselves by the exchange of latent heat. Quantitative data of the kind contained in profiles might well be incorporated into the models being developed by dynamical meteorologists.

There is no doubt that radar has a place in synoptic meteorology, and a case is made in this work for summarizing the radar data into profiles. It is exciting that equipment is already available to exploit the value of profiles on an operational basis. The work reported here has only been concerned with the most obvious features of profiles. Much more remains to be done, and it may be expected that the operational use of profiles will soon lead to a better understanding of the precipitation processes and the convection which produces them.

2. ANALYSIS OF PROFILE DATA

2.1 The Radar Measurement of Rainfall

According to simple theory (see for example Battan, 1959), the average power received by the radar from precipitation is given by

$$\overline{P}_r = \frac{C\,|K|^2\,Z}{r^2}, \tag{2.1}$$

where $Z = \sum D^6$, the sum of the sixth powers of the diameters of the precipitation particles, per unit volume,

$|K|^2$ is a dielectric factor, 0.93 for water, 0.20 for ice,

r is the range,

C is a constant of the radar.

This equation assumes that the radar beam is entirely filled with precipitation and that there are no losses by attenuation along the beam. In the McGill radar, the dependence of the received power on the inverse square of the range is accounted for electronically, and C is known. The quantity displayed may be described as the equivalent radar reflectivity,

$$Z_e = \frac{\overline{P}_r\,r^2}{C} = |K|^2\,Z. \tag{2.2}$$

Z_e is measured with a probable error of about 2 db. The McGill radar produces constant altitude maps with contours of Z_e, and it is the areas within these contours that have formed the basic data of this study.

The quantity Z has been related through many empirical studies (see Battan, 1959) to the rainfall rate R. A relation representative of most rain, and the one adopted at McGill, is

$$Z = 200\,R^{1.6} \tag{2.3}$$

where Z is in $mm^6\,m^{-3}$ and R in $mm\,hr^{-1}$. This equation may be used to deduce the rainfall rate from measurements of equivalent radar reflectivity. Further, Marshall and Palmer (1948) have given a statistical relation between the rain density M and the rainfall rate R:

$$M = 72\ R^{0.88}, \tag{2.4}$$

where M is in mg m^{-3} and R in mm hr^{-1}. This and equation (2.3) may be combined to give

$$Z = 0.0083\ M^{1.82}. \tag{2.5}$$

Thus the rain density may also be deduced from the equivalent radar reflectivity.

In the case of radar signals from snow the relevant parameter is still $Z = \sum D^6$, but now D refers to the diameter of the water droplets formed by melting the snowflakes. The appropriate relations between Z, R and M for aggregate snowflakes are (Gunn and Marshall, 1958)

$$Z = 2000\ R^{2.0} \tag{2.6}$$

$$M = 250\ R^{0.90} \tag{2.7}$$

$$Z = 0.0096\ M^{2.2}, \tag{2.8}$$

where R and M are the precipitation rate and density expressed in terms of the water equivalent. If the snow is in the form of single crystals the Z – R relation appears to be the same as that for rain, $Z = 200\ R^{1.6}$.

The radar scattering by melting snow and hail (dry or wet) have also been studied, but the resulting relations are quite complicated and need not be of concern here.

2.2 The Radar Rainfall

Following a suggestion by Marshall et al. (1947), the standard relation $Z = 200\ R^{1.6}$ may be used to define a radar rainfall rate,

$$R_r = \left(\frac{Z_e}{0.93 \times 200}\right)^{\frac{1}{1.60}} . \tag{2.9}$$

Contours of Z_e may now be relabelled with values of R_r. Except where otherwise stated, all measurements in this work are expressed as radar rainfall rates, although the description "radar" is normally omitted.

The radar rainfall rate is only a correct measure of the actual rainfall rate, or flux of precipitation, when the precipitation particles (a) satisfy the particular relation $Z = 200\ R^{1.6}$, (b) fall in air which has no vertical component of motion, and (c) are water drops. A brief discussion of the extent to which the measurements are affected when these conditions are not met now follows.

(a) Z – R Relations

Battan (1959) has given an extensive summary of Z – R relations deduced from studies of drop-size distributions in rain. The relations vary somewhat with the type of storm and geographical location, but for a given Z most of the relations give a value within a factor 2.0 of that given by $Z = 200\ R^{1.6}$. Ample direct confirmation of this relation has also been obtained with radar measurements. Recently, Austin (1963) has used it in a radar study of 40 New England storms, and found that for 30 storms it yielded radar rainfalls within a factor 2.0 of the actual values measured in a rain-gauge network; for six storms the equivalent rainfall was one-half or less of that measured, and for four storms it was twice the measured rainfall. These findings are in line with other similar investigations, and they all suggest that the use of $Z = 200\ R^{1.6}$

generally gives radar rainfall within a factor 2.0 of the actual value.

(b) Effect of Updraught on Rainfall Rate

In the present work measurements have been expressed in terms of the radar rainfall rate (2.9). An alternative quantity is the radar rain density:

$$M_r = \left(\frac{Z_e}{0.93 \times 0.0083}\right)^{\frac{1}{1.82}} . \qquad (2.10)$$

This has the advantage that in the case of vertical air motion M_r is a better measure of the actual rain density than is R_r of the actual rainfall rate. The actual rainfall rate, or flux of precipitation, R may be regarded as the product of the rain density M and a fall speed, which is the difference between the characteristic fall speed of the rain relative to the air, v, and the upward air speed, u:

$$R = M\,(v - u). \qquad (2.11)$$

The radar rainfall rate is a measure of the quantity Mv, the flux of precipitation relative to the air, and is thus in error by the factor $v/(v - u)$. On the other hand, provided the drop-size distribution remains the same, the radar measures the same rain density M, irrespective of the updraught.

In showers, vertical air speeds are certainly comparable with rain fall speeds, and the factor $v/(v - u)$ may be significantly different from unity, or even negative. In these circumstances the radar rainfall rate may be viewed either as a measure of flux relative to the air, or as an approximation to rain density. This latter approximation is possible because of the near proportionality of the relation $M = 72\ R^{0.88}$. Examples of profiles of both the total rainfall rate and rain density are

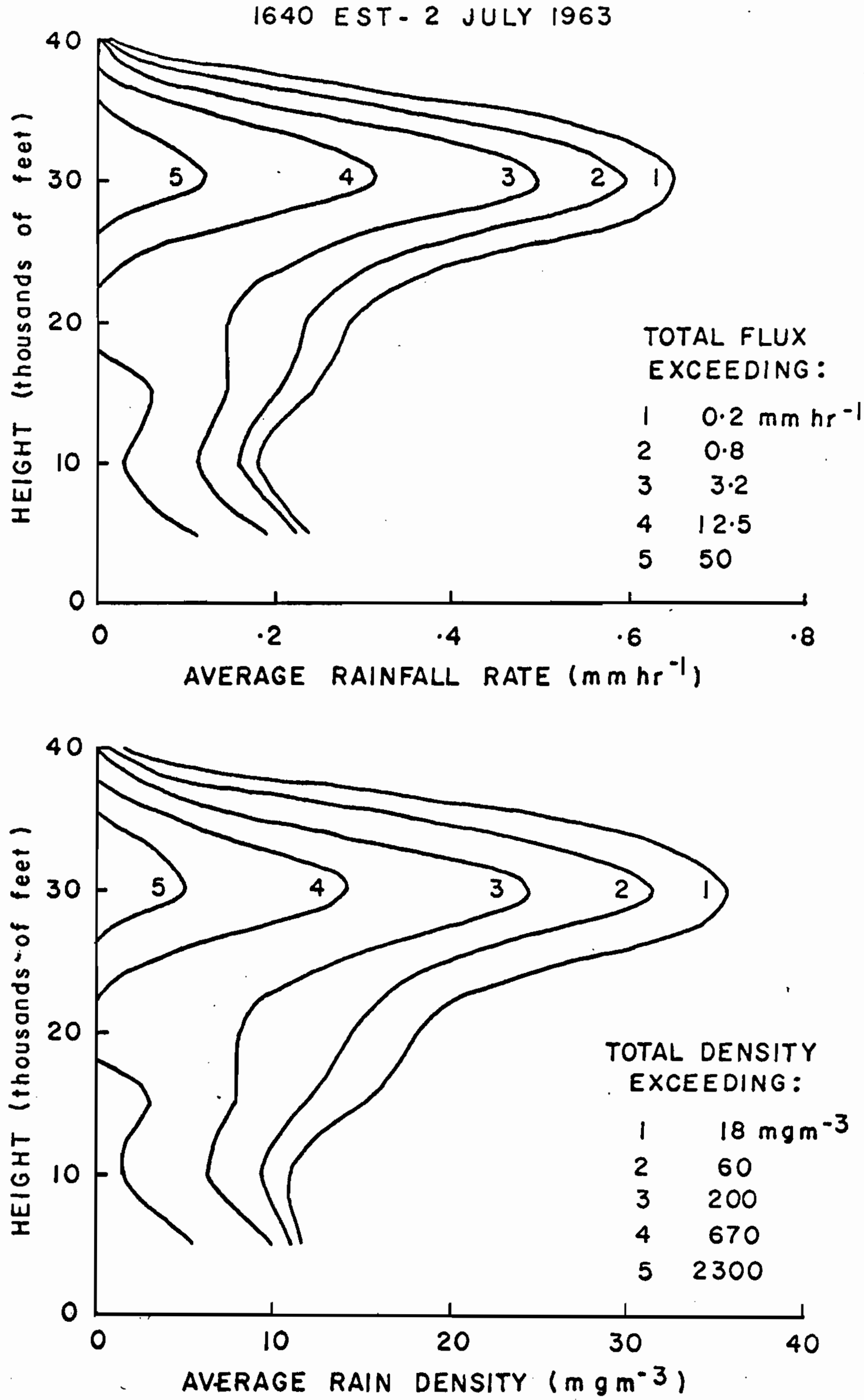

Fig. 2.1. Comparison of radar rainfall rate and rain density for an occasion during a severe storm.

shown for comparison in Fig. 2.1. It can be seen that they are quite similar, and that a factor 50 can be used to convert R (mm hr^{-1}) into M (mg m^{-3}). This factor is actually appropriate at R = 20 mm hr^{-1}, or M = 1000 mg m^{-3}, and is satisfactory because, in cases with fairly heavy rain, most of the total is due to rain of about this intensity. In cases with lighter rain the approximation is still quite good, although in these cases the updraughts may be expected to be less significant, and the radar rainfall rate is itself a satisfactory measure.

(c) The Radar Rainfall in Snow

For snow aggregates $Z = 2000\ R^{2.0}$, and for non-aggregate snow $Z = 200\ R^{1.6}$ appears to be appropriate. In practice, there is some justification for using a compromise relation, and as pointed out by Austin (1963) there is considerable merit in choosing, in particular,

$$Z = 1000\ R^{1.6}. \tag{2.12}$$

For snow satisfying this equation, the radar signal is proportional to

$$Z_e = |K|^2\ Z = 0.20 \times 1000\ R^{1.6}, \tag{2.13}$$

and the precipitation rate is thus

$$R = \left(\frac{Z_e}{200}\right)^{\frac{1}{1.6}}. \tag{2.14}$$

This is almost identical with the equation defining the radar rainfall rate, (2.9). That is, the radar rainfall rate is a reasonable approximation to the actual precipitation rate (water equivalent) in snow. It may be too high by about a factor 2.0 in heavy snow aggregates, and may be a considerable underestimate in non-aggregate snow.

Austin (1963) in a study of nine snowstorms found that, for six storms the radar rainfall compared well with the precipitation at the ground (i.e. $Z \approx 1000\ R^{1.6}$), while for the other three the radar rainfall was less than the actual precipitation by a factor 2.0 or more. Those in which the radar rainfall was satisfactory were almost all heavy snowstorms, those in which it was too low were cases of light snow.

In summary, the radar rainfall is a satisfactory measure of the actual rainfall in most rainstorms, and is almost as satisfactory in snowstorms. Where updraughts are significant, the radar rainfall should be taken as a reasonable measure of the rain density.

2.3 Correction for Attenuation

The radar equation in the form (2.1) ignored the effects of attenuation along the radar path. At the 3.2-cm wavelength of the CPS-9, attenuation by atmospheric gases, cloud and especially rain can reduce the received power considerably. Table 2.1, computed from values given by Gunn and East (1954), gives approximate values of this attenuation for conditions appropriate to this study.

TABLE 2.1

ATTENUATION AT 3.2-cm WAVELENGTH (TWO WAYS)

Rain	1 mm hr^{-1}	0.025 db mi^{-1}
	10 mm hr^{-1}	0.50 db mi^{-1}
	100 mm hr^{-1}	10.0 db mi^{-1}
Cloud		0.25 db mi^{-1} $(gm\ m^{-3})^{-1}$
Gases	1000 mb	0.05 db mi^{-1}
	500 mb	0.01 db mi^{-1}

The least important of these is attenuation by gases (oxygen and water vapour), but this could have caused losses of up to about 4 db at the maximum range (80 n mi) in this work. Attenuation by cloud can clearly be quite serious and might frequently have amounted to 5 db. However, the attenuation due to the rain itself is the most serious, often causing losses several times the others. It was felt worthwhile to apply a statistical correction for this loss, and a suitable correction was deduced from previous work at McGill (Hamilton and Marshall, 1961). A brief account of the derivation of this correction now follows.

Because of attenuation by the rain itself, the area of echo exceeding a radar rainfall rate of 0.1 mm hr^{-1} is somewhat less than the area of rain exceeding 0.1 mm hr^{-1}. In fact, the McGill study of rainfall statistics for a Montreal summer has shown that the area of echo exceeding 0.1 mm hr^{-1} is about the same as the area of rain exceeding 0.18 mm hr^{-1}. In this sense, the 0.1 mm hr^{-1} radar rainfall rate contour can be relabelled 0.18 mm hr^{-1} to compensate for attenuation. Revised values have also been worked out for other contours, and these appear in Table 2.2.

TABLE 2.2

ATTENUATION CORRECTION FOR RADAR RAINFALL RATE (mm hr^{-1})

Radar Rainfall Rate	Attenuation-Corrected Rate	Adopted Rate
0.1	0.18	0.2
0.4	0.60	0.8
1.6	2.7	3.2
6.4	15	12.5
25	61	50

It can be seen that multiplying radar rainfall rates by a factor 2.0 (5 db in equivalent reflectivity) provides a reasonable correction for all rates, and this is the correction factor that was adopted.

There is another sense in which this correction is appropriate. The McGill study showed that, for a sensitive 3-cm radar (such as the

CPS-9) looking at a point 60 miles away for a whole summer, the total radar rainfall would be about 47% of the actual rainfall because of rain attenuation. Thus the factor 2.0 correction applied to the radar rainfall throughout a summer would give very nearly the correct total. Study of attenuation in individual storms suggests that when this correcting factor has been used the resulting rainfall rates will mostly be from 0.3 to 2.0 times the actual rates, depending on the storm.

It should be mentioned that attenuation by snow is negligible at normal precipitation rates. The factor 2.0 by which all radar rainfall rates have been multiplied might therefore be expected to over-correct in the case of snow. However, in most cases, the snow concerned is above the melting level in a rainstorm. Gunn and East (1954) state that serious attenuation may take place when radar observations are made through melting snow, especially at shallow angles, so the correction factor of 2.0 may not be at all excessive.

2.4 The Sampling Area

The area within which precipitation is recorded has been restricted to that between 20 n mi and 80 n mi in range, an area of about 20,000 n mi^2. At ranges closer than 20 n mi the McGill radar does not map the precipitation at 40 kft, while at ranges beyond 80 n mi it does not map the precipitation at 5 kft. Additional reasons for this choice are the poor resolution of a 1° beam beyond 80 n mi and the inadequacy of the circuit which normalizes received signals to a standard range. However, even within this range there is some lack in the uniformity with which identical precipitation would be recorded. As an example, Fig. 2.2 shows how each of three patterns would be recorded at the limits of the sampling area.

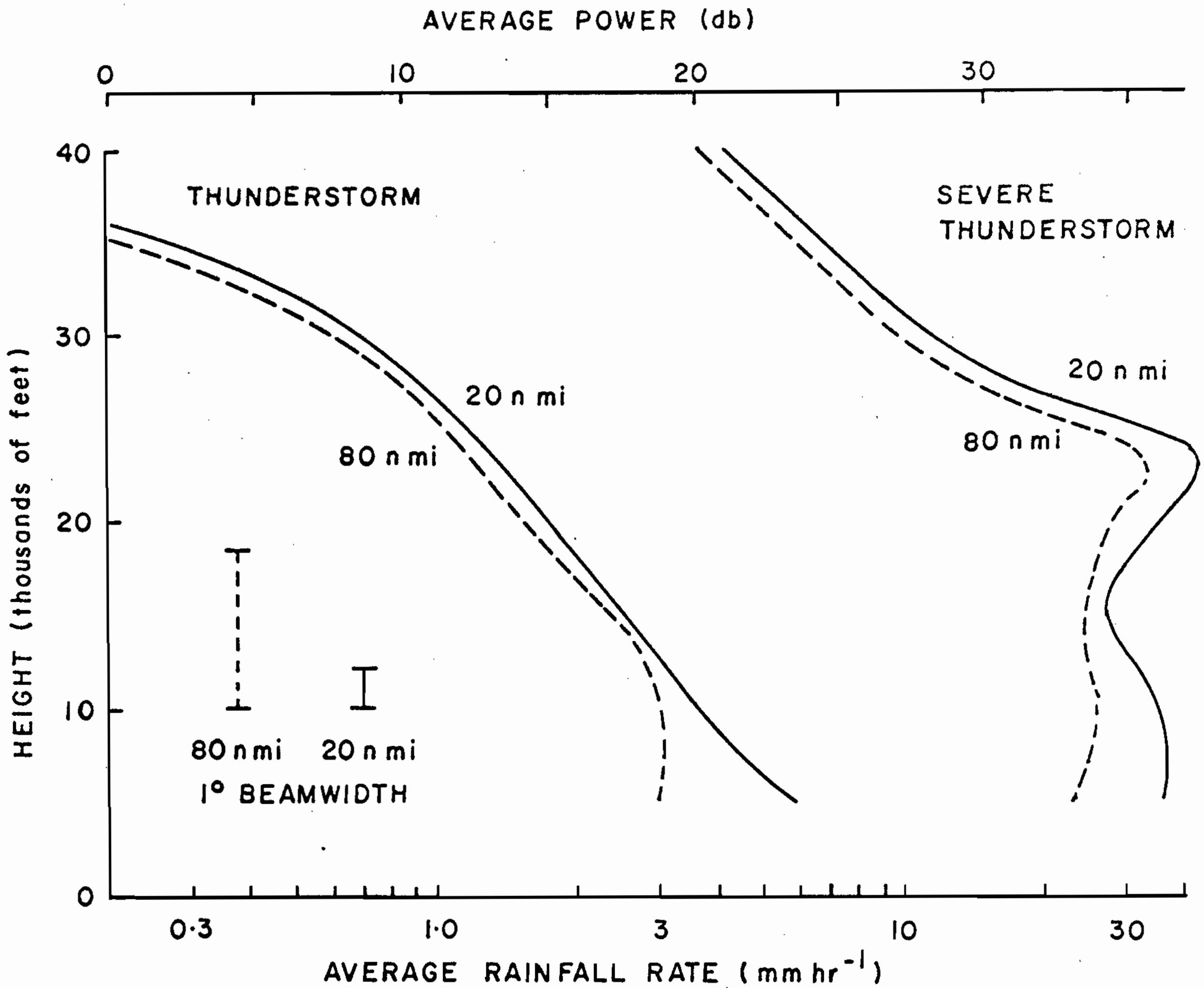

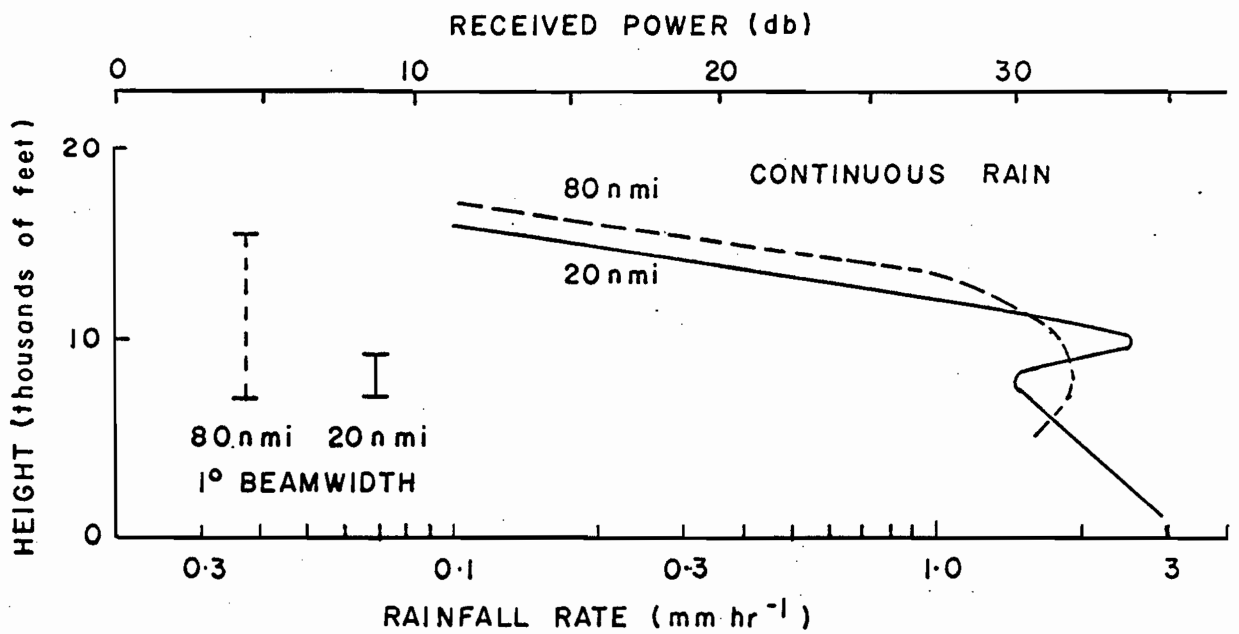

Fig. 2.2. Examples of range-distortion in profiles.

Although it is easy to calculate the effect of a divergent radar beam in observing stratified precipitation, the calculations are quite tedious for cellular precipitation. Fortunately, Donaldson (1961a) has made such calculations, giving detailed reflectivity contours for two thunderstorms viewed with a 1^{o} beam at several ranges. These were used to produce the two sets of thunderstorm profiles at the top of Fig. 2.2. Donaldson's contours are in a vertical plane normal to the radar beam, and thus it was possible to calculate the average rainfall rate at each height. It is perhaps surprising that for both cases there is a reduction in total received power of only 2 db in going from 20 to 80 n mi. The maximum reflectivities are actually reduced by 5 db, but as the beam becomes larger it records the intense echo over a greater area, and these effects tend to compensate in the average. At 80 n mi the radar beam has a radius of about 5 kft, the radar horizon is at 4 kft, and therefore when directed at heights below 9 kft part of the radar beam is lost below the horizon. Thus the reflectivity at 80 n mi falls off below 9 kft, until at 5 kft it is 5 db less than at 20 n mi. With the exception of these lower heights, it is encouraging to note that the shape of the profiles is well preserved.

The situation is not so bright on occasions of continuous precipitation. The profiles at the bottom of Fig. 2.2 have been calculated from the measurements of a vertical-pointing radar (Wexler, 1959), and assume that the precipitation is uniform in the horizontal across the radar beam. It is fairly representative of continuous rain at Montreal in the summer, and shows a bright band as snow melts to rain at 10 kft. Although much of the profile at 80 n mi is within about 3 db of the 20 n mi profile, it is poor in detail. Because of the rapid change of intensity with height, the reflectivities above 12 kft are about 5 db too high. The details at and below the bright band are missing, and at 5 kft the loss of signals below the horizon is just apparent.

It should be pointed out that the profiles of Fig. 2.2 have been presented as continuous functions of height. In the McGill radar, however, the 5 kft CAPPI map is approximated beyond 62 n mi by the beam of 0^{o} elevation. Hence echo in the outer 36% of the sampling area at 5 kft is affected by signal losses below the horizon, and could be reduced by about 3 db.

2.5 Overall Accuracy of Profiles

It seems worthwhile to collect the estimates of errors which have been made at various places in this work:

TABLE 2.3

ERROR SOURCE	PROBABLE ERROR (db power)
Radar measurement of Z_e	2.0
Sample area, 20 – 80 n mi	1.5
A-scope apparatus (Chapter 6)	1.2
Z – R relation	2.5
Attenuation (after correction by + 5 db)	3.0 (approx)
OVERALL ERROR	4.8

The overall probable error of 4.8 db means that most of the measurements of radar rainfall are within a factor 4.0, either way, of the actual rainfall. Attenuation is the greatest source of error, and at a non-attenuating wavelength most of the measurements would be correct to within a factor 3.0. The ultimate limit to accuracy is given by variations in the Z – R relation, equivalent to a factor 2.0.

It should be emphasized that these errors are errors in absolute magnitude. The errors from height to height in a given profile, and between consecutive profiles, are much less, a fact borne out by the strong consistency of the observed profiles.

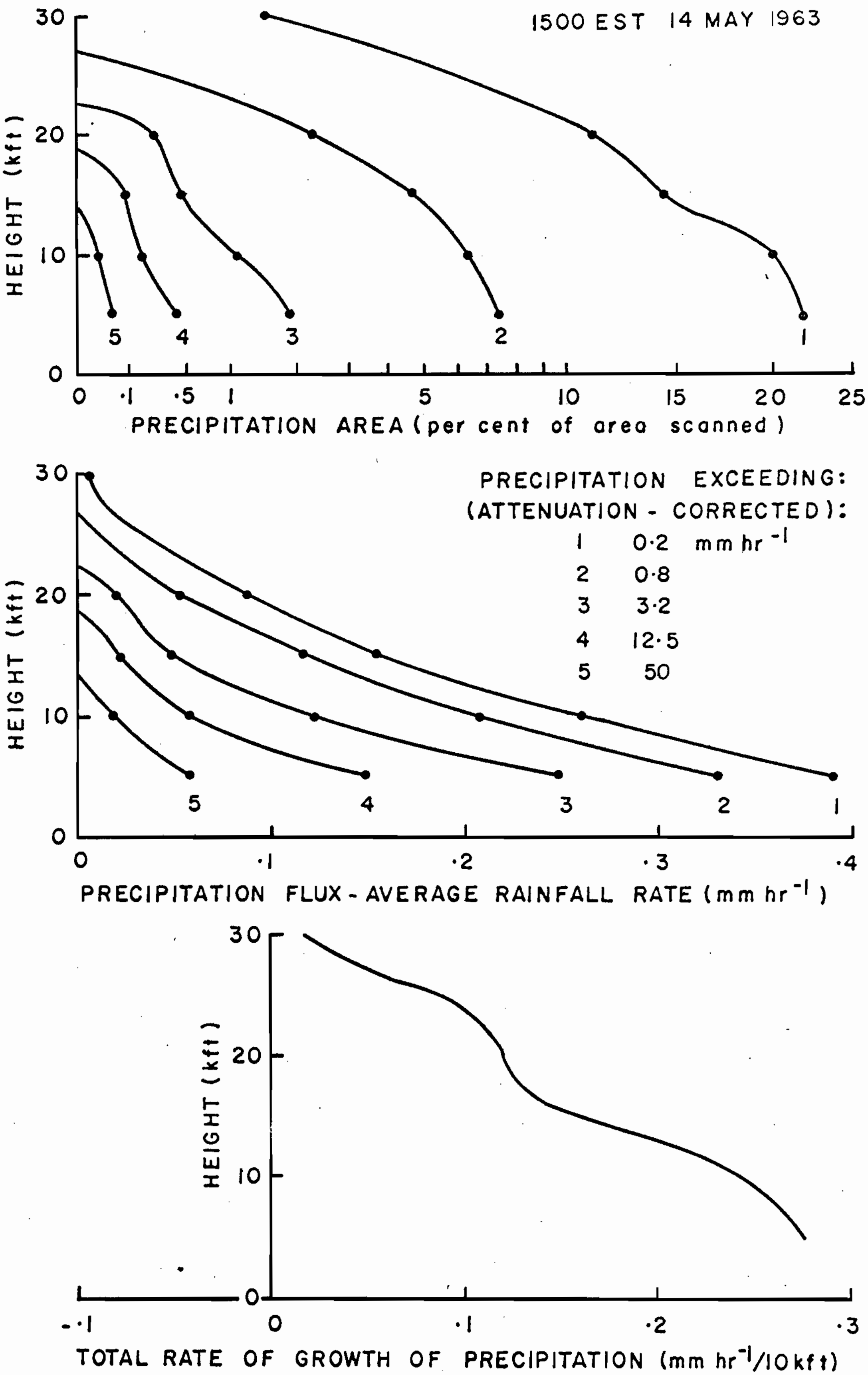

Fig. 2.3. Examples of precipitation profiles.

2.6 Types of Profiles

The basic data from which the profiles in this study have been drawn are the areas within contours of Z_e. The particular Z_e contours chosen corresponded to the boundaries between grey shades in the McGill radar. Table 2.4 gives the relevant values of Z_e and the corresponding rainfall rates, both as observed and after correction for attenuation. The first half of each double column gives values for the contours, while the second half gives the mean values used for each shade.

TABLE 2.4

McGILL GREY SHADE	Z_e - EQUIVALENT REFLECTIVITY ($mm^6\ m^{-3}$)		RADAR RAINFALL RATE ($mm\ hr^{-1}$) Observed		Attenuation Corrected	
	4.7×10^0		0.1		0.2	
1		1.4×10^1		0.2		0.4
	4.3×10^1		0.4		0.8	
2		1.3×10^2		0.8		1.6
	3.9×10^2		1.6		3.2	
3		1.2×10^3		3.2		6.4
	3.6×10^3		6.4		12.5	
4		1.0×10^4		12.5		25
	3.2×10^4		25		50	
5		9.7×10^4		50		100
	2.9×10^5		100		200	
6		8.9×10^5		200		400
	2.7×10^6		400		800	

The areas of precipitation were measured successively at heights 5, 10, 15, 20, 30 and 40 thousand feet, with 3.75 minutes being required for each. Thus it was possible to draw vertical profiles of the precipitation every 22.5 minutes. Examples of the three kinds of profiles most commonly discussed here are shown in Fig. 2.3. Each of the profiles at the top shows the area of all precipitation exceeding the given value as a function of height. The quantity plotted is actually the square root of the area which, in most situations, has the practical advantage of giving relatively even spacing between consecutive profiles. It also has some physical significance: the profiles may be looked upon as a radial cross-section of the storm that would result if all precipitation were gathered symmetrically about the radar, with the most intense at the centre.

Each of the profiles in the middle of Fig. 2.3 shows the total flux of precipitation arising from all intensities greater than the given value. It has been obtained by multiplying the area of precipitation by the attenuation-corrected mean rainfall rate for each intensity, and then adding the contributions from the various intensities. It is expressed in terms of the rainfall rate that would result if it were distributed evenly over the entire area scanned by the radar, and is plotted on a linear scale. The outer profile gives the total flux arising from all the precipitation detected by the radar, and this has been differentiated with respect to height to give the bottom curve. This is thus a plot of the rate of generation of precipitation, or rate of growth.

The discussion in section 2.2, in which it was pointed out that the radar measures rainfall rates relative to the air, is quite relevant in the interpretation of the flux and rate of growth profiles. In situations with little vertical air motion the descriptions "flux" and "rate of growth" are quite valid, but this is not the case otherwise. When there are significant updraughts and downdraughts, it is better to view the flux as an approximate measure of the rain density, and in these circumstances the rate of growth profile has no physical meaning. Nevertheless, since it will be seen that it is a valuable indicator, the rate of growth profile will be presented for many situations in which its name is misleading. For the sake of uniformity, the terms "flux" and "rate of growth" have been used throughout. It will usually be quite plain to what extent these terms are valid.

3. PROFILES OF SHOWERS

Showers are the product of local instability which is characteristically realized by convection in cells or cellular complexes with dimensions of the order of 10 miles. Updraughts ranging in speed from a few m sec^{-1} to some tens of m sec^{-1} can produce precipitation particles ranging from raindrops 1 mm across to hailstones almost 10 cm across. These precipitation particles fall at speeds comparable to the updraughts, and there is thus a complex interaction between them. Therefore, it is not surprising to find that the distribution of precipitation in the vertical is apparently largely determined by the intensity of convection. The relation between them will form the main theme in this study of showers. It will first become evident in a comparison of precipitation profiles and upper-air soundings for a variety of situations. After it has been fully established, it will be studied in relation to present knowledge of shower structure.

3.1 Relation of Profiles to Instability

By way of introduction to shower profiles a particular situation has been chosen for rather close study. Fig. 3.1 shows various facets of the situation at 1355 EST on 2 July, 1963. At the upper left, a series of constant altitude radar maps shows a sharp NE-SW line of showers to the NW of Montreal. The maps are at 10, 20, 30, and 40 thousand feet, and the range markers are at 80 n mi. At 10 kft the line of showers is about 10 mi across with closely clustered cells of moderate intensity along the near edge. The cells have their maximum intensity at 20 kft. At 20 and 30 kft there is a large area of light plume echo at the far edge of the line and especially to the NE. Radial shadows in this light echo are caused by attenuation losses in intense cells. At 40 kft separate cells are seen embedded in smaller amounts of light plume echo. Individual cells were moving from the W at about 35 knots, the speed of the 10 kft wind. The large amounts of plume echo to the NE were produced in strong upper winds from the SW, the wind shear between 10 and 30 kft being about 80 knots along the direction of the line.

An analysis of all the precipitation between 20 and 80 n mi appears in the form of the profiles at the bottom of Fig. 3.1. The profiles at the left show the area covered by precipitation exceeding 0.2, 3.2 and 50 mm hr^{-1} (after attenuation correction), expressed as a fraction of the area scanned and plotted on a scale of square roots. The radar pictures show all the precipitation exceeding 0.2 mm hr^{-1}, and the profiles show that this totals about 7% at 10 kft, 17% at 20 and 30 kft, and 10% at 40 kft. The radar pictures have been printed so that white represents precipitation of 50 mm hr^{-1} and greater. The profiles show that there are detectable amounts of precipitation of this intensity between about 12 and 25 kft, with a coverage of about 0.1% at 20 kft (the minimum detectable coverage is about 0.02%, or 4 n mi^2).

The second set of profiles shows the total flux of precipitation arising from rainfall exceeding the rates 0.2, 3.2 and 50 mm hr^{-1}. It is expressed in terms of the rainfall rate that would result if the flux were distributed uniformly over the entire area scanned. As already explained, this flux is relative to the air and differs from the absolute flux because of vertical air motion. However, in practice the total flux is almost proportional to the rain density, with 0.2 mm hr^{-1} equivalent to an average of 10 mg m^{-3}. The maximum flux occurs at 20 kft, a little lower than the height of the maximum area. It is notable that, although the precipitation exceeding 3.2 mm hr^{-1} only forms 25% of the total area of precipitation, it yields at least 85% of the total flux.

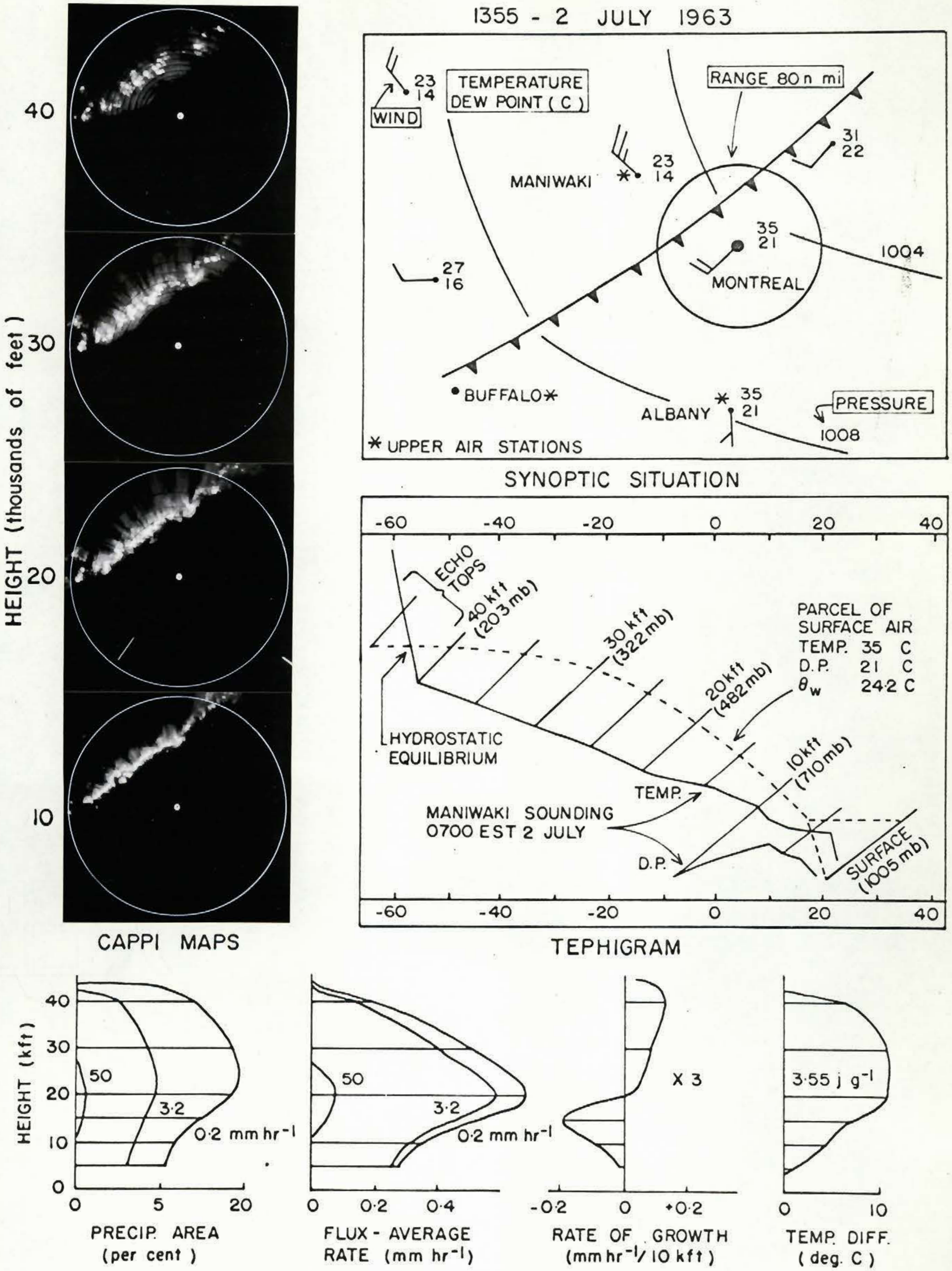
1355 - 2 JULY 1963
TEMPERATURE
DEW POINT (C)
WIND
RANGE 80 n mi
23
14
MANIWAKI
31
22
35
21
MONTREAL
1004
27
16
BUFFALO
ALBANY
PRESSURE
1008
* UPPER AIR STATIONS
SYNOPTIC SITUATION
ECHO TOPS
40 kft (203 mb)
30 kft (322 mb)
20 kft (482 mb)
10 kft (710 mb)
SURFACE (1005 mb)
PARCEL OF SURFACE AIR
TEMP. 35 C
D.P. 21 C
θw 24.2 C
HYDROSTATIC EQUILIBRIUM
TEMP.
D.P.
MANIWAKI SOUNDING
0700 EST 2 JULY
TEPHIGRAM
HEIGHT (thousands of feet)
CAPPI MAPS
HEIGHT (kft)
50
3.2
0.2 mm hr⁻¹
PRECIP. AREA (per cent)
FLUX - AVERAGE RATE (mm hr⁻¹)
X 3
RATE OF GROWTH (mm hr⁻¹/ 10 kft)
3.55 j g⁻¹
TEMP. DIFF. (deg. C)

Fig. 3.1.

The third profile shows the rate of change of the total flux with descent, which in the absence of vertical motion would be the rate of growth of precipitation. In this case there is growth above 20 kft, and apparent evaporation below. It has been found preferable to scale down a few of the more extreme profiles. Here, rates have been reduced by a factor 3.0, and thus the maximum rate of evaporation at 15 kft is 0.6 mm hr^{-1}/10 kft.

At the upper right of Fig. 3.1 is a picture of the synoptic situation, in which the circle is the circle of 80 n mi that also appears on the radar pictures. It can be seen that the showers are occurring at a well-defined cold front with temperature dropping from 35C to 23C at its passage, dew point from 21C to 14C, and wind changing from SW 20 to NW 25 mi hr^{-1}. The map has been drawn from a study of 3- or 6-hour synoptic charts, hourly station reports and climatological station reports. The data plotted are selected to represent the main characteristics of the situation.

To illustrate the technique of analysing the instability of the situation, a tephigram has been sketched and appears beneath the synoptic map. The basis of the analysis is an upper air sounding representative of the air mass producing the precipitation. Soundings were made at Maniwaki, Buffalo and Albany (see synoptic map) at 0700 and 1900 EST and either one of these or, sometimes, a suitable mean of them was chosen. On the present occasion, the Maniwaki 0700 EST sounding was representative, and is shown by the bold lines in the tephigram. The next step was to determine a potential wet-bulb temperature (θ_W) appropriate to buoyant parcels, and then the analysis followed simple parcel theory to give the parcel temperatures shown by the broken line. In this case, the buoyant parcels were probably surface air with temperature 35C and dew point 21C.

These values were arrived at by consulting hourly station reports and climatological station maximum temperatures. They were confirmed by comparing the resulting level of hydrostatic equilibrium, where parcels and environment have the same temperature, with the maximum heights of the radar echoes. The temperature and dew point adopted are those plotted beside the single bold station circle on the synoptic map, in this case Montreal.

For the present study, the quantity required from the tephigram is the maximum amount of energy available to buoyant parcels. This is given by the positive area between the environment and parcel curves, and depends on the temperature difference between them as a function of height. This temperature difference has been plotted at the bottom right of Fig. 3.1, and on 2 July the parcels were up to 11C warmer than the environment between 20 and 30 kft, the greatest difference observed in this work. The maximum amount of energy available was 3.55 j g^{-1}.

In the following pages various shower situations will be illustrated (Figs. 3.2 to 3.5), each with a 10 kft radar map, a synoptic map and plots like the bottom row of Fig. 3.1. Shower situations evolve rapidly, and frequently no single instant is representative of the whole storm. A common pattern of development in all but the weakest showers is the formation of a maximum in the flux aloft, which then varies in height, generally descending. It will be shown that there is reason to believe that the convection is at its strongest when the maximum is at its highest altitude. Since the upper air data have been analysed to determine the <u>maximum</u> amount of energy available, it is appropriate to choose an instant when the maximum flux is at its highest level. The situations which follow are thus compared at such instants. They are arranged in order of the total maximum energy available, running from the greatest down to the least. All but two of the occasions were in 1963.

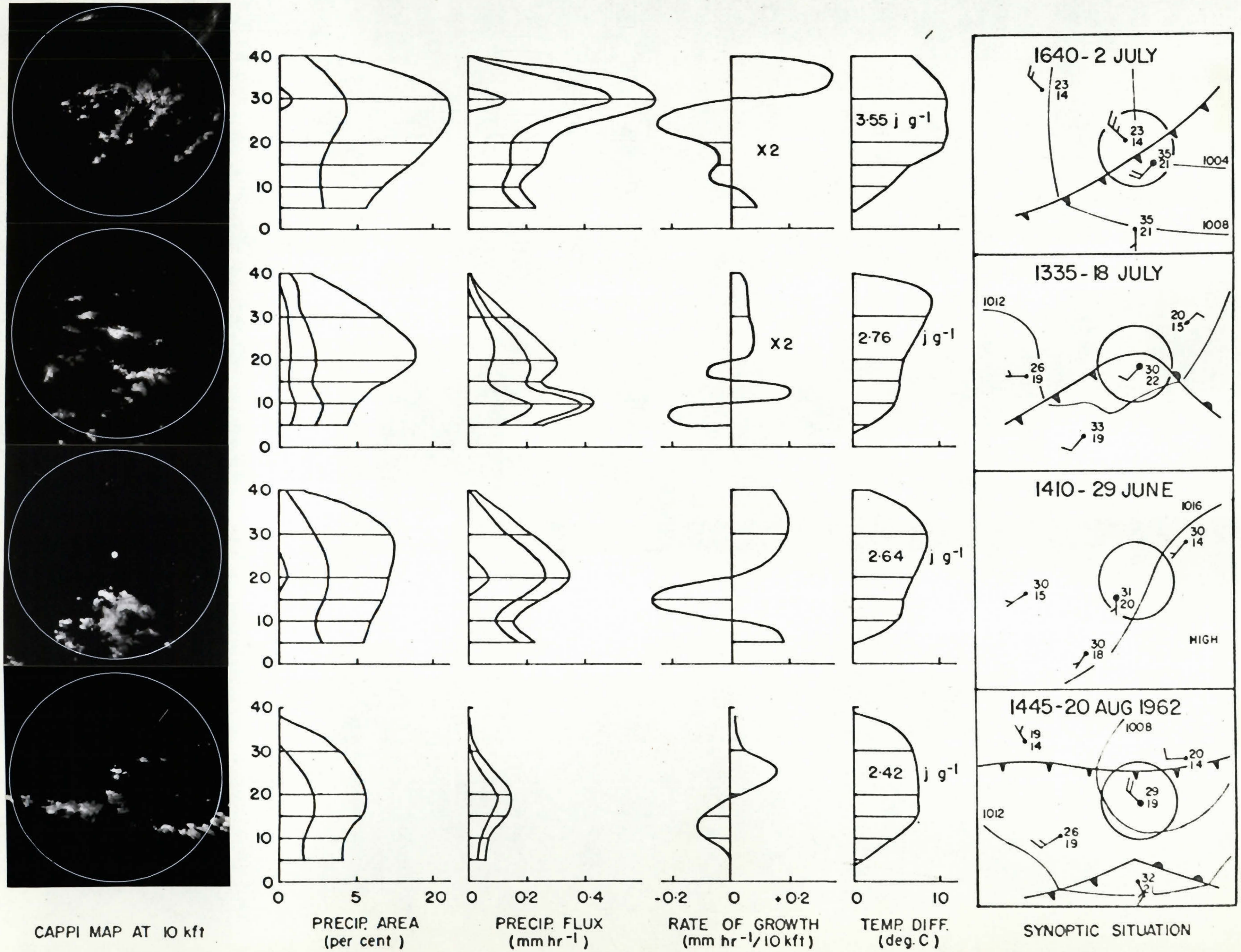
1640 - 2 JULY
1335 - 18 JULY
1410 - 29 JUNE
1445 - 20 AUG 1962
3·55 j g⁻¹
2·76 j g⁻¹
2·64 j g⁻¹
2·42 j g⁻¹
X2
CAPPI MAP AT 10 kft
PRECIP. AREA (per cent)
PRECIP. FLUX (mm hr⁻¹)
RATE OF GROWTH (mm hr⁻¹/10 kft)
TEMP. DIFF. (deg. C)
SYNOPTIC SITUATION
HIGH

Fig. 3.2

2 July. This occasion of showers at a cold front has just been discussed in detail. Here the cold front has just passed Montreal, and the line of showers is reforming after having dissipated as it passed over the St Lawrence Valley (NE-SW through Montreal). A very strong maximum in the flux has developed at the great height of 30 kft. There are large amounts of light plume echo at 20 and 30 kft, with 85% of the area of echo between 0.2 and 3.2 mm hr^{-1}, but these do not contribute greatly to the total flux.

18 July. Cellular complexes are drifting at 30 knots from the W in the warm sector of a minor frontal wave. Even though the wind shear between 10 and 30 kft is less than 20 knots, there is considerable plume echo, with 90% of the echo area at 20 kft between 0.2 and 3.2 mm hr^{-1}. The flux has maxima at 10 and 20 kft, and the upper maximum subsequently intensified and descended. Soon after it descended below 15 kft a tornado was reported 25 n mi NW of Montreal. In accord with the considerably smaller amount of energy available, the maximum is much lower than on 2 July.

29 June. An area of shower activity has developed over the Adirondack Mountains to the S in a situation with light winds. There is considerable pluming toward the SE at 20 and 30 kft, the wind shear between 10 and 30 kft being from the NW at 25 knots. Again, there is a maximum in the flux at 20 kft.

20 August 1962. An E-W line of showers has formed, with a cold front to the N and a minor frontal wave to the S. The cells were moving almost along the direction of the line from the W at 35 knots, so the line advanced only very slowly to the S. One station along the line reported prolonged heavy rain and scattered hail amounting to over 60 mm in less than 3 hours. There is reason to believe that values in the 1962 measurements are too low, but there is a definite maximum in the flux at 20 kft.

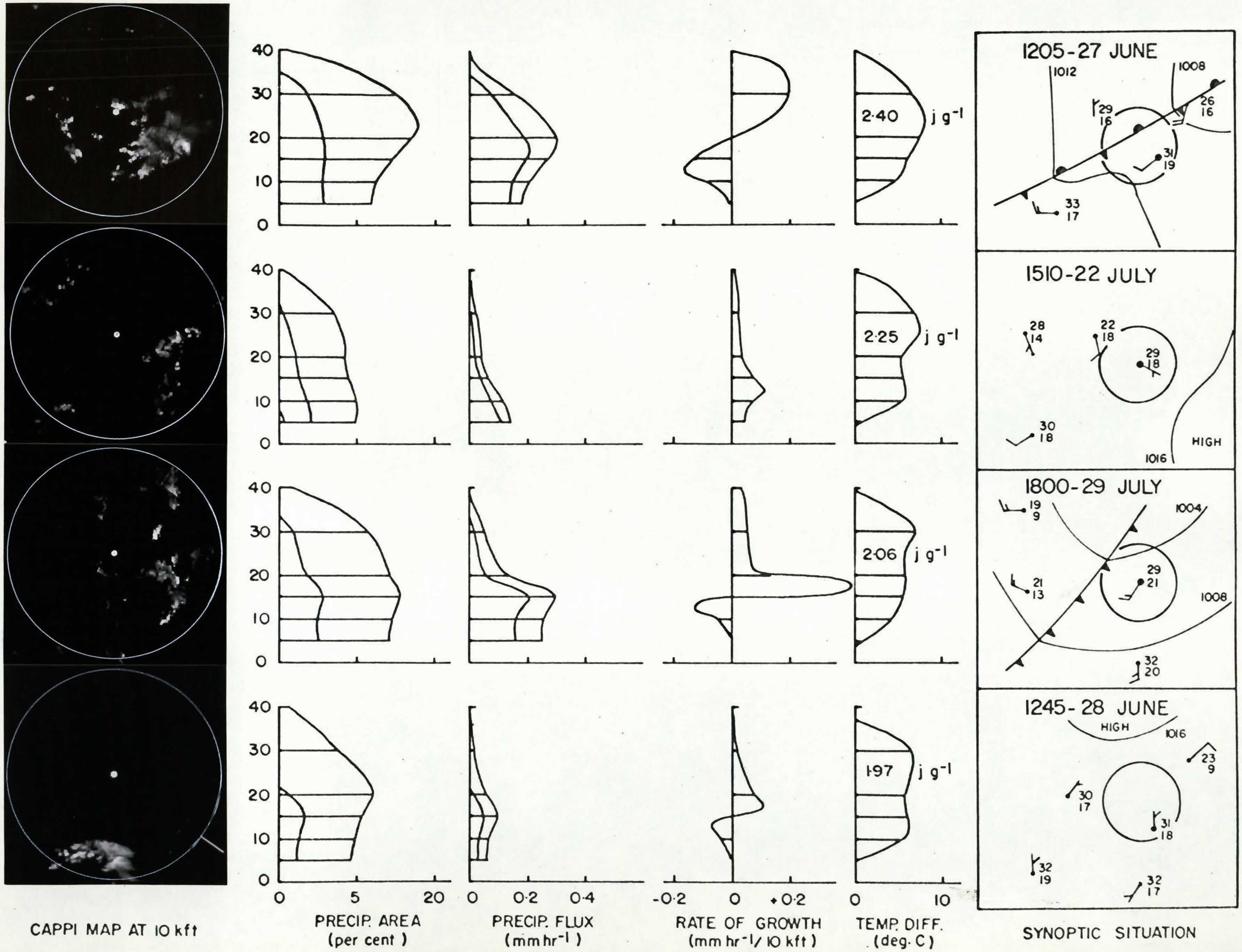
1205-27 JUNE
1510-22 JULY
1800-29 JULY
1245-28 JUNE
2·40 j g-1
2·25 j g-1
2·06 j g-1
1·97 j g-1
HIGH
CAPPI MAP AT 10 kft
PRECIP. AREA (per cent)
PRECIP. FLUX (mm hr-1)
RATE OF GROWTH (mm hr-1/10 kft)
TEMP. DIFF. (deg. C)
SYNOPTIC SITUATION

Fig. 3.3.

27 June. Numerous groups of cells are forming in the region of a stationary front and drifting from the NW at 35 knots. A maximum in the flux has developed at about 18 kft, and this intensified and descended. As it reached 10 kft at about 1245, the area of precipitation to the SE gave heavy rain, hail and strong winds at points 60 n mi SE.

22 July. Widely scattered isolated showers have developed in a region of light winds, and are drifting very slowly from the E. At no height did the wind exceed 15 knots, and the winds at 10 and 30 kft were identical. This case is exceptional, for the flux shows no maximum aloft. The cells did not show the usual tendency to cluster, and were more isolated than in any other of the cases discussed here. Possibly, because of their small size, entrainment of environmental air might have prevented the cells from realizing more than a small portion of the available energy.

29 July. Scattered groups of showers are drifting from the SW at 35 knots in air ahead of a well-defined cold front advancing from the NW. Precipitation amounts ranged up to 50 mm. There are no significant plumes aloft, but there is a maximum in the flux at 15 kft. It is lower and much less pronounced than in previous cases.

28 June. This occasion was quite similar to 29 June. An area of showers has developed and is almost stationary over the Adirondack Mountains to the S. At 20 kft there are prominent plumes to the E produced by 40-knot winds. Since the total area of precipitation is rather low (about 5%) the total flux is also low. However there is a definite maximum at 15 kft.

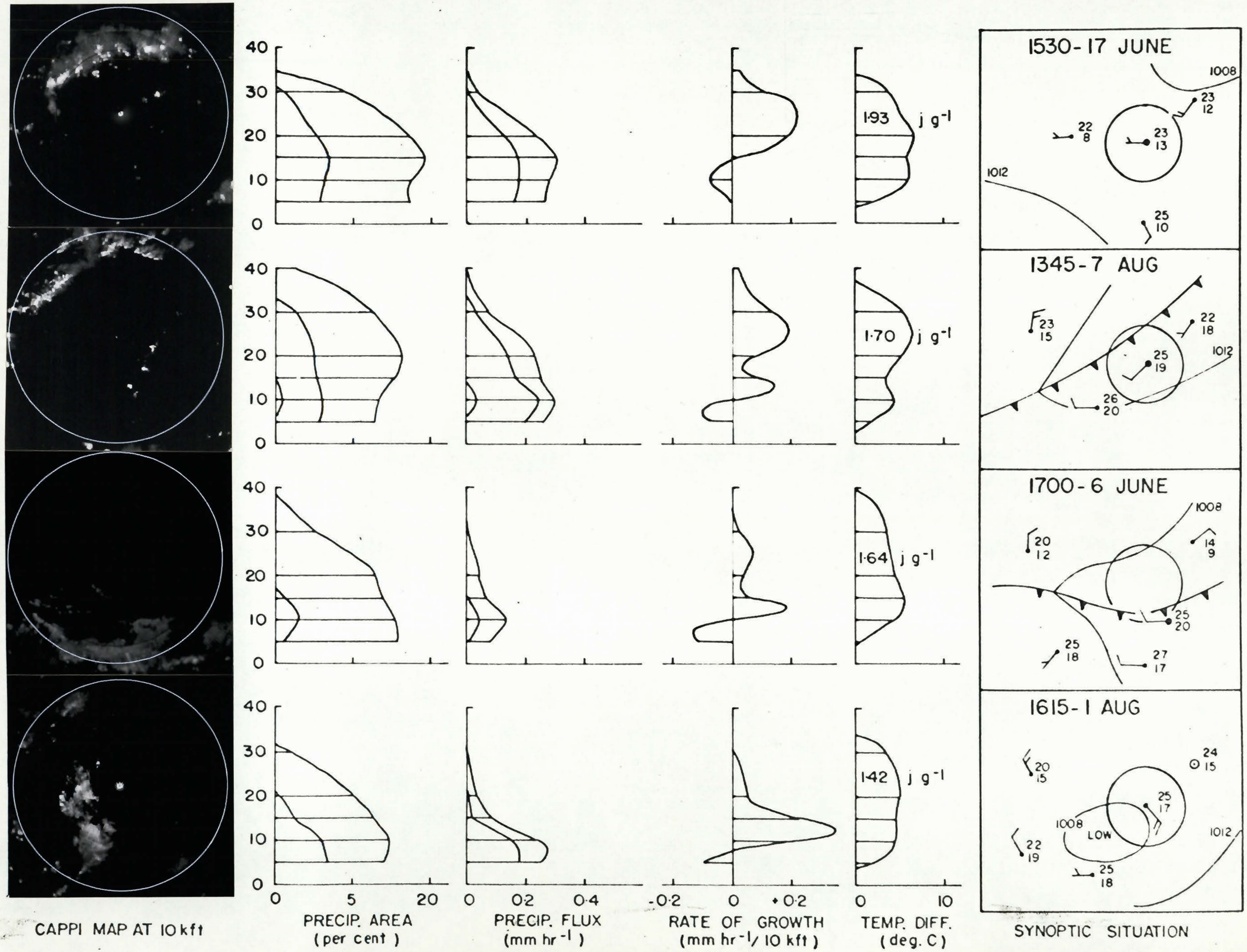
1530-17 JUNE
1345-7 AUG
1700-6 JUNE
1615-1 AUG
1·93 j g⁻¹
1·70 j g⁻¹
1·64 j g⁻¹
1·42 j g⁻¹
CAPPI MAP AT 10 kft
PRECIP. AREA (per cent)
PRECIP. FLUX (mm hr⁻¹)
RATE OF GROWTH (mm hr⁻¹/ 10 kft)
TEMP. DIFF. (deg. C)
SYNOPTIC SITUATION

Fig. 3.4.

17 June. The main feature on this occasion is an E-W line of cells embedded in a band of light precipitation. The individual cells are moving along the line from the W at 15 knots, many apparently being generated at a point about 80 n mi to the WNW. The precipitation pattern was fairly uniform with height and persisted with little overall change for several hours. It extended only up to 35 kft, rather lower than previous cases. The upper winds were generally W 15 knots and did not vary much with height. A few stations along the line reported rainfall amounts up to 25 mm. Although the precipitation flux is fairly uniform up to 20 kft, it does show a slight maximum at 15 kft.

7 August. Again the radar map shows a line of cells embedded in light precipitation, but in this case the cells are along a cold front. The winds aloft are fairly uniform with height at NW 20 knots, and this is also the velocity of the cells. Extensive areas of light precipitation are generated at 20 kft, but because of the uniform winds it persists around the cells at that height. One station near Montreal reported a rainfall of 40 mm. As on 17 June, the flux does not vary much up to 20 kft, although on this occasion there is a maximum at the rather lower height of 10 kft.

6 June. Here the precipitation is in a broad E-W band at a cold front to the S of Montreal. It is drifting from the NW at 20 knots. As the front passed Montreal three hours earlier a narrow line of cells moved obliquely over the city, with a very small component of motion normal to the line. Rainfall amounted to 50 mm in less than 2 hours, including a 5 min burst at 130 mm hr^{-1}. Unfortunately, attenuation was so severe that no useful radar observations were possible at that time. However, after a period in which there was no maximum in the flux aloft, one developed at 10 kft at 1700 EST.

<u>1 August</u>. Shower areas are drifting with a local depression at 15 knots from the SW. The precipitation pattern is uniform up to 10 kft, but then the amount and intensity of precipitation decrease with height, with tops just over 30 kft. There is a maximum in the flux at about 8 kft.

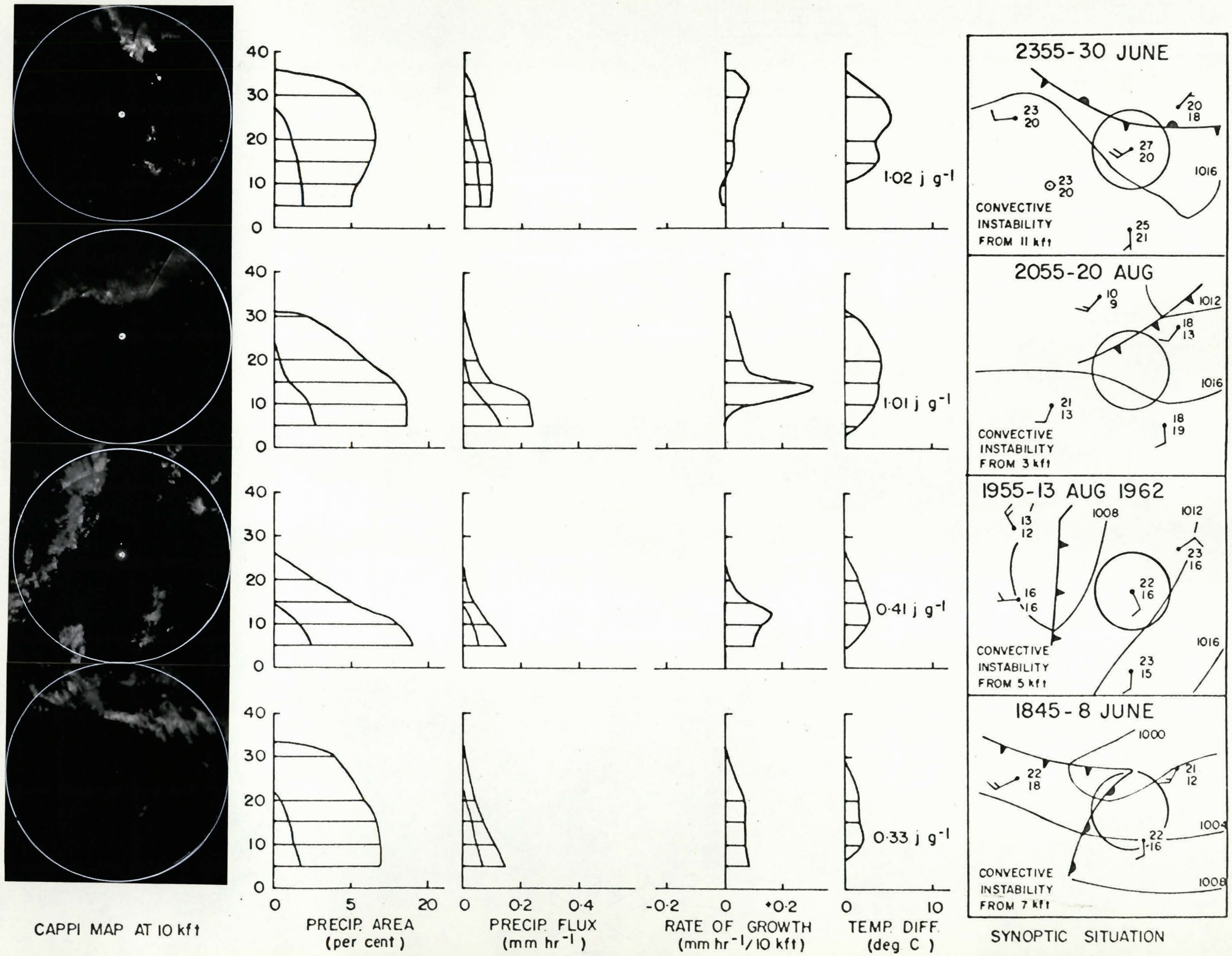

2355-30 JUNE
CONVECTIVE INSTABILITY FROM 11 kft
1·02 j g⁻¹
2055-20 AUG
CONVECTIVE INSTABILITY FROM 3 kft
1·01 j g⁻¹
1955-13 AUG 1962
CONVECTIVE INSTABILITY FROM 5 kft
0·41 j g⁻¹
1845-8 JUNE
CONVECTIVE INSTABILITY FROM 7 kft
0·33 j g⁻¹
CAPPI MAP AT 10 kft
PRECIP. AREA (per cent)
PRECIP. FLUX (mm hr⁻¹)
RATE OF GROWTH (mm hr⁻¹/10 kft)
TEMP. DIFF. (deg C)
SYNOPTIC SITUATION

Fig. 3.5.

30 June. The significant precipitation on this occasion is occurring at a well-defined stationary front to the N of Montreal. The area is drifting along the front from the W at 25 knots. Whereas all previous cases have occurred before 1800 EST and convection has been from the surface, in this and the following cases the convection is in the upper levels after 1800 EST. In this particular case convective instability is realized between 11 and 36 kft. The upper height is given by the echo tops, and the lower height can then be deduced from the tephigram. This lower height is beautifully confirmed by a study of the profiles, which show steady growth from the top almost down to this height and no growth below it. There is actually a slight maximum in the flux at about 13 kft, 2 kft above the condensation level. On this occasion there were also prominent plumes at 20 kft.

20 August. This is a similar situation, with an area of precipitation to the N drifting with a well-defined cold front at 25 knots from the NW. Again convection is produced by the realization of convective instability, this time between 3 and 31 kft. There are no plumes on this occasion and the precipitation decreases steadily in area and intensity above 10 kft. The flux profiles are rather suggestive of a maximum at about 5 kft, 1 kft above the condensation level. This is very similar to the height of the maximum on 30 June.

13 August 1962. Precipitation in a NE-SW band about 100 n mi ahead of a cold front is drifting from the W at 30 knots. Convective instability is realized between 5 and 27 kft. There is apparently no upper maximum in flux, though it is interesting to note that there is still an upper maximum in the rate of growth.

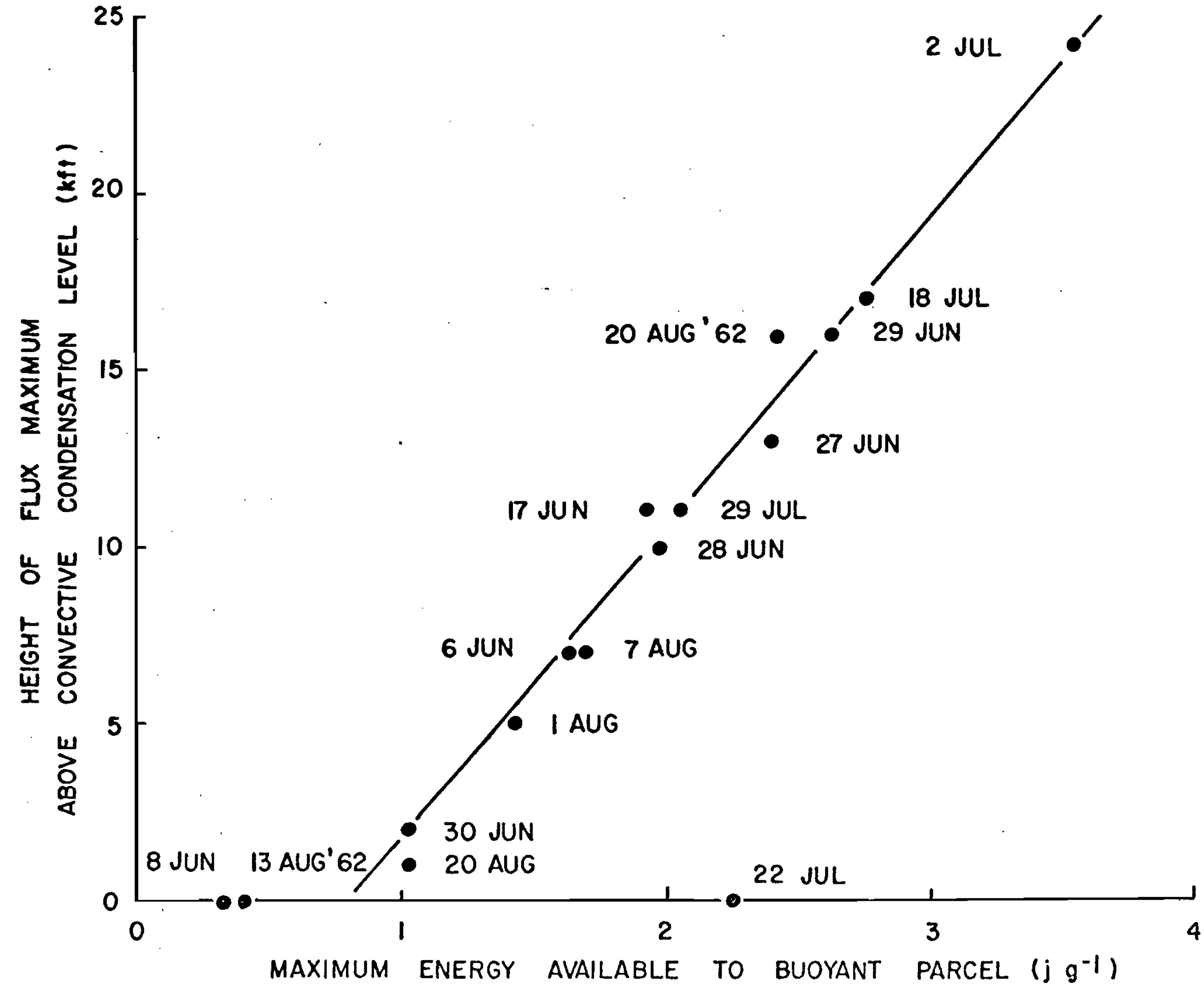

Fig. 3.6. Relation between height of maximum flux above convective condensation level and maximum amount of energy available to buoyant parcel.

<u>8 June</u>. On this occasion there is an area of cellular precipitation to the N. It seems to be due to convective instability which is realized as rather moist air is lifted in the region between warm and cold fronts. The pattern was moving at 35 knots from the NW. Like 13 August, there is no upper maximum in the flux. In contrast to that occasion, however, there is now no upper maximum in the rate of growth.

Now that the main characteristics of a wide variety of situations have been discussed, the pattern that has emerged can be studied. The most notable feature is undoubtedly the existence of a maximum in the flux at a height which depends on the amount of available energy. This relation has been put into graphical form in Fig. 3.6, which shows the height of the maximum above the convective condensation level (from the tephigram) as a function of the maximum amount of energy available to a buoyant parcel. It is indeed a striking relation: roughly, 1 j g^{-1} is required to produce a maximum at all, and thereafter each additional j g^{-1} lifts the maximum 10 kft. Even the single exception of July 22 is of some interest, and will be discussed later.

Such a striking relation strongly invites an explanation. Some insight into the possible explanation can be obtained by looking closely at the observed features of the maximum in flux in the light of other research on shower structure, and this will be done later in this chapter. At the same time it will be found that profile observations reinforce this other research.

Returning to the profiles in Figs. 3.2 to 3.5, it can be seen that there is frequently a maximum in the total area near the level of maximum flux. It generally lies a few thousand feet above the maximum flux, but can be as much as 10 kft above or 2 kft below. There is little correlation between the height of this maximum area and the available energy.

There is an erratic tendency for the value of the flux at the maximum to decrease with decreasing available energy from an average rainfall rate of 0.65 mm hr^{-1} to 0.1 mm hr^{-1}. The value of the flux at 5 kft does not show any dependence on available energy, although the way in which its average of 0.2 mm hr^{-1} arises is somewhat dependent on the energy. In severe storms it may be the product of 5% coverage at 4 mm hr^{-1}, in weak storms 15% at 1.3 mm hr^{-1}. The ratio of the maximum flux to that at 5 kft was also studied, and it decreased erratically with decreasing energy from about 2.7 to 1.0. However, none of these other relations is as striking as that between the height of the maximum flux and the available energy.

3.2 Case Studies of Shower Situations

The main features of various shower situations have now been studied. Before discussing the implications of these features, the four most severe storms will be looked at more closely. In Figs. 3.7 to 3.11 profiles of area and flux have been drawn every 22.5 minutes throughout the most interesting periods of the storms. CAPPI maps are given at several heights every 45 minutes. Upper maxima are evident in all cases, and attention will be directed particularly to the trends these maxima show with time.

It should be noted that the CAPPI maps and profile data at the various heights are not quite simultaneous. Data are acquired successively at 5, 10, 15, 20, 30 and 40 kft and it takes 3.75 minutes to record each height. The times given are those at the beginning of the sequence when the 5-kft data are being recorded, and are all EST.

In analysing the trends of the maxima it was found helpful to plot the data at points in a grid with coordinates of time and height. The contours on this diagram quickly showed up maxima and their trends, even where the maxima lay between the points of the grid. Such an analysis is particularly necessary when the maximum lies between two grid points 10 kft apart in height. It was used in preparing all the following profiles.

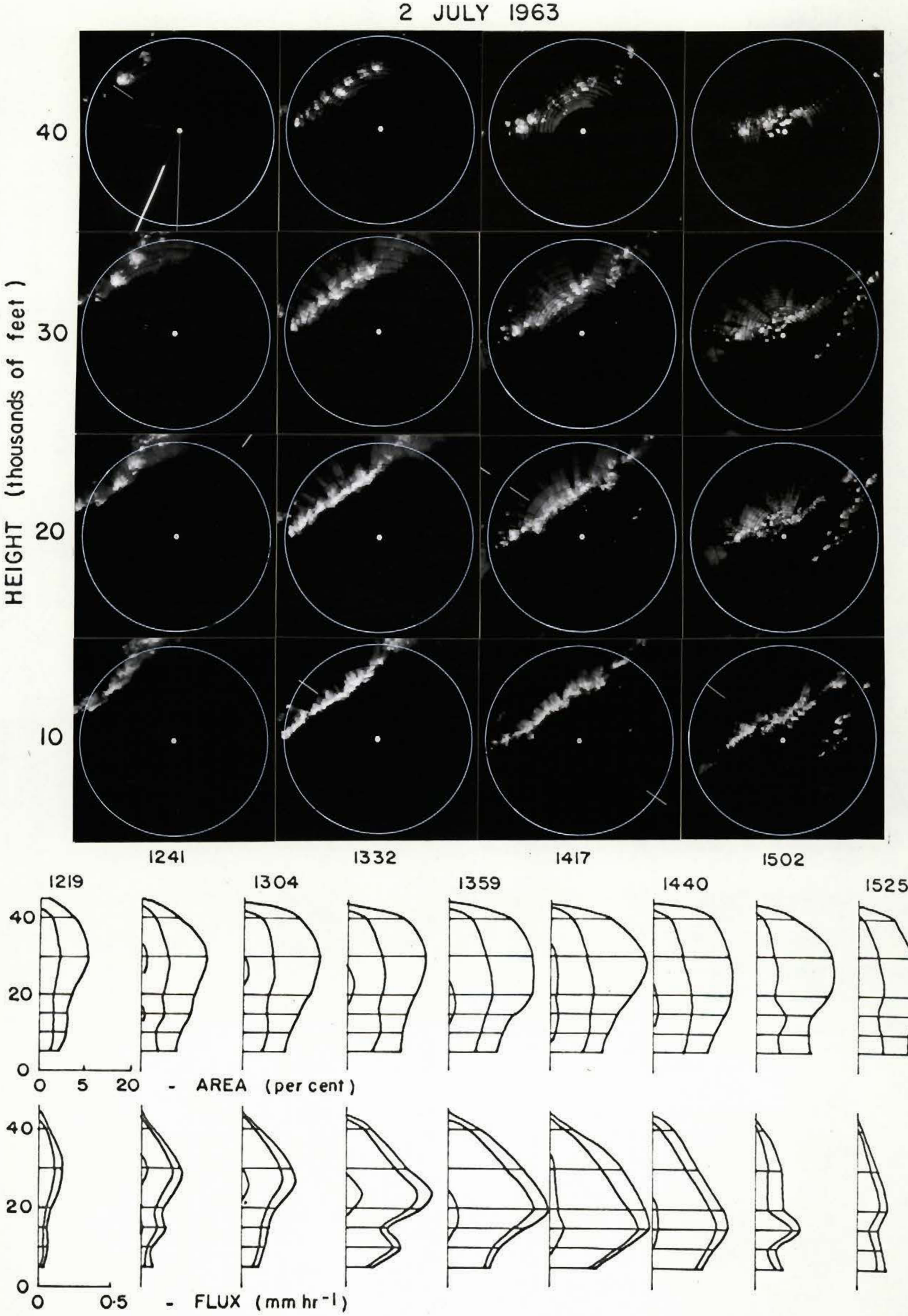
2 JULY 1963
HEIGHT (thousands of feet)
40
30
20
10
1241
1332
1417
1502
1219
1304
1359
1440
1525
40
20
0
0 5 20 - AREA (per cent)
40
20
0
0 0·5 - FLUX (mm hr⁻¹)

Fig. 3.7.

<u>2 July</u>. The profiles of this day, the most exciting of the 1963 season, have already received some attention at the beginning of section 3.1. Here, two sequences of profiles and maps are presented in Figs. 3.7 and 3.8. A line of showers oriented NE-SW moved into the region from the NW, with individual cells moving from the W at 35 knots. It dissipated as it passed over the St Lawrence Valley, reforming again to the SE. The first sequence is during the approach of the line, the second during its departure, and it will be seen that the two sequences of profiles are remarkably similar.

The first sequence starts about 90 min after the line had formed, and after the line had moved within the 80 n mi limit of the sampling area. Most of the overall increases in area and flux at the beginning are due to the fact that the line is moving into the region. Thus the total flux at 5 kft increases from an amount equivalent to 0.03 mm hr^{-1} over the whole area at 1219 to 0.17 mm hr^{-1} at 1332, while the average rate over the area of precipitation remains constant at about 2.5 mm hr^{-1}. However, provided a sufficient area is within the sampling region the variations with height are still significant, and it happens that it is the changes in the vertical pattern that are especially interesting.

The maximum in flux characteristic of shower situations is quite apparent. It has probably just become established at 30 kft at 1219. Having formed, it steadily descends as the sequence progresses, reaching 15 kft soon after 1440. The maximum then dissipates rapidly, but the observations are beginning to suffer seriously from attenuation losses (most evident in the 20 and 30-kft CAPPI maps), and one cannot be too confident of measurements at this time. The line certainly weakened as it passed over the radar and the St Lawrence Valley, giving very small

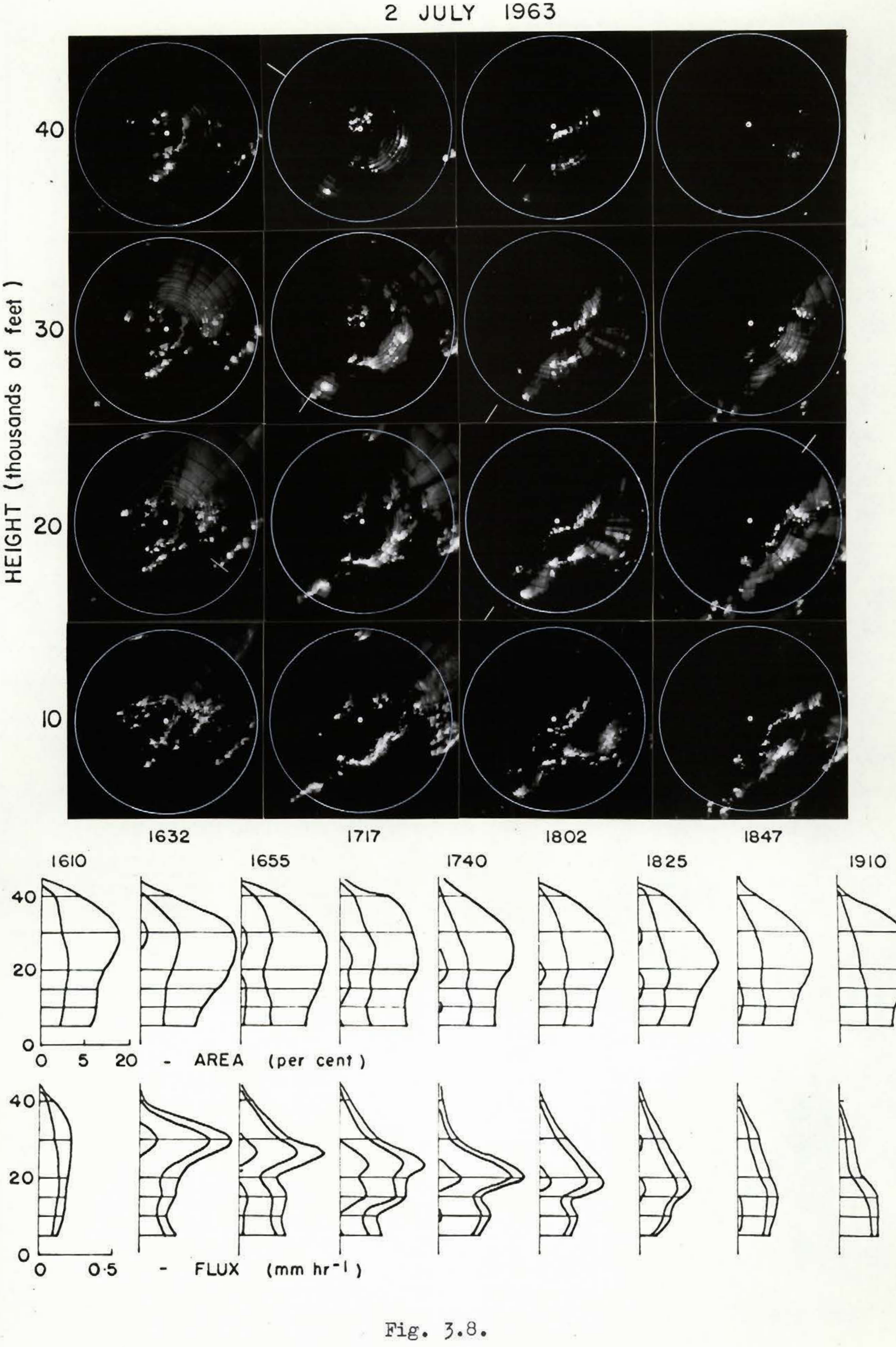
2 JULY 1963
HEIGHT (thousands of feet)
40
30
20
10
1610
1632
1655
1717
1740
1802
1825
1847
1910
0 5 20 - AREA (per cent)
0 0·5 - FLUX (mm hr⁻¹)

Fig. 3.8.

rainfall rates. Immediately prior to dissipating, at the time the maximum reached 15 kft, raingauges beneath the line recorded rainfall amounts two or three times those recorded previously. It is interesting, and perhaps significant, to note that the melting level was at 14 kft.

The second sequence begins with the reformation of the line. The line is much less clearly defined now, but it can be seen at 1717 and subsequently. At 1632, a prominent maximum in flux has developed, again at 30 kft. It is probably due to the new groups of cells which have developed about 30 n mi S and 70 n mi E of the radar and are seen in the 30-kft CAPPI map. At this time there is very little light plume echo around these new cells, but this has appeared 45 min later. Meanwhile the maximum in flux has descended to 23 kft, and as before continues to descend, reaching 15 kft just before 1847. As it reaches 15 kft it again dissipates rapidly. Because the precipitation is in several groups rather than the well-defined line it assumed during its approach, it is not readily possible to tell whether an intensification of rain occurred at the ground at this time. There is a need to study the individual groups of showers separately in cases like this.

In both sequences, the maximum in flux descended from 30 kft to 15 kft in a little over two hours, at about 110 ft min^{-1} (0.6 m sec^{-1}). This period is almost certainly considerably in excess of the lifetime of any of the component cells in the line.

Although the area profiles have been somewhat neglected in this discussion they are also interesting. The maximum in area, like the flux maximum, forms at 30 kft. But, in the first sequence, it remains at about the same height. During the second sequence it descends rather slowly from 30 kft to 20 kft at about half the rate of descent of the flux maximum.

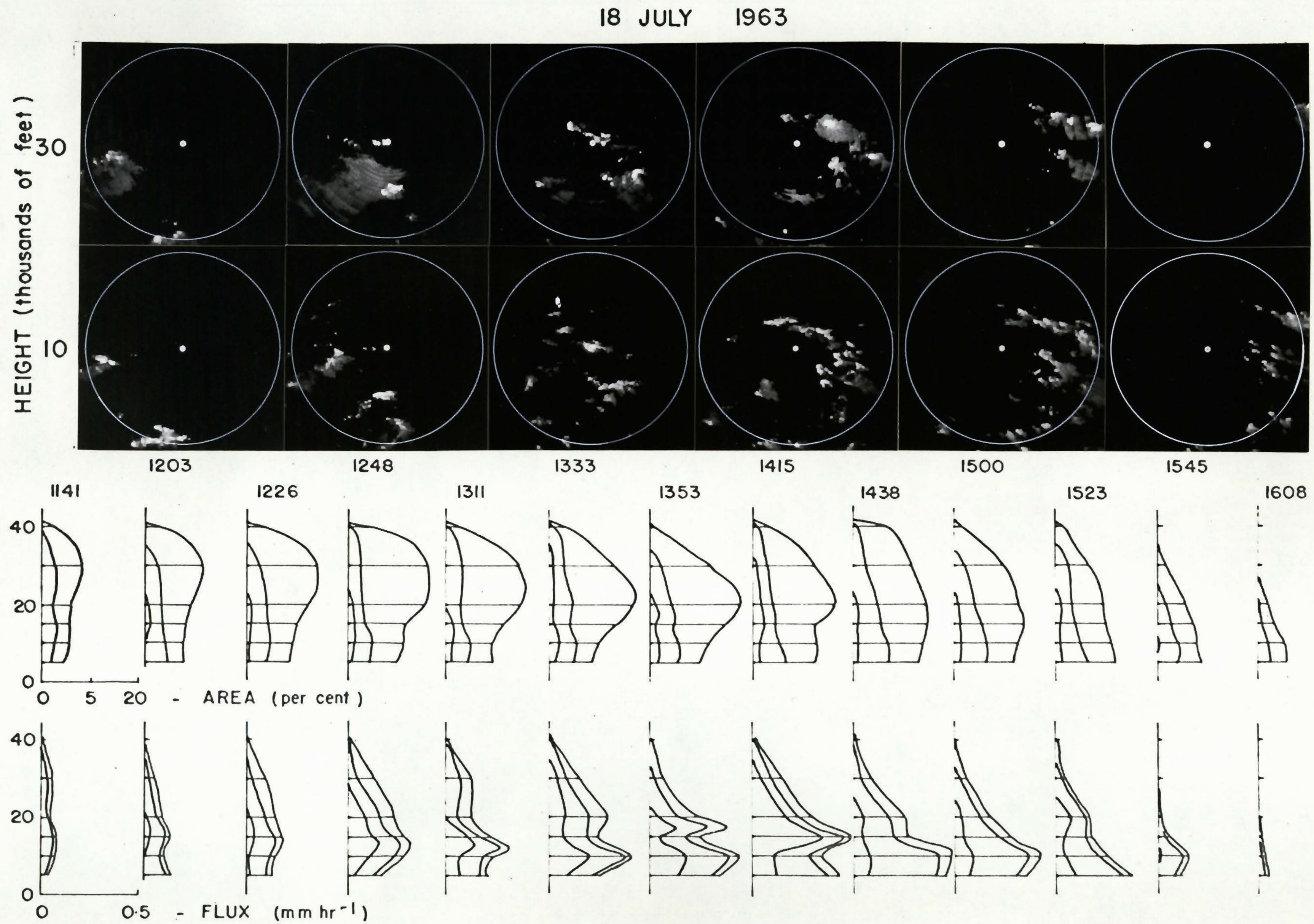
18 JULY 1963
HEIGHT (thousands of feet)
30
10
1203
1248
1333
1415
1500
1545
1141
1226
1311
1353
1438
1523
1608
40
20
0
0 5 20 - AREA (per cent)
0 0·5 - FLUX (mm hr⁻¹)

Fig. 3.9.

18 July. On this day scattered groups of showers were moving from the W at 30 knots. At 1203, two groups of showers which had formed 90 min earlier are 70 n mi to the W and S, and have just developed plumes at 30 kft. There is a slight maximum in the total flux at 15 kft. This persists as the two groups of showers develop, eventually descends slowly and then apparently lingers at 10 kft before finally disappearing after 1353. Meanwhile, by 1333, new groups have formed about 40 n mi to the NW and the flux profile is apparently forming a second maximum at 20 kft. At 1415 this second maximum has descended to 15 kft, just above the melting level. A few minutes later, at 1430, the rather small group of cells 25 n mi to the NW produced the season's only reported tornado. A slight maximum is present at 10 kft after this time, eventually disappearing after 1500.

It is not known how much of the maximum at 15 kft just prior to the tornado is due to the particular group of cells which produced the tornado, but an unusually large proportion of it was due to a small area of very intense precipitation. In fact, 18 July was the only day of showers when precipitation with an equivalent reflectivity greater than 3×10^5 mm^6 m^{-3} (200 mm hr^{-1}, attenuation corrected) was detected, and the pre-tornado maximum included the greatest observed amount of such intense precipitation. The 0.05% (10 n mi^2) area accounted for almost 40% of the total flux. It is remarkable that, with precipitation covering about 1700 n mi^2, 40% of the total can be contained in 10 n mi^2. Considering that the density of raingauges is rarely much better than one per 100 n mi^2, this is an eloquent reminder of the value of radar as a tool in precipitation measurements.

The major maximum in flux descended from 20 to 15 kft in 40 min at 125 ft min^{-1} (0.7 m sec^{-1}), and possibly continued down to 10 kft at the same rate. The maximum in area formed at 30 kft as on 2 July, descended to 15 kft in 3 hours at 80 ft min^{-1} and then dissipated.

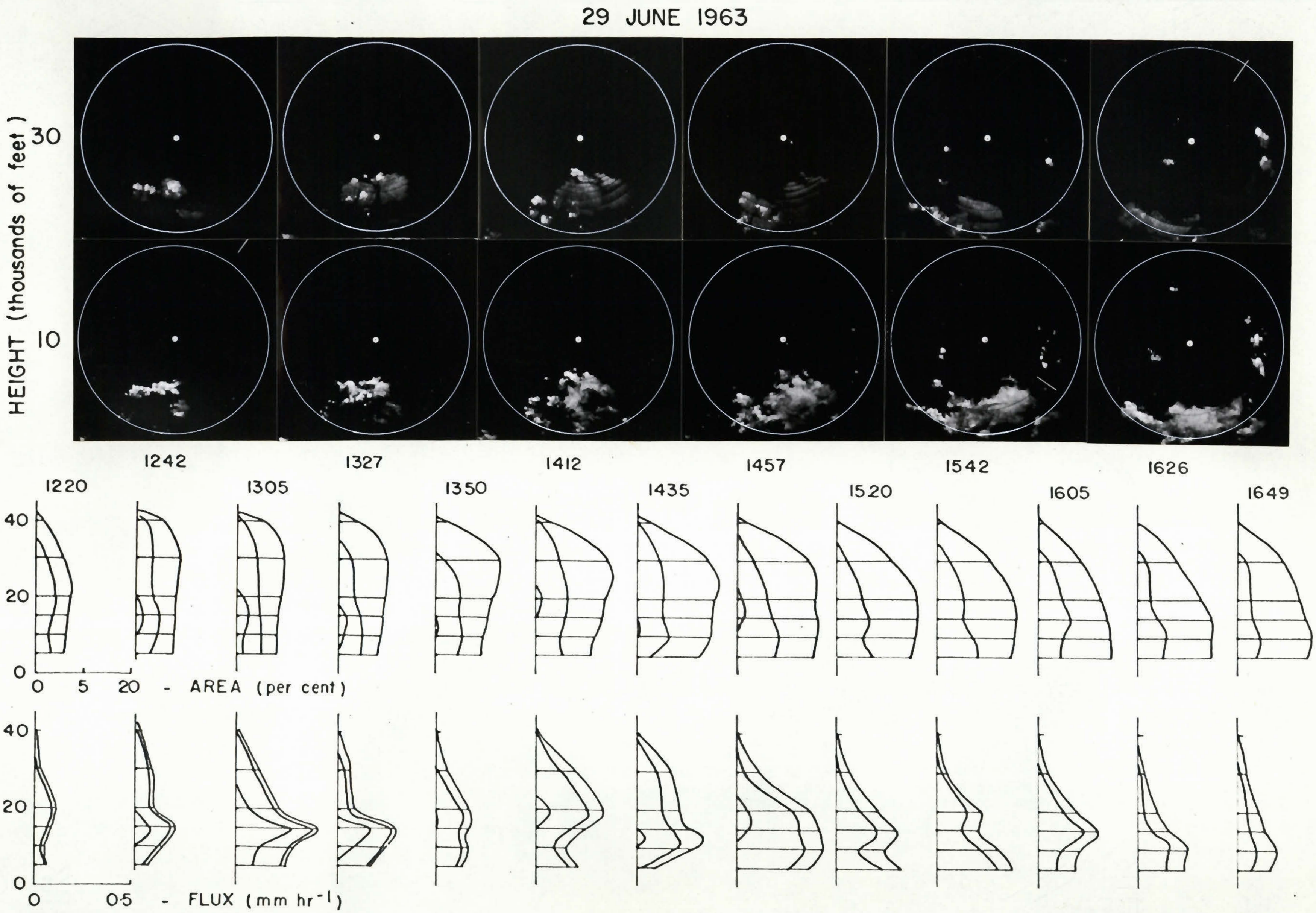
29 JUNE 1963
HEIGHT (thousands of feet)
30
10
1220
1242
1305
1327
1350
1412
1435
1457
1520
1542
1605
1626
1649
40
20
0
0 5 20 - AREA (per cent)
40
20
0
0 0·5 - FLUX (mm hr^{-1})

Fig. 3.10.

29 June. On this day an area of shower activity has developed over the Adirondack Mountains to the S. It will be seen that although there are upper maxima in flux, it is more difficult to follow their trends than in the previous two cases. The first cells were detected at about 1130 with maximum flux at 13 kft. The maximum steadily ascended until it was at 20 kft at 1220. At the time of the first CAPPI maps (1242), there is a compact area of cells 50 n mi SSE, and the 30-kft map shows the first signs of the formation of a plume. The flux maximum has descended to 15 kft, remains there for 45 min, and then dissipates. At 1412, a maximum has formed at 20 kft, and this seems to coincide with the development of new cells at the N edge of the shower area. This maximum descends quickly, reaches 10 kft by 1457 and dissipates. Yet another maximum has formed at 20 kft at 1542, this time coincident with the formation of new cells 60 n mi to the E. A particularly intense member of this group is clearly seen on the 30-kft CAPPI map 60 n mi to the ESE. This maximum again quickly descends to 10 kft and dissipates.

On this occasion, at least three maxima were observed to descend from 20 kft, though they were quite difficult to follow. This is probably because they descended much more quickly than in previous cases. Twice, the rate of descent appeared to be about 220 ft min^{-1} (1.2 m sec^{-1}).

Although plume echo formed at 30 kft, and the total area at 30 kft was double that at 5 kft by 1350, it was not as prominent as in the two previous cases.

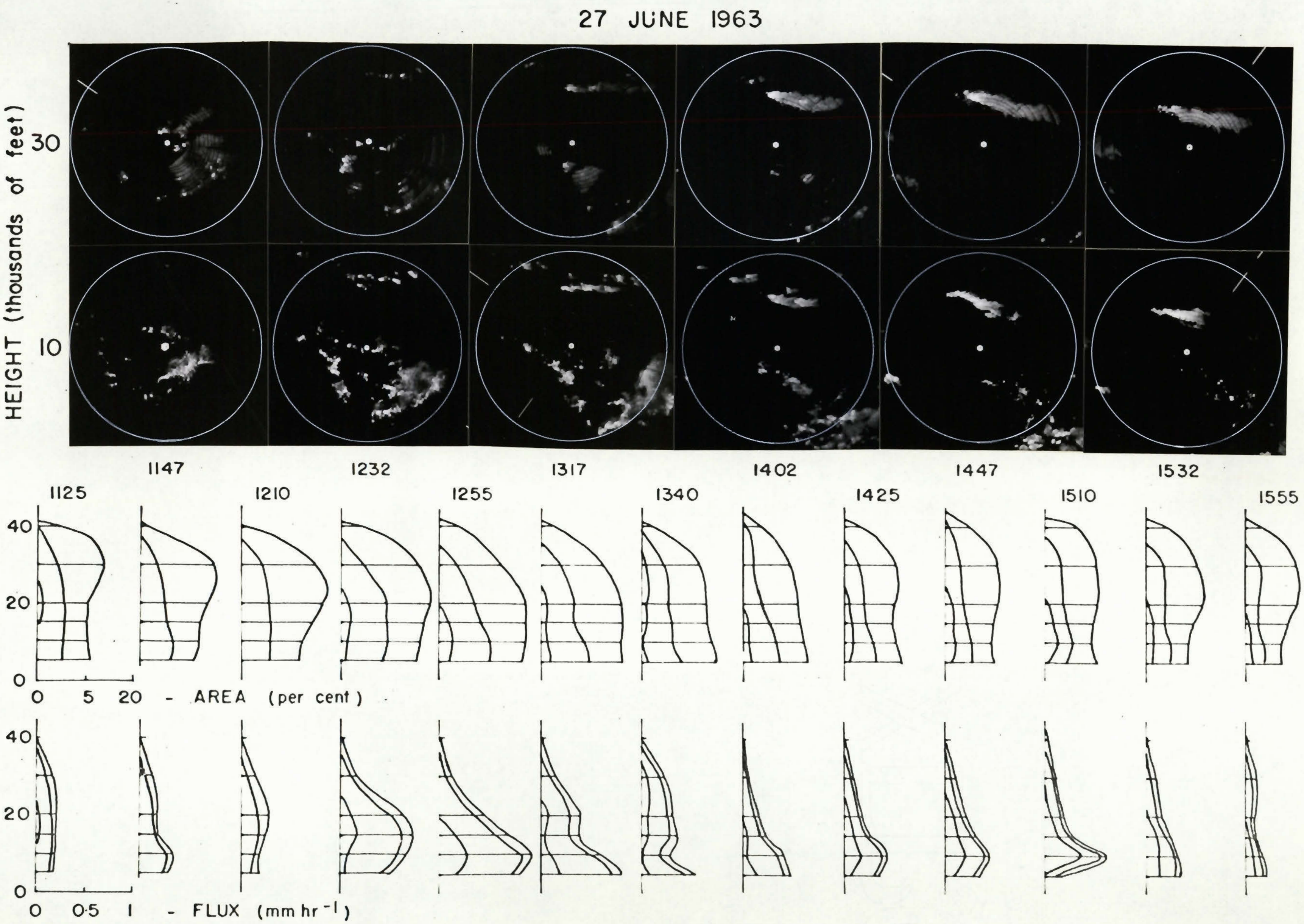
27 JUNE 1963
HEIGHT (thousands of feet)
30
10
1147
1232
1317
1402
1447
1532
1125
1210
1255
1340
1425
1510
1555
40
20
0
0 5 20 - AREA (per cent)
40
20
0
0 0·5 1 - FLUX (mm hr^{-1})

Fig. 3.11.

27 June. Numerous groups of showers are forming and moving from the NW at 35 knots. At 1147 a compact group with a considerable amount of plume echo is located to the SE. By 1210 a maximum in flux has developed a little below 20 kft, and subsequently this appears to descend quickly to 10 kft at 1255 before dissipating. At this time wind gusts strong enough to uproot trees, heavy rain and hail were associated with the group 60 n mi to the SE. It may be noted that the melting level was at 11 kft. The rate of descent of the maximum was about 220 ft min^{-1} (1.2 m sec^{-1}).

By 1317 a new group has formed to the N, and there is a suggestion of a maximum just below 20 kft. In the next profile this has descended to 15 kft. Later, this group gave a maximum which persisted at 10 kft for almost an hour.

The general pattern that has emerged from these case studies is the formation of maxima in flux at a height characteristic of the day, and their subsequent descent. It is this characteristic height which has already been related to the maximum amount of energy available to a buoyant parcel (Fig. 3.6). The well-organized line of showers of 2 July produced prominent maxima which descended slowly to the melting level and there dissipated. In the other cases showers developed in separate groups and, since each group can apparently produce its own maximum, the pattern was much more confused. There is some evidence that severe conditions at the surface occur as a maximum reaches the melting level. However, this evidence is much weakened by the lack of separate sets of profiles for each group.

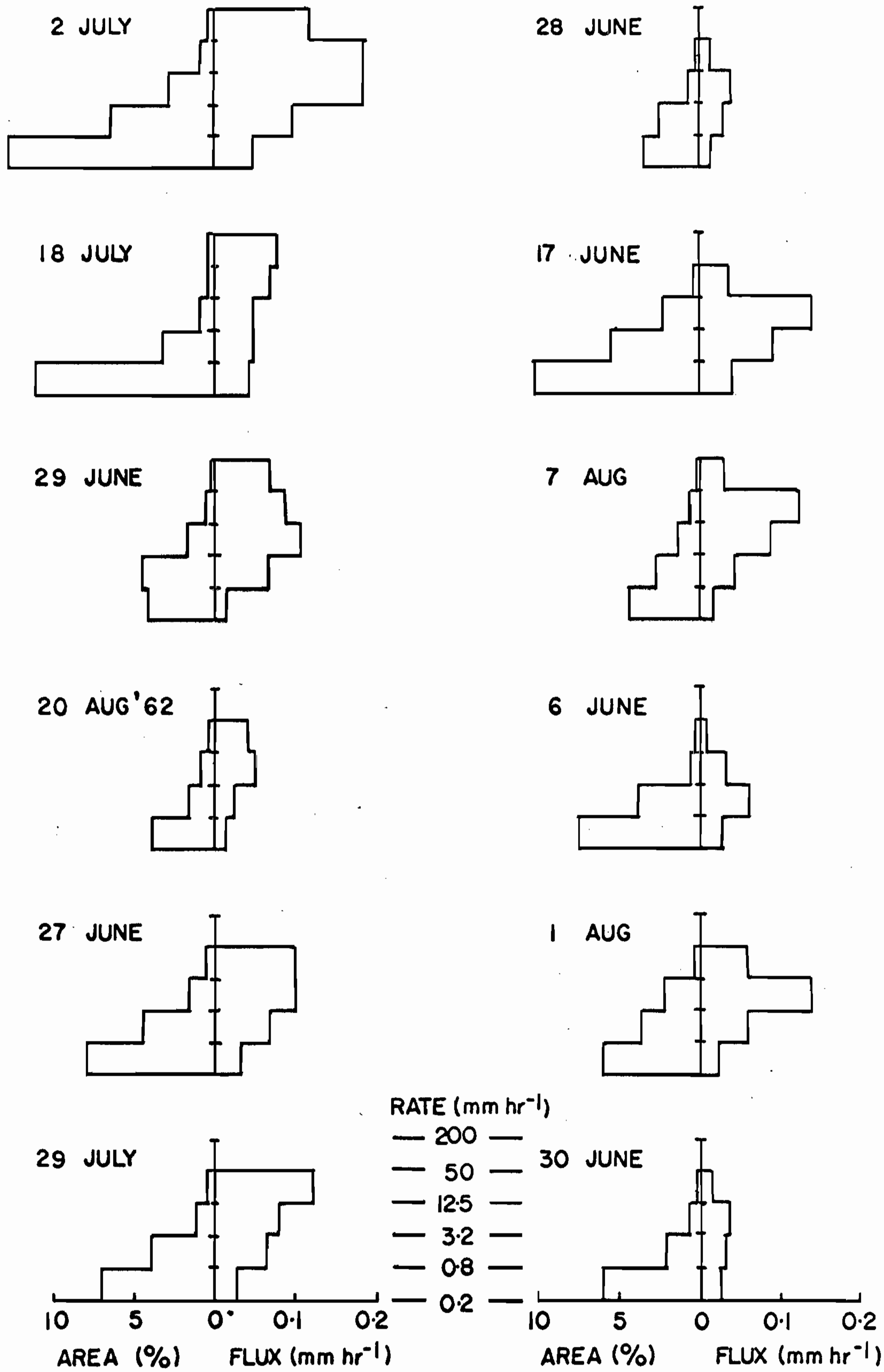

Fig. 3.12. The distribution of area and flux with rainfall rate at the height of maximum flux.

3.3 The Nature of the Maximum in Flux.

It is appropriate to begin a study of the nature of the maximum in flux with a look at the proportions contributed by rainfall of each intensity, as shown in Fig. 3.12. The cases shown are those with the highest maxima, and they are arranged in order of decreasing height of maximum in each of the two consecutive columns. For each case, histograms of precipitation area appear at the left, while histograms of flux are at the right. The intervals of rainfall rate for which the histograms have been prepared are shown at the bottom (all values are attenuation-corrected). Looking first at areas, they almost invariably decrease with increasing intensity. The only exception is 29 June, for which the areas in the first two intervals are about the same. Further, in all cases but 29 June, the area in the first interval forms at least 50% of the total area, with an average of about 60%. Turning from areas to fluxes, it can be seen that the contributions to the total flux from the first interval are quite small, and in fact they average about 12%. Thus, the large amount of light plume echo which is often present near the height of the maximum flux generally contributes only insignificant amounts to it.

There is considerable variation from case to case in the distributions of flux with intensity, but a few features are worth comment. It has just been pointed out that the contribution to the total from the light rain less than 0.8 mm hr^{-1} is quite small. The same is usually true for the heavy rain greater than 50 mm hr^{-1}. There are significant amounts of heavy rain in the first three cases, but in only one of the other nine was there any. In a general way, about 80% of the total flux lies between 0.8 and 50 mm hr^{-1}, the remainder being contributed mainly by heavy rain when the maximum is high, and mainly by light rain when it is low. The median rainfall rate,

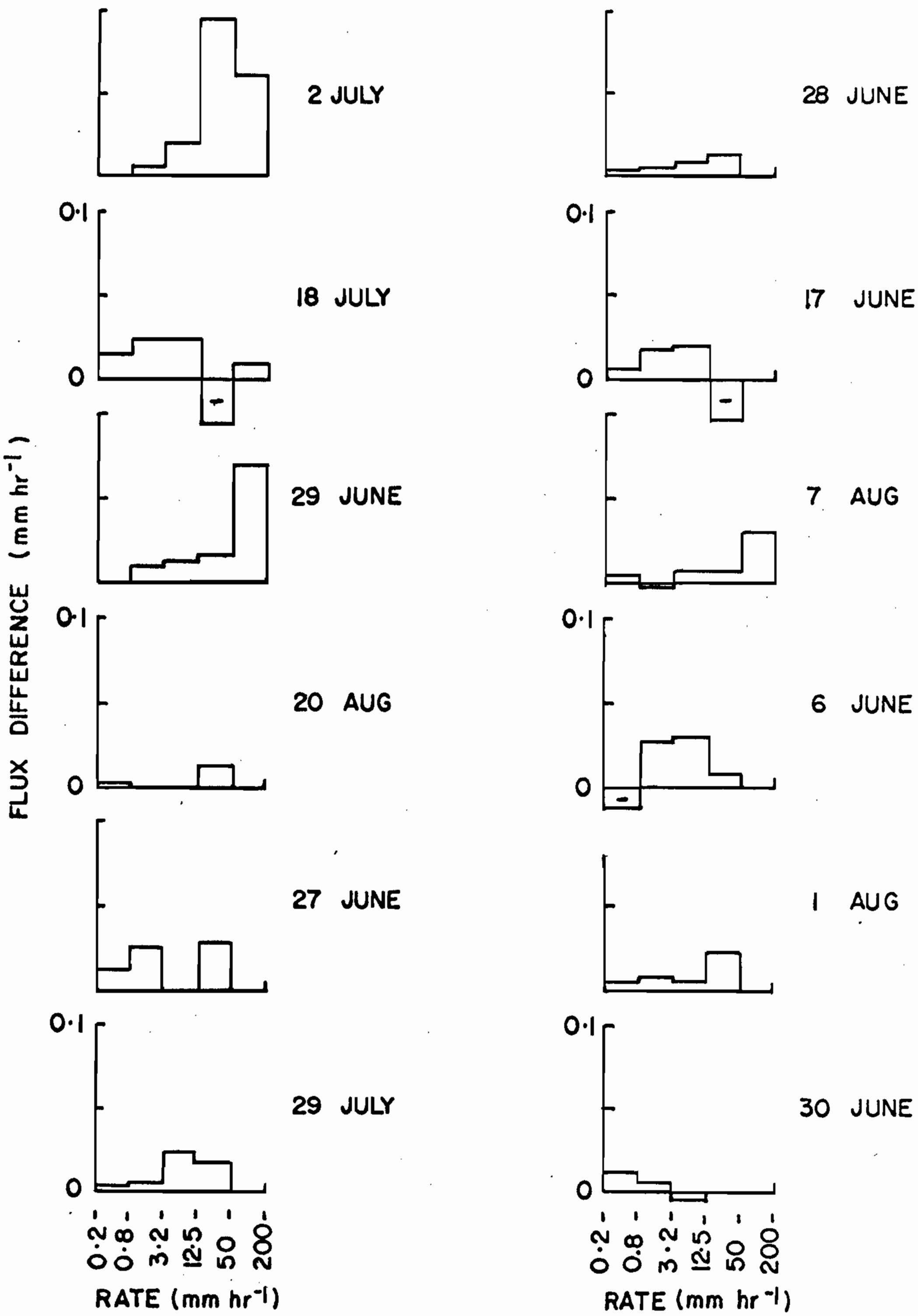

Fig. 3.13. The distribution of the difference between the flux at the maximum and that 5 kft below with rainfall rate.

or the rate which divides the flux into equal portions, decreases rather erratically with decreasing height of maximum from 12 mm hr^{-1} to 2 mm hr^{-1}.

These facts all suggest that the maximum in flux is largely determined by the area and intensity of the moderate rainfall. This suggestion is confirmed by looking at the difference between the maximum flux and that 5 kft below. Fig. 3.13 shows how this difference is distributed with rainfall rate. In most cases the excess flux at the maximum over that below is made up of excesses in all the individual intensities, although there are occasions in which there are deficits in some intensities. Notably, there were deficits in the interval 12.5-50 mm hr^{-1} on 18 July and 17 June. However, there is always a net excess for the interval 0.8-50 mm hr^{-1}, and in a majority of cases it forms more than half the total excess.

It is particularly necessary to draw attention to the importance of the moderate rain. The greatest total flux normally occurs together with the greatest intensity, but an explanation of the greatest intensity is not sufficient explanation for the existence of the maximum in total flux. There is one other point to make. Evaporation of falling precipitation is probably not a major factor in producing the maximum in flux. This may be inferred from the fact that the moderate precipitation at the height of the maximum occupies only 40% of the total area of rain, being well protected by the surrounding light rain both at that height and 5 kft below.

3.4 Profiles of Individual Showers.

The existence of a maximum aloft in profiles of all the precipitation over an area can only be understood in the light of the characteristics of the component cells. The structure of individual cells can be studied on the McGill grey-scale CAPPI maps, but this has not yet been done.

Accordingly, this section contains a review of other studies of shower structure. These can then be used to throw light on profiles of the total precipitation.

Marshall et al. (1947), in describing shower structure as observed by radar, suspected the accumulation of great quantities of rain aloft in the strong vertical air currents. This was soon confirmed by Langille and Gunn (1948), who presented vertical cross-sections through showers. They found that precipitation often accumulated aloft in showers, and they also noted frequent subsequent descent of such accumulations. The detailed pattern was observed to change rapidly, and on one occasion an accumulation was observed to descend at 1000 ft min^{-1}. Bowen (1950) observed similar accumulations aloft, and gave a reasonable explanation for them in terms of the trajectories of growing precipitation particles in updraughts. Later, Battan (1953a, 1953b) made an extensive study of the initiation and growth of precipitation in shower cells, and observed that precipitation in isolated Ohio cells was generally initiated between 8 and 16 kft. This observation, and others similar, stimulated East (1957) to provide an explanation. This was done in a full treatment of the growth of raindrops in cloud updraughts, along the lines of, but more realistic than, Bowen (1950).

Most of the observations up to this time were of fairly modest storms, and there was considerable excitement over observations of severe storms by Donaldson (1958, 1959, 1961b). An accumulation aloft was commonly observed at the core of a severe thunderstorm, and on one occasion reached the almost unbelievable radar rainfall rate of 3800 mm hr^{-1} at a height of 22 kft. Donaldson found that a high and intense maximum in radar reflectivity was present in the most severe thunderstorms, and that the height and intensity declined as a function of the decreasing severity of the storms. Various

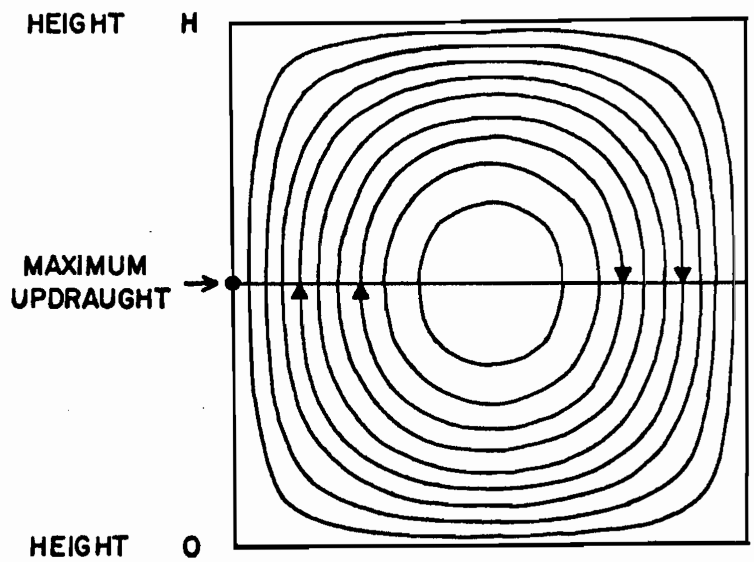

CONVECTIVE CELL

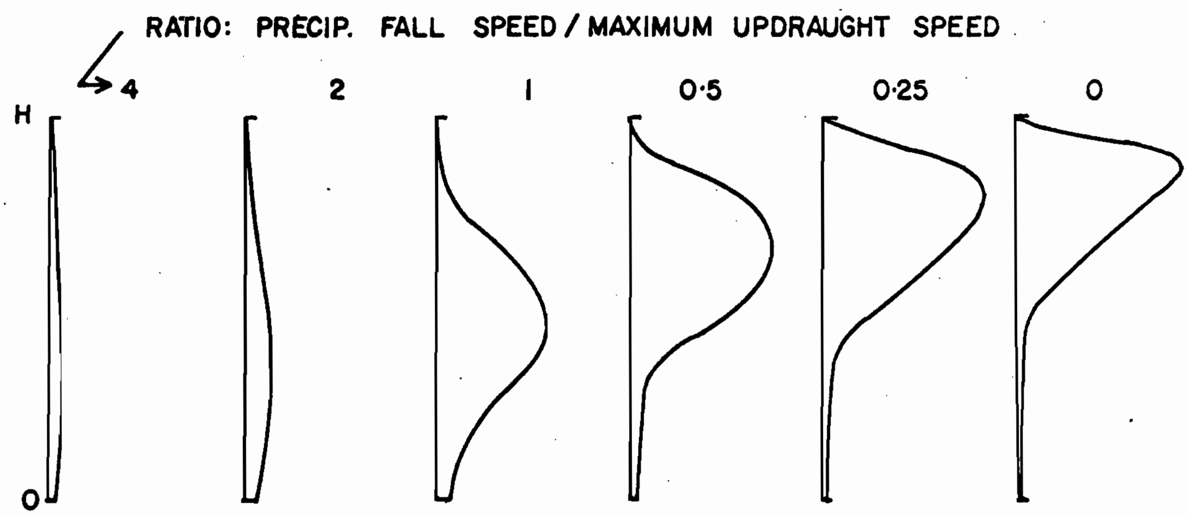

PROFILES OF TOTAL STORED PRECIPITATION

Fig. 3.14. Vertical profiles of the total precipitation developed in a model convective cell. The streamlines of the wind field are shown above. Profiles below are in each case at time = 1.35H/max. updraught speed. (After Kessler, 1961)

possible explanations of the strong reflectivity maximum were considered such as the storage of precipitation aloft during growth, the presence of strongly reflecting large dry hail, evaporation below the maximum, and severe attenuation losses at the lower levels (the observations were at 3-cm wavelength). Of these the storage of precipitation aloft, either in the form of hail or rain, was considered to be the most likely explanation.

Computations of the precipitation development in a model convective cell by Kessler (1961) bear this out. Vertical profiles of the total precipitation in the cell were computed for various updraught speeds, and some of these are shown in Fig. 3.14. For the stronger updraughts they show large accumulations of precipitation aloft. The nature of the wind field adopted for the model convective cell is indicated by the streamlines in the picture at the top. The profiles were obtained by starting with a just-saturated cell and studying the subsequent development of precipitation within it. Profiles are shown for various values of the ratio: precipitation fall speed/maximum updraught speed. The third profile, for example, is for a situation in which they are equal, and shows a pronounced accumulation near the height where they are equal. The profiles for which the maximum updraught speed exceeds the fall speed show similar accumulations which become higher and more intense with increasing updraught speed. There is even a slight maximum aloft in the total precipitation for cases in which the updraught speed is less than the fall speed.

It can be seen that Kessler's profiles bear a considerable resemblance to those observed in the present work. Further, just as the observed maxima appear at a height which increases with increasing available energy of buoyancy, so the height of the maxima in Kessler's model increases with

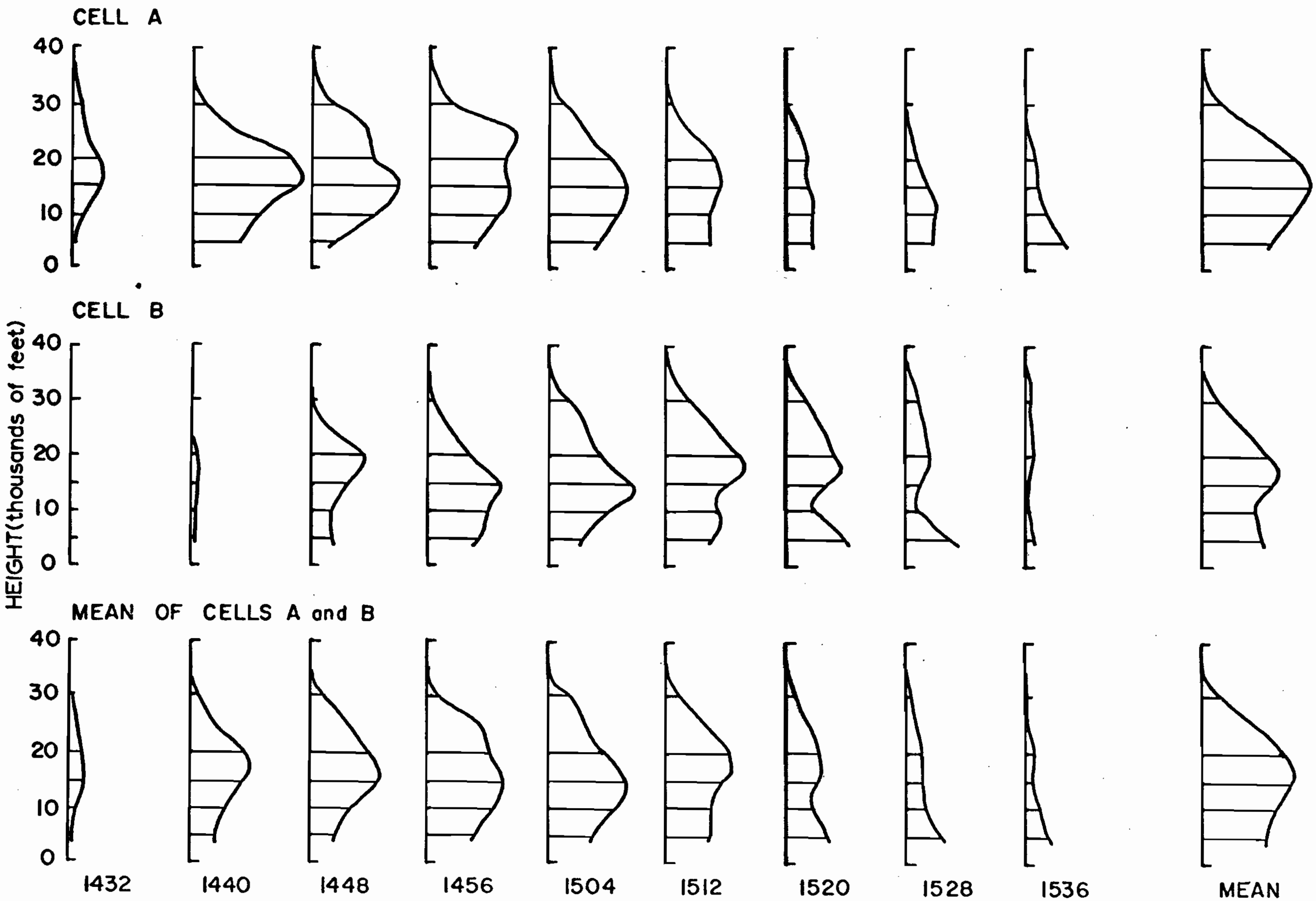

Fig. 3.15. Profiles of liquid water concentration at cores of two thunderstorm cells in Texas, 24 May 1961. Also the mean of the two cells, and the means of the series of observations. (From data given by Runnels et al., 1963b)

the updraught speed. But, the present profiles are for the total radar coverage, and the total precipitation is generally composed of many cells at different stages of development. Kessler's calculations have not been carried out with updraught speeds which vary with time, as they would during the lifetime of a real cell. In any case, without a knowledge of the way in which they do vary in nature, it is not possible to use the model in calculating the overall effect on profiles of the total precipitation in many cells.

However, there are available several radar studies of the development of precipitation throughout the lifetime of single shower cells. Runnels et al. (1963a, 1963b) have studied two isolated thunderstorm cells in Texas. They presented values of the liquid water concentration at the cores every few minutes throughout the lifetime of the cells. Profiles of these core concentrations have been drawn at the top of Fig. 3.15. Those in the top row are at 8-minute intervals during the life of the most intense cell observed that day, and those in the second row are simultaneous profiles for another cell more than 100 miles distant. In both cases, pronounced maxima develop aloft and are maintained at a fairly constant height for at least two-thirds of the cell's lifetime, finally dissipating quite quickly. Consequently, prominent maxima appear in the mean profiles for the period, shown at the ends of the rows. For both cells the maximum in the mean lies a little above 15 kft.

Although there are rapid variations in the detailed pattern, the overall pattern of development and decay of each cell is quite similar. In is interesting, therefore, to take the mean of the profiles of the two cells at each time, and this has been done in the bottom row. The maximum in these mean profiles mostly lies between 15 and 20 kft, and it varies much more slowly with time than do the maxima in the individual cells. The overall mean profile for both cells for the whole period is shown at the bottom right, and it has a definite maximum at about 17 kft.

The profiles just shown are of the liquid water concentration at the cores of cells, whereas this work is concerned with profiles of the total precipitation. However, for an individual cell, the maximum concentration should be a fair indicator of the total precipitation. Certainly, a maximum at the core generally accompanies a maximum in the total and, at least qualitatively, profiles of total precipitation may be expected to resemble core profiles. The Texas study shows that a maximum in the total precipitation at a fairly constant height is such a dominant feature in the life of a cell that a maximum appears in the mean profile. Thus, many different cells at various stages of development can be expected to produce a similar maximum aloft in the aggregate profile. It is interesting that the two widely separated cells observed in Texas showed parallel and simultaneous development, but this is not necessary for a maximum to appear in the aggregate profile. The maximum in each cell was maintained above 15 kft for at least 40 min. If at least one new cell developed every 30 min or so, a maximum would be maintained aloft in the aggregate indefinitely.

In summary, calculations by Kessler (1961) predict the existence of a maximum aloft in the total precipitation within single convective cells. Its height and value increase with increasing updraught speed. Numerous observations confirm the existence of such a maximum. In particular, observations by Runnels et al. (1963a, 1963b) show that it is sufficiently intense and persistent to dominate in profiles of an aggregate of cells. Therefore, it is not surprising that a relation exists between the height of

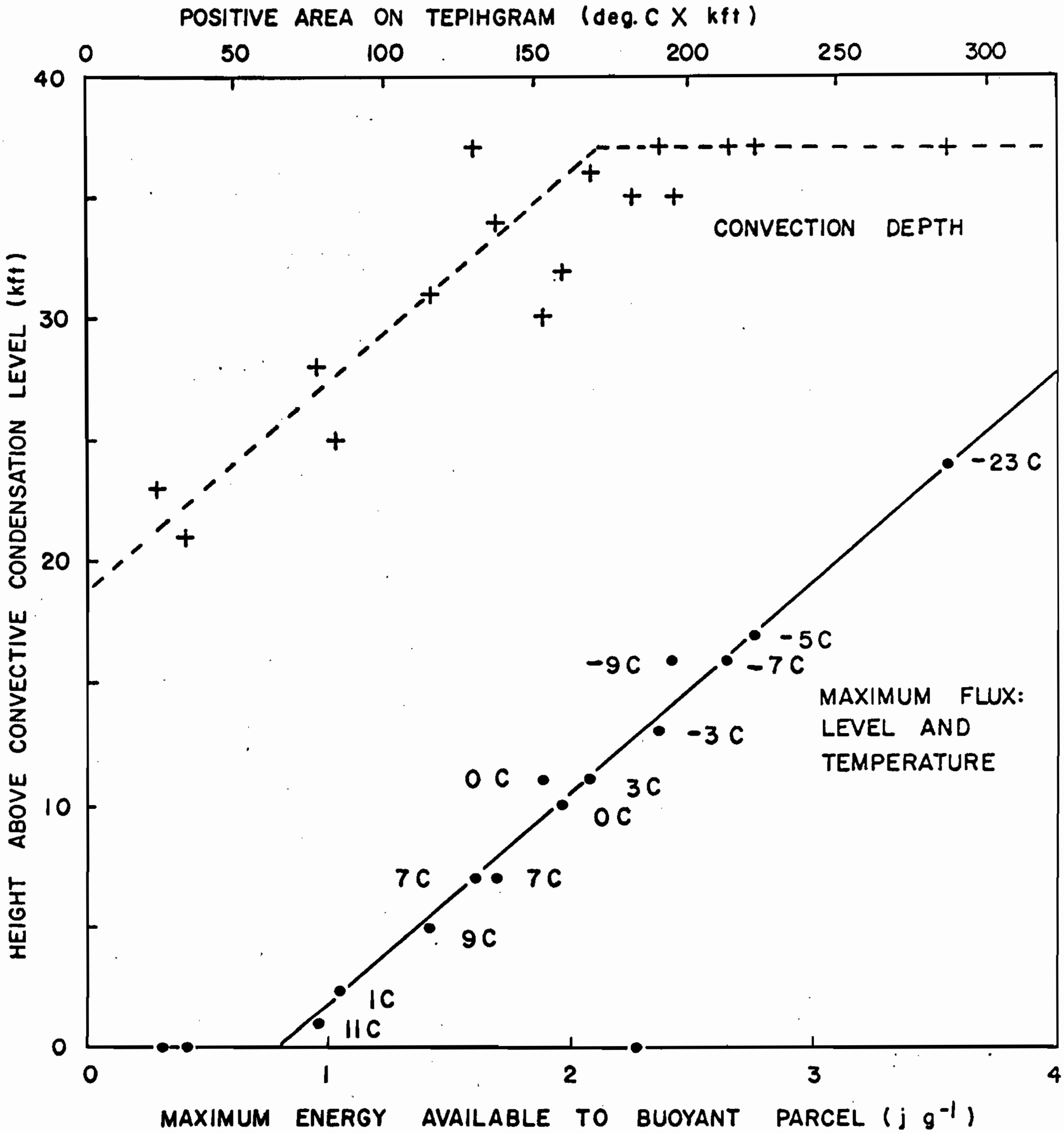

Fig. 3.16. The height of the maximum flux and the temperature of a buoyant parcel there, and the depth of convection as functions of available energy.

the maximum in flux characteristic of profiles in shower situations and the total available energy of convection.

3.5 Relation of Height of Maximum in Flux to Available Energy

Before attempting to discuss the relation between the height of the maximum in flux and the available energy, there are a few further observations to make. The relation, which was first seen in Fig. 3.6, has been re-plotted in Fig. 3.16 together with additional data. Again the abcissa is the maximum energy available to a buoyant parcel and the ordinates are heights above the convective condensation level. For each case, the spot represents the height of the maximum flux, and is annotated with the temperature of a buoyant parcel there. Although there were not many cases in which this temperature was well below OC, the relation does not appear to be sensitive to the position of the maximum with respect to the OC level. Turning attention to the crosses, these show the depth of convection between the condensation level and the level of hydrostatic equilibrium. This level of equilibrium increases with increasing height of maximum flux, but is limited by the tropopause to a maximum of 37 kft. The scale at the top of Fig. 3.16 gives the energy of the positive area on the tephigram directly in units of height (kft) x temperature difference (deg C). For example, on a day with maximum flux at 11 kft and convection depth 36 kft, the positive area was 165 (deg C.kft), and hence the mean temperature difference throughout the convection depth was about 165/36 = 4.6C.

One striking point about Fig. 3.16 is that a minimum of 0.8 j g^{-1} is required to produce any maximum at all. Kessler's (1961) calculations show that the very modest updraught of about 1 m sec^{-1} would produce a maximum at 8 kft. A 1 m sec^{-1} updraught requires 5 x 10^{-4} j g^{-1} energy and, although 0.8 j g^{-1} represents the total positive area rather than that up to the level of the maximum, the discrepancy is enormous. Thus, one wonders what factor could have been left out of the elementary parcel theory that led to Fig. 3.16. Marshall (1961) has impressively demonstrated the tremendous damping effect that large rain concentrations could have on updraughts. However, it has been emphasized that the maxima in flux are largely due to the moderate rain less than about 50 mm hr^{-1}, in which case the effective loss of buoyancy from precipitation would not amount to more than 1 deg C. But there is another load that every buoyant parcel must bear, and that is the cloud water. Since parcels may enter the cloud base with as much as 15 g kg^{-1} vapour, and 4 g kg^{-1} produces an effective loss of buoyancy of about 1 deg C, it can be seen that losses due to cloud loading may amount to almost 4 deg C. In the cases presented in Fig. 3.16 the effective loss almost invariably exceeded 2 deg C at 20 kft.

The effect of cloud loading is particularly devastating where the instability is small. In two cases, the parcel buoyancy of about 2 deg C was equalled (or even exceeded!) by the cloud loading. These were cases in which convective instability was realized by lifting a moist air mass, and it is especially in such cases that the near balance of the two quantities is of great significance. Even on the occasion of greatest buoyancy, when the cloud loading had its least effect, it was equivalent to one third of the total positive area. The attractive feature of including the cloud loading effect in parcel theory is that it is quite intrinsic. Cloud loading and buoyancy are inseparable, and even if a parcel sheds some of its cloud load it remains to be borne by succeeding parcels. Accordingly the cloud loading effect has been calculated for all the cases in Fig. 3.16, and subtracted from the total available energy to give what has been termed the

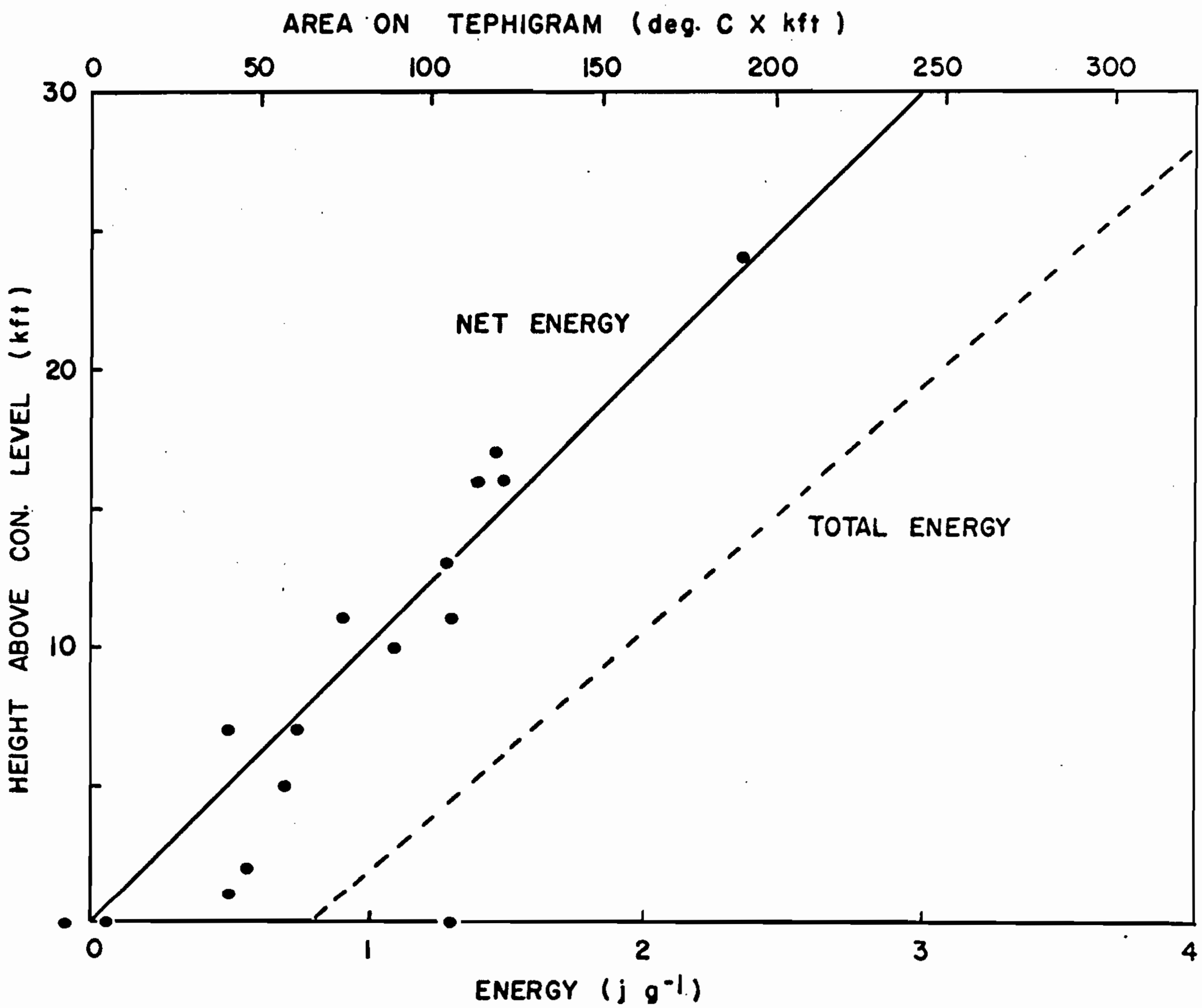

Fig. 3.17. The height of the maximum flux as a function of the net energy, that is the total energy available to a buoyant parcel less the amount expended in lifting the condensate.

net energy. Fig. 3.17 shows the height of the maximum flux as a function of this net energy. The points scatter more than previously, but they now lie on a line that goes through the origin. The new relation has been displaced from the original relation (the broken line in Fig. 3.17) by the amount of the cloud loading, and since the cloud loading is a fairly constant term the lines have nearly the same slope. Fig. 3.17 is justification for including a cloud loading term, even if only as an empirical correction.

So far, a relation has been demonstrated between the height of the maximum in flux and the positive area on a tephigram. Calculations by Kessler (1961) show that a model cell produces an accumulation of precipitation at a height which depends on the updraught speed. The observations of core profiles by Runnels et al (1963) were presented in the last section as evidence that an accumulation seen in a profile of the total precipitation arises from accumulations in one or several cells. Thus it is natural to try and relate the presently observed energy-dependent maxima to Kessler's updraught-dependent maxima, and thereby obtain an estimate of the updraught speed as a function of the available energy.

The profiles of the precipitation produced in Kessler's model have been shown in Fig. 3.14. To compare them with the present study, a cell with height H = 35 kft, and precipitation falling at 10 m sec^{-1} were chosen. Thus the first five profiles in Fig. 3.14 are respectively representative of maximum updraughts of 2.5, 5, 10, 20, and 40 m sec^{-1}. The mean updraught speed, averaged over the entire left half of the cell and 90% of the depth of the cell, is about half the maximum updraught. It is this mean updraught speed which has been related to the height of the maximum in Fig. 3.18. It can be seen that a mean updraught of 1 m sec^{-1} produces a maximum at 8 kft,

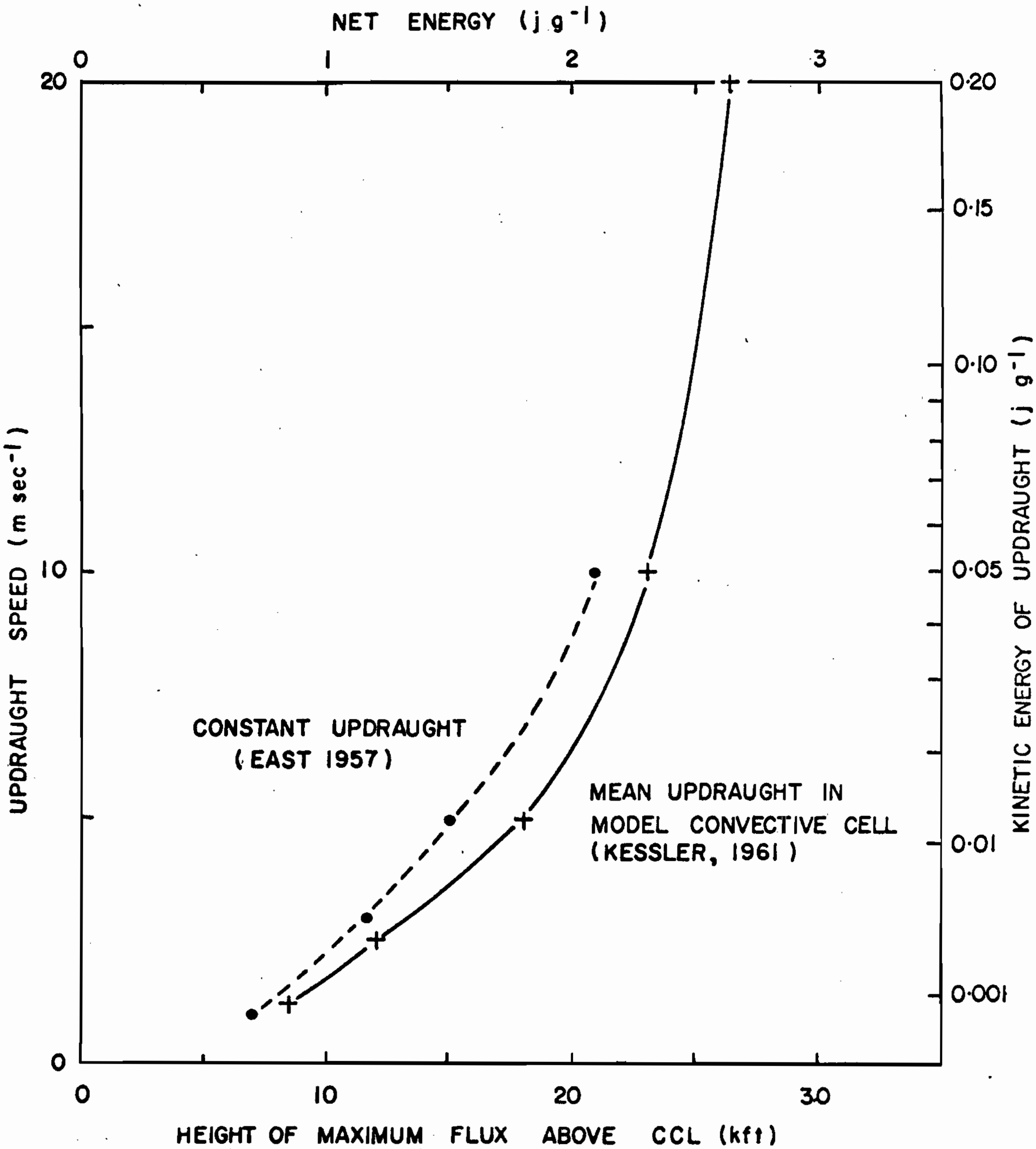

Fig. 3.18. Mean updraught speed as a function of height of maximum flux, based on work by East (1957) and Kessler (1961). Scale of net energy at top added from Fig. 3.17.

5 m sec^{-1} at 18 kft and 10 m sec^{-1} at 23 kft. To lift maxima higher than this requires a considerable increase in updraught speed, so that an extra 10 m sec^{-1} only lifts it another 3 kft to 26 kft.

In Kessler's (1961) model the cloud phase is omitted, and condensation immediately produces precipitation of constant fall speed. This defect has been remedied in later work (e.g. Kessler, 1964), but the more realistic models still produce very similar results. There is also an independent check available from work by East (1957), who was predominantly concerned with the microphysical processes in precipitation. East calculated the trajectory of a droplet growing in a 3 m sec^{-1} updraught, and showed that it would first be detected by radar about 11 kft above cloud base, a figure in keeping with observation. The calculations went on to show that the droplet reached the top of its trajectory at 13 kft and had reached the maximum stable size of 4.5 mm diameter at 9 kft. Thus, in the early stages of development, one would expect a maximum concentration of water near the level of first detection. The observations of Runnels et al. (1963) show that the maximum concentration indeed develops at about the same height that precipitation is first detected by radar (when that level is about 15 kft above cloud base, anyway). Data given by East enable one to calculate the level of detection in updraughts ranging from 1 to 10 m sec^{-1}, and these have been plotted in Fig. 3.18.

The agreement between East and Kessler is surprisingly good, suggesting that the kinematical effects and the microphysical processes in a convective cell both conspire to produce a maximum concentration at about the same level. When the maximum flux is between 15 and 20 kft, the mean updraughts range from 5 to 10 m sec^{-1}, which are entirely consistent with values observed in thunderstorms (Byers and Braham, 1949). The occasional reports of mean updraughts exceeding 15 m sec^{-1} are also consistent with occasional observations of maxima more than 20 kft above the condensation level. There is reason for believing that in the case of weak updraughts, the level of maximum concentration would fall below the level of initial radar detection of precipitation. Thus the updraughts which can maintain a maximum in flux at 7 kft are probably somewhat greater than the 1 m sec^{-1} given by the graphs. Otherwise, the updraughts in Fig. 3.18 are believed to be quite reasonable.

Now that the updraught speed has been related to the height of the maximum flux, it is possible to go the one stage further and relate it to the net available energy of convection. Fig. 3.17 gave the observed relation between the height of the maximum in flux and the net energy, or the energy of the positive area less the cloud loading effect. A scale of net energy can thus be added alongside the scale of height of maximum in Fig. 3.18, and this has been done at the top. A tephigram could now be used to estimate the mean updraught speeds on a given occasion.

The fact that it has been possible to relate an updraught speed to tephigram-derived energy raises the interesting point of the significance of the energy of the positive area. Although there are fairly successful hail-size forecasting techniques (Foster and Bates, 1956) which are based on a literal interpretation of positive area in terms of updraught speeds, it is generally regarded as a rather crude measure of instability. Its significance probably depends a great deal on the characteristics of the systems it is used to explain. Almost all the storms in the present study could be accounted for quite reasonably by convection from the surface, and it is in such storms that positive area is most meaningful. Browning and Ludlam (1962) have produced a beautiful detailed analysis of

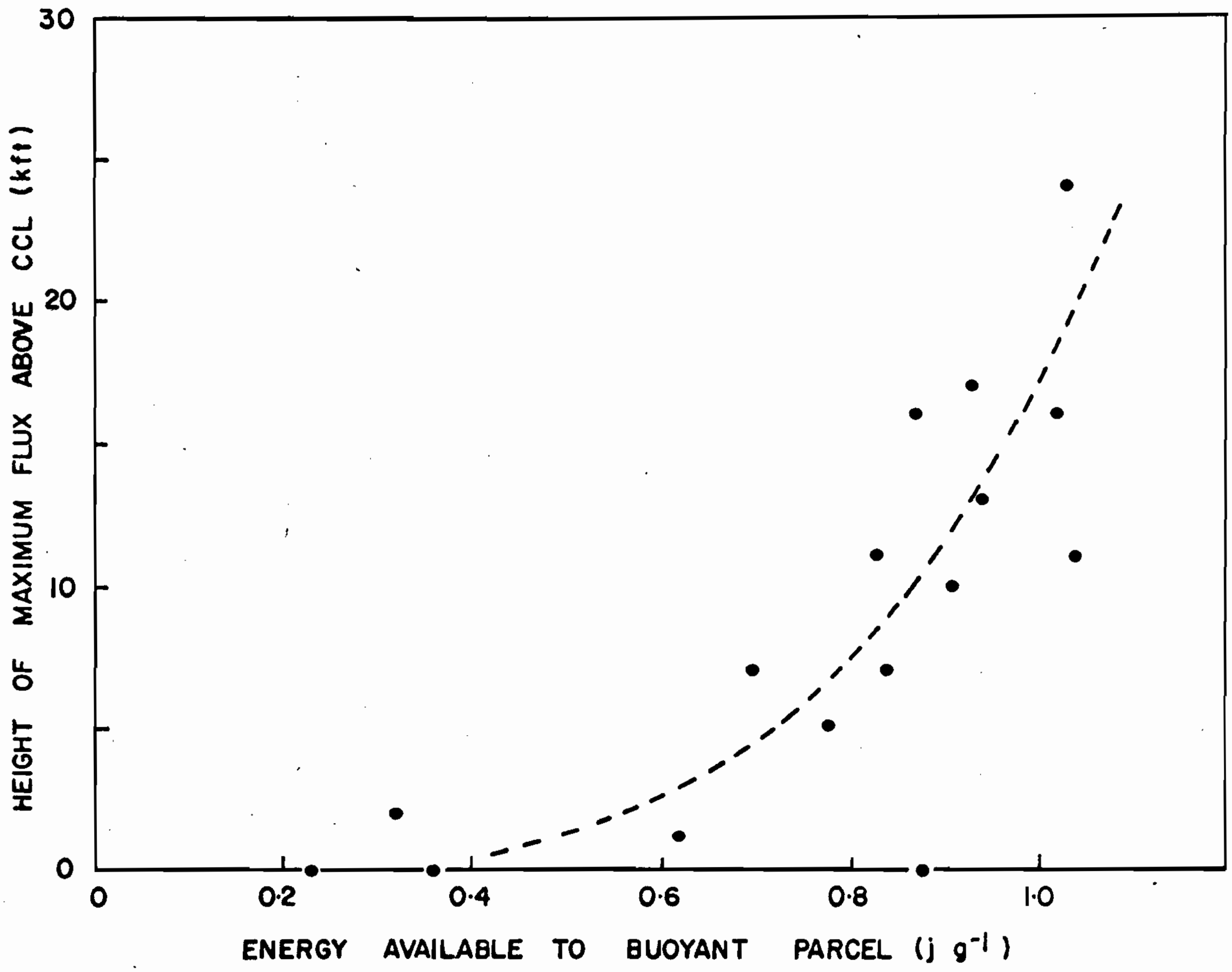

Fig 3.19. Relation of height of maximum flux to the energy available to a buoyant parcel only up to 20 kft.

a severe travelling storm which could not be accounted for in this way. They considered that both the descent of potentially cold air and the updraughts produced by the upward deflection of low level horizontal winds were major factors. However, the severe travelling storm is probably a much more complex system than the majority of thunderstorms. The success of the present study in using positive area is really the best evidence that the storms studied were relatively simple.

Even if a storm is the simple product of convection from the surface it is difficult to interpret the positive area rigorously. Elementary parcel theory shows that the energy of the positive area is the kinetic energy acquired by a parcel in its buoyant ascent to the top of the storm. But it would be interesting to know what effect energy available at the top of the storm has on the circulation much lower in the storm. Fig. 3.19 is strongly suggestive of the fact that it has a considerable effect. It shows a plot of the height of the maximum flux in the sixteen shower cases against the amount of energy available only up to 20 kft (that is, positive area below 20 kft). The relation is much weaker than in the similar plot of height against the total energy available throughout the depth of convection, Fig. 3.16. Even though all but one of the maxima lie below 20 kft, the energy available above 20 kft apparently has a strong influence on them. On a similar basis, the energy available above 30 kft also has some effect, though a much smaller one, on the circulation at lower levels.

Since it is apparently the total energy which determines the general intensity of convection, it is reasonable to compare it with the actual energy of the updraughts. Returning to Fig. 3.18, a scale showing the kinetic energy of the updraught has been added at the right side. With net energy of 0.5 j g^{-1} the maximum forms at 5 kft in an updraught of about

1 m sec^{-1}, and the kinetic energy of such an updraught is 5×10^{-4} j g^{-1}. This is a fraction 10^{-3} of the net energy. As the net energy increases this fraction increases, so that for a net energy of 1.8 j g^{-1} it is 10^{-2} and, extrapolating a little, for 2.7 j g^{-1} it is 10^{-1}. The kinetic energy of the updraught is roughly proportional to the fourth power of the net energy. Or to put in another way, the mean updraught speed is given by the square of the net energy rather than the square-root suggested by simple theory. In a review of bubble theory, aufm Kampe and Weickman (1957) show that the limiting upward velocity of a bubble is proportional to the square root of its temperature difference from the environment, and cite measurements of the rate of rise of cumulonimbus tops in confirmation. The present work indicates that the mean updraught velocity is proportional to the square of the temperature difference. Although bubbles emerging from the tops of cumulonimbus are certainly different from mean updraughts at the lower levels, the fourth power discrepancy is rather substantial. It would certainly be nice to reconcile this difference.

It should perhaps be emphasized that the updraughts just considered are mean updraughts. There are undoubtedly cores with updraught speeds several times the mean. Donaldson (1961b) has given median profiles of core reflectivities for different categories of storm severity. It is possible to estimate from his data that profiles with a maximum intensity 13 kft above cloud base would just be capable of producing ½ in diameter hail. Assuming that Donaldson's core profiles of New England storms can be compared with the data of the present study, and that the hail was produced in an updraught comparable to its fall speed, speeds of at least 20 m sec^{-1} would be present on occasions with net energy of 1.3 j g^{-1}. The mean updraught in these circumstances would not be more than about 4 m sec^{-1}.

Enough has been said to indicate that precipitation profiles probably can contribute to a more complete understanding of the way in which shower structure is determined by the conditions of instability in the atmosphere. The few calculations that have been made in this section are just a beginning.

3.6 Shower Structure from Profiles

In the preceding sections, updraught speeds in convective storms have been related to the energy of buoyancy which produces them. This was done by studying precipitation profiles in the light of other research into shower structure. It must be remembered that the resulting relations have been derived only for the initial stages of a convective storm. There are several reasons for this. For one thing, the instant in a storm for which a representative profile was chosen was the instant when a maximum in flux had just developed at the greatest height observed on that day. These maxima had almost always only just formed, and so the profiles are representative of the initial stages of a storm. Since it is conceivable that storms modify their surroundings during their development, the upper air soundings with which the profiles were compared were also probably more relevant to the initial stages. Finally, East's (1957) calculations were devoted to explaining the formation of the initial radar echo from a developing storm, rather than any accumulation during a storm.

Nevertheless, there is reason to hope that the height of the maximum flux continues to indicate the general level of convection throughout the life of a convective storm. The line of showers of 2 July twice produced maxima, each of which took over two hours to descend from 30 to 15 kft. This period is surely much greater than the lifetime of any of the individual cells. In fact, one pictures series of cells such as those observed

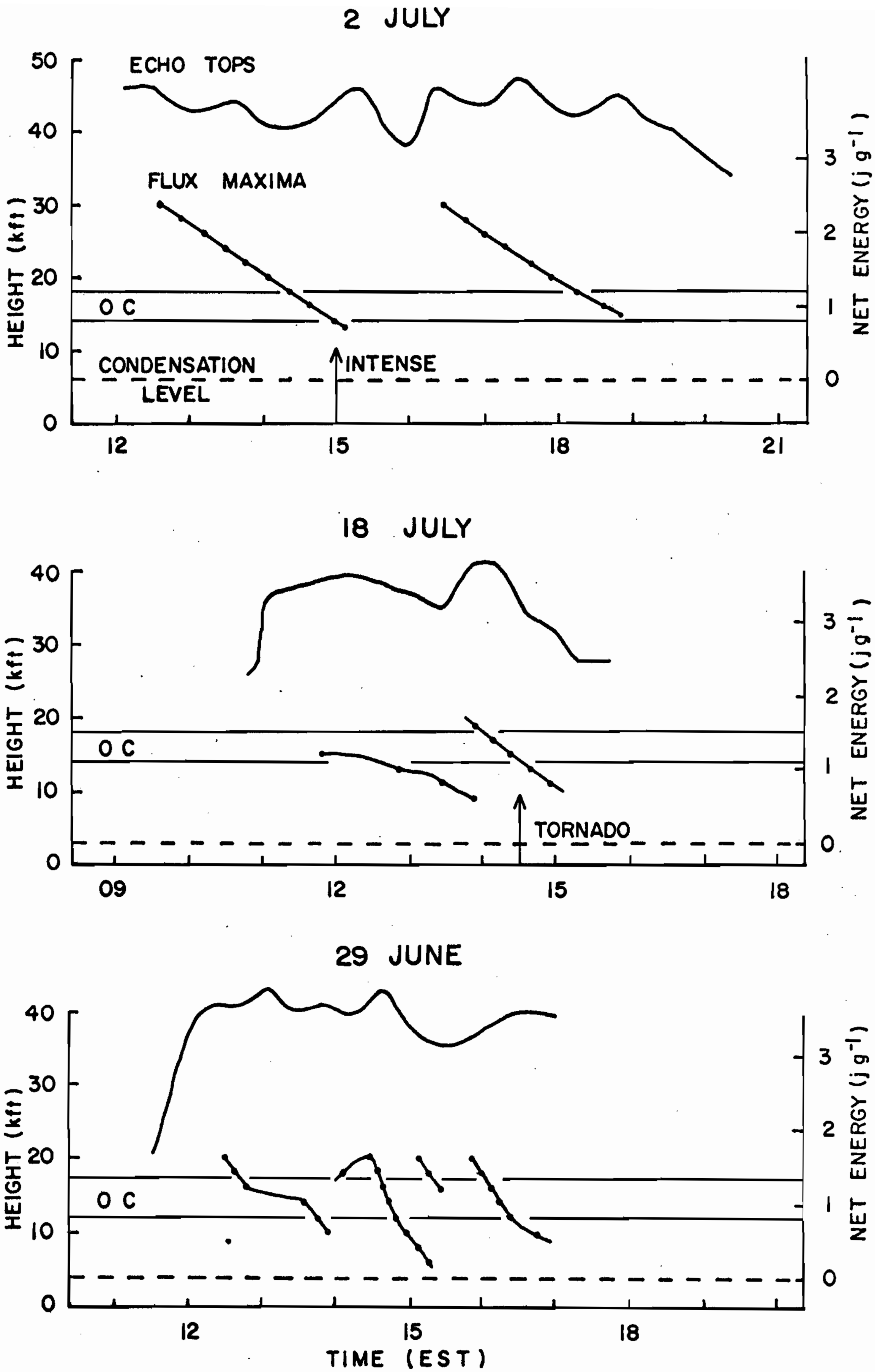

Fig. 3.20. The variation with time of the height of maximum flux for three storms in 1963.

by Runnels et al. (1963), each producing a maximum throughout the initial two-thirds of its lifetime, but with the maxima successively forming at ever lower heights. If this is the case, then the height of the aggregate maximum still indicates the general intensity of convective activity.

There is even reason for thinking that the height of the maximum in an individual cell also continues to depend on the updraught speed throughout the life of the cell. Kessler's (1961) model maxima remain at about the same height throughout their formation and development in a constant updraught. If the updraught were changed, the trajectories of the precipitation particles would change and the maximum concentration would vary in response.

If the height of the maximum in the profiles does continue to depend on the updraught speed and the available energy, then it is a most valuable monitor of these quantities during the life of a storm. It is interesting to look at the profiles in these terms. In Fig. 3.20, the heights of the maxima in flux have been plotted as they vary in time. The data were taken from the sets of profiles presented in section 3.2, and are for the three most intense storms of the season. A scale against which to measure the net energy of a storm system has been taken from Fig. 3.17 and added at the right side of the diagram.

Perhaps a few words should be said about the term "system". In the case of 2 July, the line of showers was most uniform in character along its 150-mile length. An examination of the radar maps suggests that the profiles for any short segment of the line would have been similar to those for any other. It seems reasonable to think of the whole line as a system. In the other cases the system was more difficult to identify, but it was most likely a group of showers. Such a group might typically be contained within an area of 1000 mi^2, and there might simultaneously be several such relatively independent groups. The frequent maxima of 18 July and especially 29 June (Fig. 3.20) which seemed to be associated with separate groups rather support this view. However, it does need some confirmation, and this would require profiles of individual groups.

Returning to Fig. 3.20, 2 July will be singled out to show the value of profiles in the analysis of convective storms. Both maxima formed when the system had net energy of 2.4 $j\ g^{-1}$. The spots on the trajectories are every 2 kft or 0.2 $j\ g^{-1}$. Since the maxima descended at 6.5 kft hr^{-1} the net energy was decreasing at 0.65 $j\ g^{-1}\ hr^{-1}$. The net energy is made up of the total energy of the positive area less the cloud loading effect. Thus either the energy of the positive area was decreasing or the cloud (and precipitation) loading was increasing, or both were occurring.

The positive area can be reduced either by a decrease in the potential wet-bulb temperature of ascending parcels, or by an increase in the environment temperature by subsidence. Calculations show that the observed rate of decline of the net energy can be accounted for by a surface potential wet-bulb temperature (θ_w) decrease at the rate of 0.8 deg C hr^{-1}. The system formed at about 1200 EST in a region where θ_w = 24.5C, and the observations would be accounted for by θ_w = 22.5C in the region where it dissipated at 1500 EST. The Montreal region is unfortunately rather sparsely covered with meteorological stations, and it is only with great hesitation that one draws conclusions which properly require a meso-meteorological network. Nevertheless, the available evidence suggests that θ_w was indeed rather less in the St Lawrence Valley where the system dissipated than in the rather hilly source region to the NW, and that the difference was of the right order. Further, θ_w in the region where the storm reformed at 1630 EST was certainly higher than in the region where it dissipated at 1500 EST, and again the difference was just about right to account for the observations. These differences in θ_w are fairly reasonable in relation to the geography of the Montreal region, and thus it is entirely possible that they could have accounted for the behaviour of the storm.

Alternatively, the required decrease in positive area could have been produced by subsidence of the environment at the rate of 15 cm sec^{-1}. However, if this were in compensation for the storm updraughts it would decrease as they decreased in response to the decreasing energy of the system. This would lead to a decreasing rate of decline in the storm intensity, rather than the uniform rate that was observed. Thus subsidence does not seem to have been a major factor in this particular case. Even large scale dynamical subsidence is not probable, for the storm reformed an hour after its dissipation at 1500 EST with greatly enhanced net energy.

The other possible cause of a decrease in net energy would be an ever-increasing cloud and precipitation load. The relations that have been developed in this work can be used to estimate mean updraught speeds, and these can be used to estimate the cloud load. Unfortunately, just as in the case of subsidence, the calculations show that the cloud loading effect would probably decrease with decreasing updraughts. Without making a rather doubtful assumption in the calculations it is not possible to account for the steady rate of decline in the storm intensity.

The most likely explanation for the development of the storm of 2 July thus appears to be a variation in the potential wet-bulb temperature of the air which fed the storm. Because of the scarcity of surface data, one must necessarily accept this explanation with reservation. However, this example was presented not so much to provide an explanation of the storm as to illustrate the power of profiles in the analysis of convective storms. If profiles do indeed indicate the degree of convective activity in a storm, then they will be a valuable aid in studying the energy budget of the storm.

The heights of the storm top (or the radar echo top) have most frequently been used as indicators of storm activity. Fig. 3.20 shows the variations with time of the echo tops, as well as the variations of the maxima in flux. It can be seen immediately that the usefulness of echo tops as an indicator is rather limited in comparison with profiles. It is interesting to note that on 2 July and 18 July the birth of maxima tended to be accompanied by an upward surge in echo tops. The really notable surge on 18 July preceded the tornado by 30 minutes. On 2 July, surges seemed to occur at the formation of a maximum, as it descended through 23 kft and as it dissipated. While echo tops provide a valuable supplement to profiles, they are probably of limited use in themselves.

It is significant that it has been possible to determine so precisely a fundamental relation (Fig. 3.6) between the height of the maximum in flux and the available energy of buoyancy. The fact that it has, strongly suggests that the amount of available energy limits the degree of storm activity, that all storms but one reached this limit at some time during their life, and that the line specifies the limit. The one exception is 22 July, and it is natural to try and determine why it was exceptional. The most notable difference between the synoptic conditions of this day and any other was the complete absence of wind shear between 10 and 30 kft. On every other day this shear was at least 10 knots. Possibly because of this absence of wind shear, the showers failed to cluster into the usual groups and remained isolated and relatively small. Thus entrainment of environmental air could have prevented them from reaching their full potential. Ludlam (1963) suggests that the role of wind shear is to tilt the updraughts so that they are not burdened with the precipitation they produce. This would also account for the weak showers of 22 July. It is interesting to note that, though the profiles clearly indicated that the showers failed to reach their potential, the echo tops at 40 kft would not have given the same indication.

Almost the whole of this chapter has been devoted to the discussion of the upper maximum in flux which is characteristic of shower profiles. This maximum has been shown to have valuable quantitative significance as an indicator of convective activity, and should therefore be of great value in studying the energy budget of storms. This significance was certainly not anticipated by the author, and in many ways its discovery distracted the course of this work from other potentially more profitable avenues. Clearly, the real value of precipitation profiles lies in their quantitative interpretation, and not even a beginning has been made on this. They should lead to a knowledge of the water budget of a storm far more detailed than has been possible before. When this knowledge is added to the rather unexpected knowledge of storm dynamics which they also give, profiles offer exciting new prospects for further research into the nature of convective storms.

4. PROFILES OF CONTINUOUS PRECIPITATION

Continuous precipitation is essentially the product of large-scale almost horizontal convection. It may extend over many hundreds of miles and be of many hours duration. Updraughts limited to a few tens of cm sec^{-1} often take a few hours to produce precipitation particles large enough to fall. The precipitation is considerably more uniform in the horizontal than are showers, though it is just as variable in the vertical. Vertical radar cross-sections in situations of continuous rain commonly show a region of snow separated from the rain below by a bright band at the melting level (see, for example, Fig. 2.2). This is one of the most striking features in radar observations of continuous precipitation, and has received a great deal of attention, particularly in an effort to determine the overall effect of the melting process on the precipitation rate. Radar observations of the region of snow frequently reveal long trails of snow falling from small cells at the top of the storm. They are actually convective cells in which the convection results from the release of latent heat of sublimation by growing ice crystals.

Convective snow generating cells most frequently occur in air which is hydrostatically stable. But large-scale convection can also produce convective cells through the realization of convective instability. Precipitation profiles in such cases may be indistinguishable from the profiles of showers. In fact, a few cases of convective instability were included amongst the cases of showers in the last chapter (Fig. 3.5). The large scale convection which produces the convective instability may simultaneously be producing continuous rain, resulting in a pattern of continuous rain with embedded showers.

This chapter will begin with a brief discussion of the place of CAPPI techniques in the study of continuous precipitation. This will be followed by a close study of the profiles of a particular rainstorm. Finally, the profiles of several continuous storms will be compared and discussed.

4.1 CAPPI Observations of Continuous Precipitation

Much of the present knowledge of continuous precipitation has been obtained from vertical beam radars, in which the vertical pattern of precipitation is continuously recorded during the passage of a storm. In many ways they are especially well-suited to this purpose with their great sensitivity and high resolution. However, they do sample only a tiny pencil of the atmosphere, and it is often not possible to relate precipitation processes along a vertical line. This is especially the case with snow, which may reach the earth's surface as much as 100 mi from the point where it was generated. If the wind direction varies with height it is not even possible to study the precipitation process in a vertical plane. The other deficiency of the vertical beam radar is that it provides no knowledge of the areal distribution of precipitation other than what may be inferred by treating the records as a sample. This information can only be obtained from CAPPI maps. If these maps are complete with contours of precipitation intensity, then they form a most valuable means of studying the processes of continuous precipitation. It is then possible to measure total flux of precipitation over a large area at each of several constant altitudes. In this way the measurements will reflect the true growth of the precipitation, and will not depend to any extent on the particular three-dimensional paths that precipitation follows as it falls through the wind field.

It is appropriate to give a brief review of some of the work that has been done on continuous precipitation. An excellent picture of the complete three-dimensional structure of a winter cyclone has been synthesized by Boucher (1959) from observations of many storms with a vertical beam radar. Several composite vertical cross sections of the precipitation pattern are presented and they show all the main features commonly observed in continuous precipitation. This study emphasized the potential value of vertical beam radar observations to the synoptic meteorologist, and Wexler (1959) has discussed suitable methods of presentation of such data. He found that individual vertical soundings often contained too much detail, and preferred to summarize them over 30-minute periods. These summaries were quite similar to the present area profiles, except that the abscissa was duration rather than area.

The limitation of observations to a vertical cross section was keenly felt in the study of snow generating cells, which are fairly small and occur at a fairly constant altitude. Accordingly Langleben (1956) made the first use of CAPPI in a study of these cells and their trails, and at the same time made a few measurements of the total area of precipitation at each of several altitudes. Hitschfeld and Gunn (1958) also used CAPPI maps to measure areas, and presented the first vertical profiles of the total area for both continuous precipitation and showers. Their presentation contained a qualitative breakdown of the precipitation into intensities, but this was rather limited. At about the same time Boucher (1958), in a study of the value of CAPPI maps in continuous precipitation, also gave what were effectively profiles of total area at frequent intervals throughout entire winter storms.

Thus, there have been many studies using high resolution vertical radar soundings of the precipitation intensity. At best these can only give an idea of the areal coverage of precipitation on a statistical basis. The

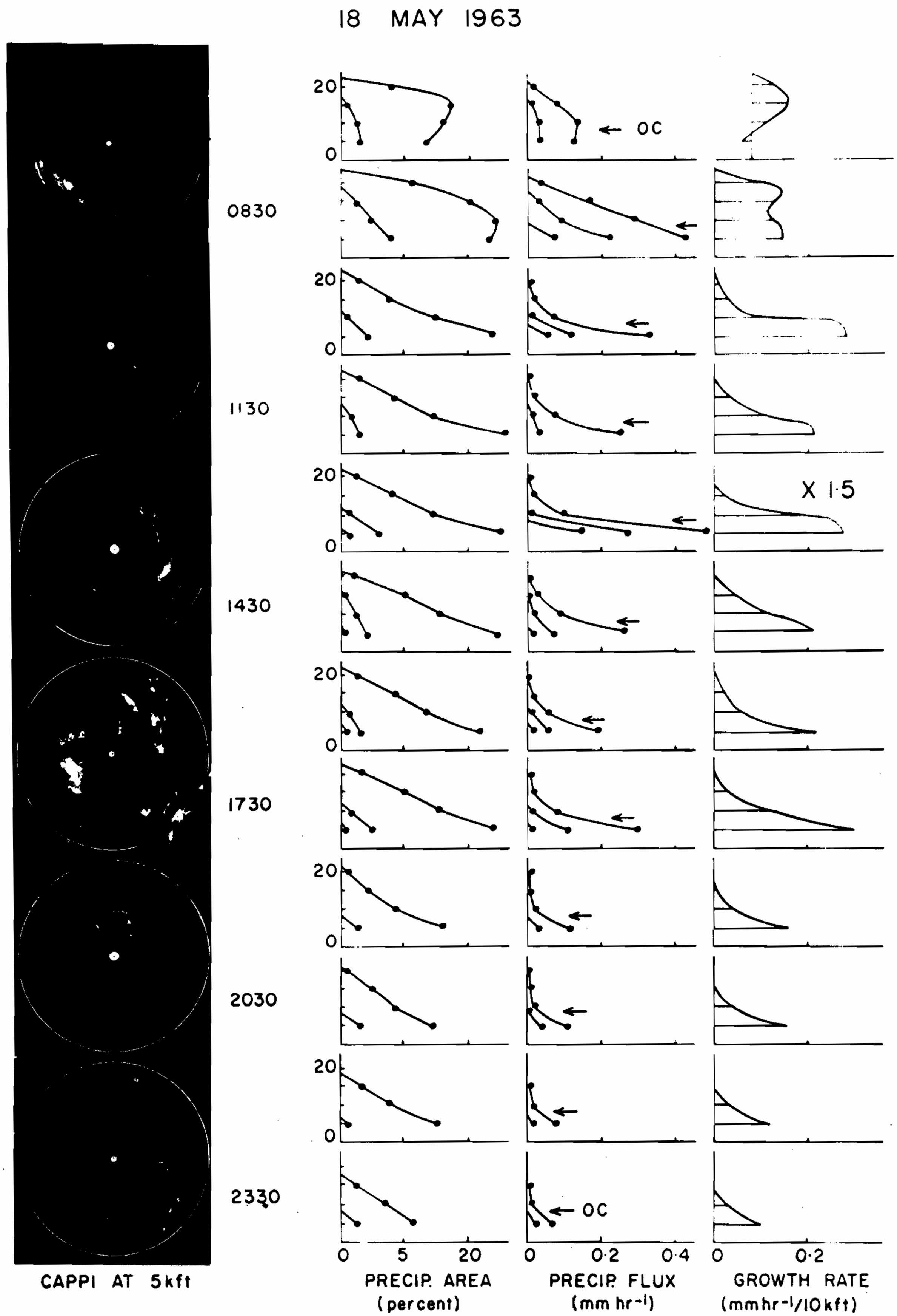
18 MAY 1963
0830
1130
1430
1730
2030
2330
OC
X 1·5
CAPPI AT 5kft
PRECIP. AREA (percent)
PRECIP. FLUX (mm hr⁻¹)
GROWTH RATE (mm hr⁻¹/10 kft)

Fig. 4.1.

advent of CAPPI led to a few direct measurements of the areal coverage of precipitation at each of several heights, but these have not contained much useful information about intensity. The present profiles give both area and intensity of precipitation as a function of height. They fill a need for a quantitative summary of large areas of precipitation.

4.2 A Continuous Rainstorm in Profiles

The storm that has been chosen for detailed study was a fairly modest one which moved from the SW to the NE at about 30 knots. It was originally a small independent low pressure area, but it was carried through Montreal in the circulation of a more vigorous low 1000 mi NE, and eventually weakened to become a trough of low pressure. From the present point of view, one of the advantages of this particular storm is that the melting level was at about 8 kft, midway between the 5- and 10-kft sampling levels. Thus the measurements at these two levels should not contain appreciable contributions from the bright band, and it will be possible to compare them with other previous measurements above and below the bright band.

Profiles and CAPPI maps at frequent intervals throughout the storm are shown in Fig. 4.1. CAPPI maps at 5 kft are given every 3 hours, and profiles of area, flux and rate of growth every 1.5 hours. The contours in the profiles are at 0.2, 3.2 and 50 mm hr^{-1} (attenuation-corrected values). The most notable thing about the profiles is the fact that apart from the initial 3 hours they do not vary much with time. After 1000 EST all the profiles show a steady increase with descent.

At the time of the first profile, 0700, there is considerably more precipitation at upper levels than below. The rather structureless precipitation was advancing from the SW, and at 5 kft the leading edge was 60 n mi distant while at 15 kft it was only 40 n mi away. Then the total area decreased from about 14% at 15 kft to 10% at 5 kft. This overhang is a feature of the initial stages of most continuous rainstorms. Although the total area increases with height, in this case, the area of moderate precipitation remains fairly constant or decreases with height, as shown by the inner area profile. Accordingly the total flux does show a slight maximum at 10 kft but then decreases steadily above 10 kft. The rate of growth shows a maximum at about 15 kft, and below this the growth declines, eventually becoming zero at 7 kft with evaporation beneath. By 0830, the precipitation is about 20 n mi from Montreal, and there is no longer any evaporation. In fact the rate of growth is constant over the entire layer from 18 kft down to 5 kft. At 1000 there has been a great decrease in the area and flux at and above 10 kft, although those at 5 kft have remained constant. Whereas previously the total flux at 5 kft was about 1.5 times greater than that at 10 kft, now it is 5 times greater. This change is also reflected in the rate of growth profiles which show much lower growth rates in the upper levels and much greater rates below. After 1000 the profiles remain very similar until about 1800, when the rain is beginning to move away to the NE, and they then gradually decline.

It is interesting to look at the period from 1000-1800 more closely, and in particular to compare the precipitation at 5 kft and 10 kft. The total area at 5 kft is between 2.3 and 3.5 times greater than that at 10 kft, with an average of about 2.7. The total flux is between 2.9 and 5.2 times greater, with an average of 4.2. This average difference in flux from 2 kft above the melting level to 3 kft below has been compared with those in a few published records of vertical beam radar soundings (Boucher, 1959; Wexler, 1959). These soundings show an average reflectivity difference between the corresponding levels of about 10 db or a factor 4 in rainfall

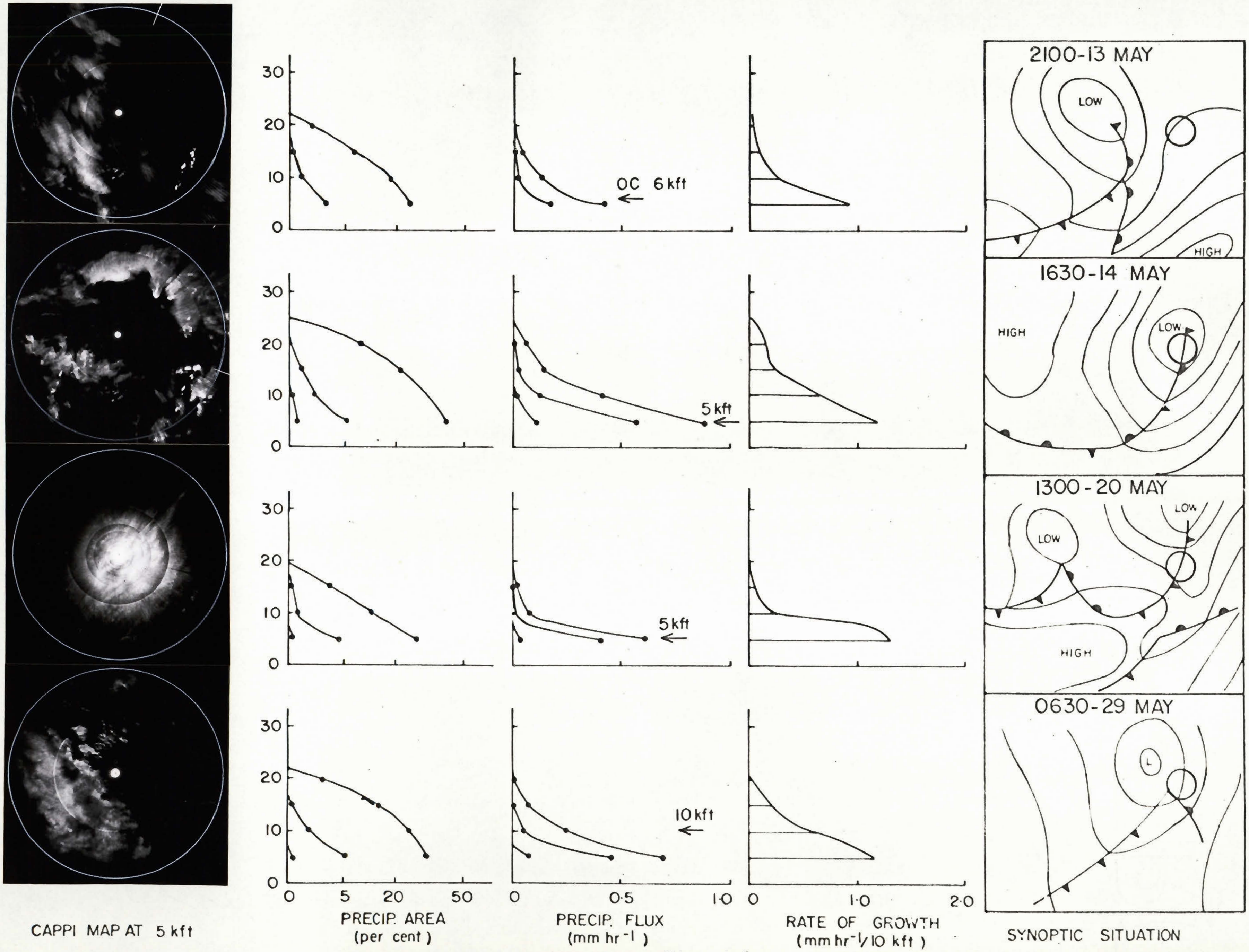
2100-13 MAY
LOW
HIGH
1630-14 MAY
HIGH
LOW
1300-20 MAY
LOW
LOW
HIGH
0630-29 MAY
L
OC 6 kft
5 kft
5 kft
10 kft
30
20
10
0
0
5
20
50
0
0·5
1·0
0
1·0
2·0
CAPPI MAP AT 5 kft
PRECIP. AREA
(per cent)
PRECIP. FLUX
(mm hr⁻¹)
RATE OF GROWTH
(mm hr⁻¹/10 kft)
SYNOPTIC SITUATION

Fig. 4.2.

rate, which is very similar to the present figure. It should be emphasized that this figure was obtained by averaging the published vertical reflectivity profiles over the total duration of the observation. The similarity of the two results is an indication that the duration of precipitation of a certain intensity observed at a point is statistically proportional to the areal coverage of that precipitation. Apparently it would be reasonable to interpret duration in the records of vertical beam radars as area.

During the last stages of the storm the amount of precipitation at and above 10 kft dwindles more quickly than that at 5 kft. The total flux at 5 kft is an average 6.0 times greater than that at 10 kft, compared with the factor 4.2 during the middle stages. With a little experience the various stages during the passage of a storm can be readily identified.

4.3 The Pattern of Profiles in Continuous Precipitation

In the storm examined in the last section a long period was observed in which the profiles did not vary much. This is quite typical of continuous precipitation situations, and consequently the profiles of several such situations are rather more easily compared than are the profiles of shower situations. Eight continuous rain storms have been chosen from the summer of 1963, and they are compared in Figs. 4.2 and 4.3. At the left of each row is a 5-kft radar map, with a range marker at 80 n mi, showing all the precipitation exceeding 0.2 mm hr^{-1}. The next two columns show area and flux profiles for the region between 20 and 80 n mi, with individual curves for the precipitation exceeding 0.2, 3.2 and 50 mm hr^{-1} respectively. The fourth column shows rate of growth profiles, and since updraught speeds are generally much less than the precipitation fall speeds they may fairly be interpreted as the rate of growth. At the right of

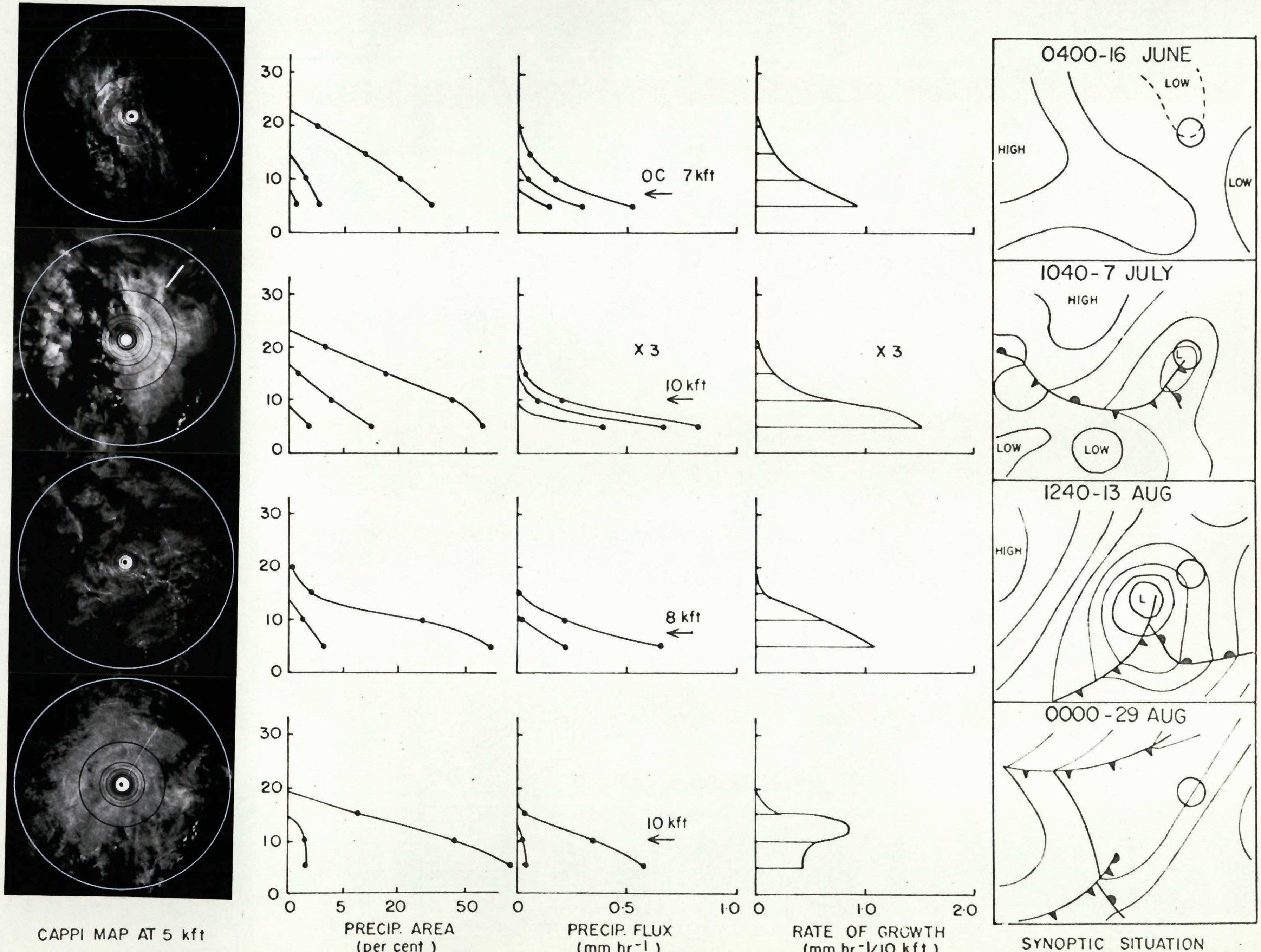
0400-16 JUNE
LOW
HIGH
LOW
1040-7 JULY
HIGH
L
LOW
LOW
1240-13 AUG
HIGH
L
0000-29 AUG
OC 7 kft
X 3
X 3
10 kft
8 kft
10 kft
30
20
10
0
0
5
20
50
0
0·5
1·0
0
1·0
2·0
CAPPI MAP AT 5 kft
PRECIP. AREA
(per cent)
PRECIP. FLUX
(mm hr⁻¹)
RATE OF GROWTH
(mm hr⁻¹/10 kft)
SYNOPTIC SITUATION

Fig. 4.3.

each row is a sketch of the synoptic situation. The circle on these maps is the 80 n mi circle that also appears on the radar maps. The instant for which a storm is compared is that at which the greatest flux was measured at 5 kft. This moment is usually soon after the beginning of the steady period that was noted in the example of 18 May, and is normally fairly representative of the whole of that period.

The most notable thing about profiles of different continuous rainstorms is their great similarity. Thus all the area and flux profiles of Figs. 4.2 and 4.3 show a steady increase with descent, and only one of the rate of growth profiles (29 August) fails to show the same trend. Thus most of the precipitation in a continuous storm is in the lower layers. Only on 14 May is there any significant amount of precipitation at 20 kft, and the flux at 15 kft is typically only one-tenth of that at 5 kft. Almost all the growth occurs below 15 kft at an ever-increasing rate, and more than one-half of the total flux at 5 kft is usually generated below 10 kft. The CAPPI maps show generally similar continuous precipitation, although there may have been a few convective cells embedded in the continuous precipitation of 14 May.

One thing worth some discussion is the possible influence of the melting level on the flux profiles. It is not surprising that the melting level cannot be picked out from the flux profile even when it coincides with one of the sampling levels. The example of Fig. 2.2 showed that the resolution of a 1° radar beam is so poor at 80 n mi that the detail of the bright band is completely lost. In fact it can barely be resolved beyond 40 n mi, that is over 80% of the sampling area. Nevertheless one would expect it to enhance the flux at a sampling level with which it coincides, but with the possible exception of 29 August this is not at all apparent.

The eight cases and the example studied separately (18 May) have been analyzed to try and detect bright-band effects. They were divided into three groups according to the melting level, and the fluxes at 5 and 10 kft were studied for each group. For those cases in which the melting level was at 5 or 6 kft the flux at 5 kft was an average 3.7 times greater than that at 10 kft. When the melting level was at 7 or 8 kft the factor was 3.3, and for 10 kft it was 2.6. Vertical radar soundings show that the rate of growth is generally greater in the region of snow than rain. Growth by a factor 3.7 in 5 kft (melting level 5 kft) is quite appropriate to snow, and a factor 2.6 (melting level 10 kft) is similarly appropriate to rain. Thus there is not much evidence of enhancement by the bright band in these cases. Further the growth by a factor 3.3 (melting level 7 kft) is suitably intermediate. It is just possible that there was some enhancement of the flux at 10 kft on 29 August due to the bright band, but on other days its effect is difficult to detect.

A final point to make about the profiles of Figs. 4.2 and 4.3 is that they are much more characteristic of the radar pattern than the synoptic situation. Continuous precipitation may be produced in the general circulation of a cyclone, or at a warm front, a cold front, an occlusion or a trough of low pressure. The radar pattern in any one of these cases is probably indistinguishable from that in any other, and the profiles are likewise indistinguishable. The profiles effectively identify the precipitation character irrespective of the particular synoptic feature which produced it.

Now that profiles from several continuous storms have been seen it is worth looking at their value. There is no doubt that their resolution leaves much to be desired when compared with the records of a vertical beam radar. This sacrifice is the inevitable consequence of extending the sampling area from a vertical pencil to an area. A suitable compromise must be chosen between resolution and sampling area. For instance, the bright band would still be resolved in profiles taken over the area within 30 n mi of the radar, but this is only 15% of the sampling area used in the present work. It is worth noting that in three of the eight cases in Figs. 4.2 and 4.3 a vertical sounding would have shown nothing. The profiles for the area out to range 80 n mi already showed a fully developed continuous rainstorm. This demonstrates that there is at least a considerable operational need for profiles of the precipitation over a fairly large area.

5. PROFILES IN SYNOPTIC METEOROLOGY

Radar weather maps have been used by synoptic meteorologists for many years, but these maps have never really exploited the potential of radar. The synoptic meteorologist attempts to follow and forecast the atmospheric convection which may lead to the formation of precipitation. The pattern of the precipitation is largely determined by the pattern of the convection which produces it, and the analysis of the precipitation will greatly strengthen the meteorologist's analysis of the convection. The precipitation pattern is a three-dimensional one and yet the meteorologist commonly only has two-dimensional knowledge of it. In many ways the missing vertical dimension is the most important to the synoptic meteorologist. At the most he may know the vertical extent of the precipitation, but he normally knows nothing of its distribution with height. The profiles which have been introduced and studied in this work provide a knowledge of this distribution.

This chapter will open with a discussion of the place of profiles in synoptic meteorology, drawing on the results described in the previous two chapters. The rest of the chapter will be devoted to a discussion of possible techniques of transmission and presentation of profile data.

5.1 Characterization of Precipitation by Profiles

The characteristics of the two types of precipitation, showers and continuous, have already been discussed separately in some detail. In this section, profiles of the two types will be presented again for comparison. Although the two basic types of precipitation appear to be well defined they can occur simultaneously. In fact the two basic types of precipitation, when occurring separately, do not account for more than one half

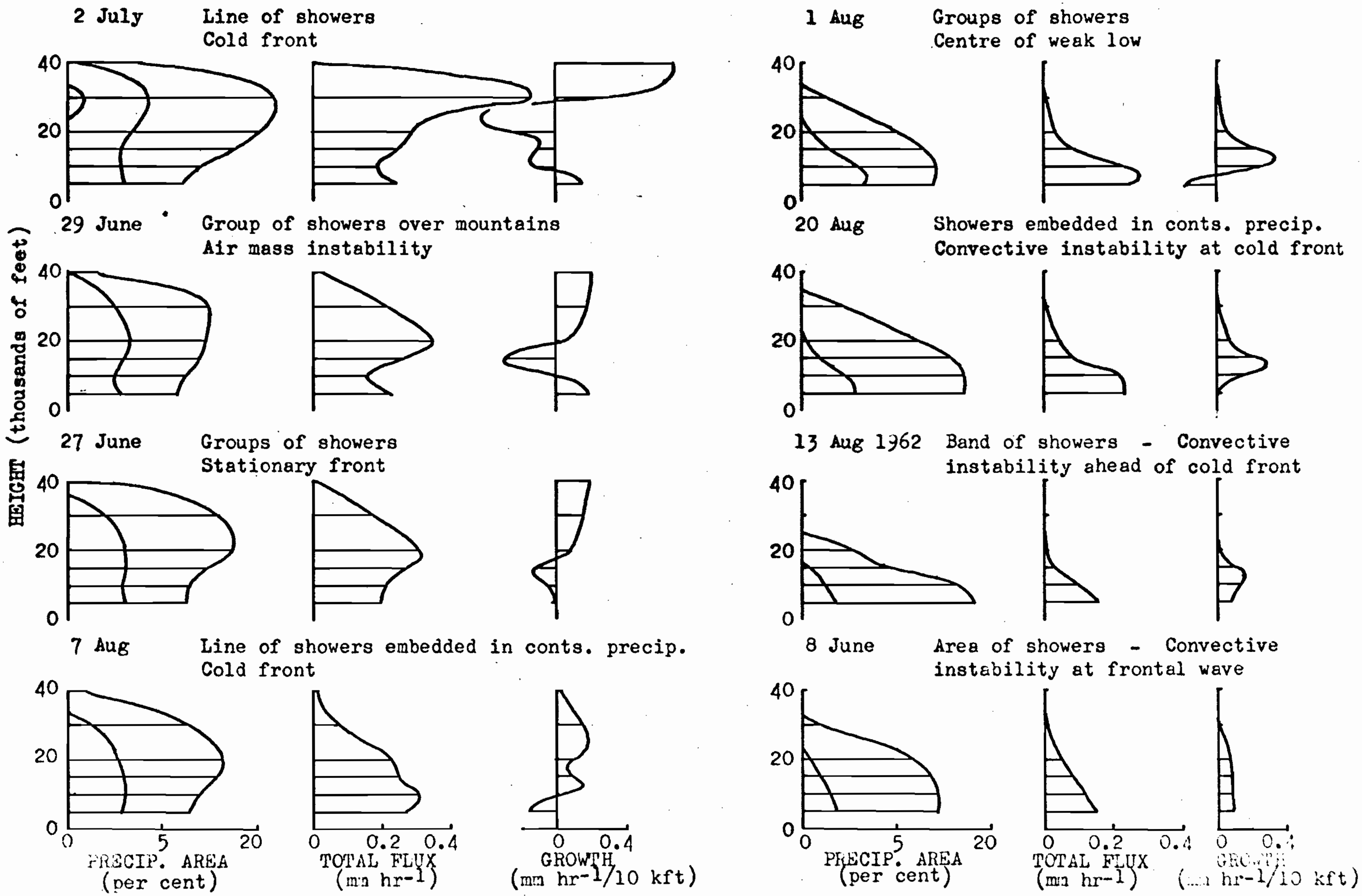
2 July
Line of showers
Cold front
29 June
Group of showers over mountains
Air mass instability
27 June
Groups of showers
Stationary front
7 Aug
Line of showers embedded in conts. precip.
Cold front
1 Aug
Groups of showers
Centre of weak low
20 Aug
Showers embedded in conts. precip.
Convective instability at cold front
13 Aug 1962
Band of showers - Convective
instability ahead of cold front
8 June
Area of showers - Convective
instability at frontal wave
HEIGHT (thousands of feet)
40
20
0
0
5
20
0.2
0.4
PRECIP. AREA
(per cent)
TOTAL FLUX
(mm hr-1)
GROWTH
(mm hr-1/10 kft)

Fig. 5.1

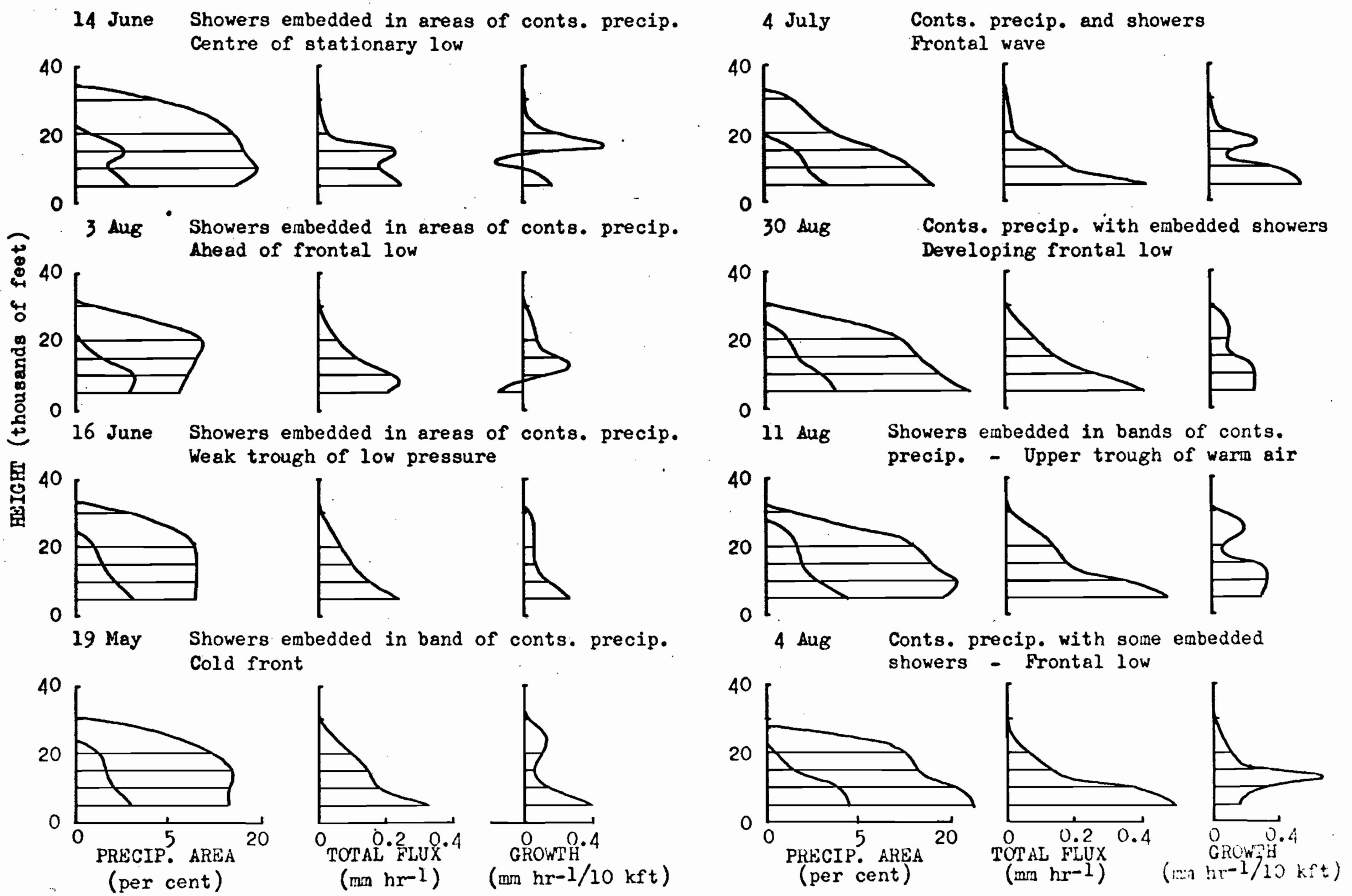
14 June
Showers embedded in areas of conts. precip.
Centre of stationary low
4 July
Conts. precip. and showers
Frontal wave
3 Aug
Showers embedded in areas of conts. precip.
Ahead of frontal low
30 Aug
Conts. precip. with embedded showers
Developing frontal low
16 June
Showers embedded in areas of conts. precip.
Weak trough of low pressure
11 Aug
Showers embedded in bands of conts.
precip. - Upper trough of warm air
19 May
Showers embedded in band of conts. precip.
Cold front
4 Aug
Conts. precip. with some embedded
showers - Frontal low
HEIGHT (thousands of feet)
40
20
0
0
5
20
PRECIP. AREA
(per cent)
0
0.2
0.4
TOTAL FLUX
(mm hr-1)
0
0.4
GROWTH
(mm hr-1/10 kft)
Fig 5.2

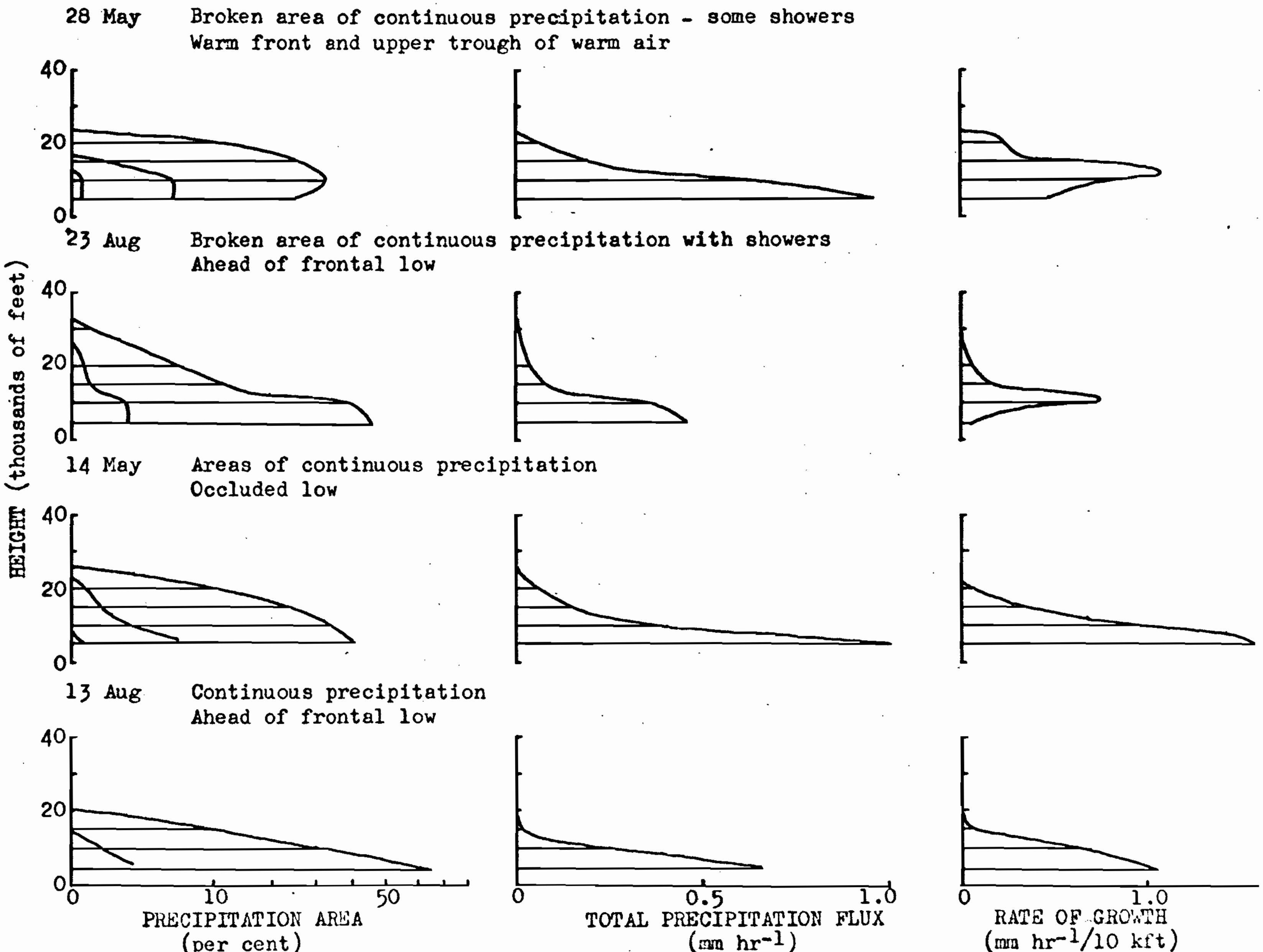

28 May
Broken area of continuous precipitation - some showers
Warm front and upper trough of warm air
23 Aug
Broken area of continuous precipitation with showers
Ahead of frontal low
14 May
Areas of continuous precipitation
Occluded low
13 Aug
Continuous precipitation
Ahead of frontal low
HEIGHT (thousands of feet)
40
20
0
10
50
0.5
1.0
PRECIPITATION AREA
(per cent)
TOTAL PRECIPITATION FLUX
(mm hr⁻¹)
RATE OF GROWTH
(mm hr⁻¹/10 kft)

Fig. 5.3

of a summer's precipitation at Montreal. For the rest of the period the two types occur in combination. Accordingly, profiles of a number of situations are presented in Figs. 5.1 to 5.3, ranging from definite showers through mixed showers and continuous precipitation to definite continuous precipitation.

All of the cases shown in Fig. 5.1 have been taken from amongst the shower situations presented in Figs. 3.2 to 3.5. The cases are arranged in consecutive columns in order of decreasing instability. Each case is represented by three sets of profiles: area of precipitation exceeding 0.2, 3.2 and 50 mm hr^{-1}, total flux and rate of growth. Brief descriptions are given of the radar precipitation pattern and the synoptic situation on each occasion. Fig 5.2 shows similar profiles for situations in which there were both showers and continuous precipitation. It is not really possible to arrange these in any order, but an attempt has been made to put those in which showers dominate at the beginning and those in which continuous rain dominates at the end. The first two cases in Fig. 5.3 are also examples of mixed precipitation types, but they are certainly cases in which the continuous precipitation is dominant. The final two cases of Fig. 5.3 are examples of pure continuous precipitation and were originally presented in Figs. 4.2 and 4.3.

Perhaps the best way of appreciating the spectrum of examples in Figs. 5.1 to 5.3 is to compare the two extremes, 2 July and 13 August. On 2 July the total area increased from about 6% at 5 kft to over 20% at 30 kft with a maximum height of more than 40 kft, whereas on 13 August the area decreased from over 60% at 5 kft to zero at 20 kft. The area of precipitation exceeding 3.2 mm hr^{-1} was quite similar in both cases at 5 kft, but it increased with height in the showers and decreased rapidly in the continuous rain. The total flux profiles show exactly the same differences as the total area: for the showers, modest at 5 kft and great at 30 kft; for the continuous rain, great at 5 kft and then decreasing very rapidly with height. Finally, the growth profile of 2 July shows very strong growth in the upper levels and strong evaporation below, while on 13 August there was very strong growth only in the low levels.

A glance down the columns of area profiles shows a fairly steady change from the one extreme to the other. The flux profiles also change fairly steadily, except that there is some overlap in Figs. 5.1 and 5.2. However, the rate of growth profiles do not vary steadily at all, especially in Fig. 5.2. It is especially apparent from them that the profiles of mixed showers and continuous precipitation can be considered to be the sum of profiles of the separate components. Thus, for example, the rate of growth profile of 4 August (bottom right, Fig. 5.2) is very closely reproduced by adding 1.5 times that of 1 August (upper right, Fig. 5.1) to 0.25 times that of 13 August (bottom right, Fig. 5.3). It is not pretended that there is any value in this kind of calculation, but it does emphasize that the profiles of mixed precipitation are determined by the components.

It should be plain from the examples of Figs. 5.1 to 5.3 that the great virtue of profiles is that they characterize the precipitation, regardless of the synoptic situation which produced it. In fact an attempt was made at grouping profiles of similar synoptic type, but it was most unrewarding. It quickly became apparent that the profiles were more fundamental than the synoptic analyses. Much more rewarding was a comparison of the profiles with the character of the radar precipitation pattern. It was found that the presence of shower cells in precipitation was almost invariably obvious from the profiles, especially the rate of growth profile. Qualitatively, it was also apparent that the frequency and intensity of the showers was reflected in the profiles. The profiles in thus characterizing the precipitation offer a means of studying the convection which generates it. Their analysis might even lead to estimates of the relative amounts and intensities of small and large scale convection, especially if coupled with conventional thermodynamic and dynamical analyses.

The area profiles are the basic set from which the flux and rate of growth profiles can be derived, and with a little experience it is possible to estimate the form of these two derived sets from the area profiles. For example, there is often a significant similarity between the shape of the second area profile (3.2 mm hr^{-1}) and the total flux. However, although they are interdependent, each of the three profiles contributes to the ready interpretation of a situation. The rate of growth profile is the most irregular of the three, and for this reason it is a most valuable indicator. It is very sensitive to the relative amounts of showers and continuous precipitation, and thus it is a good monitor of changes in a situation. But even this profile is only fully useful in the context of the others.

It is also important to look at profiles in their synoptic context, particularly the upper-air sounding. In the chapter on shower profiles it was shown that the upper maximum in flux was essentially a dynamical effect, but this is not the cause of all upper maxima. They can also result from evaporation in the lower levels. The two different effects would not be confused if the profiles were studied together with the sounding. The profiles can also be a valuable aid to interpreting the sounding. For example, in one case presented in Fig. 3.5 (30 June), the profiles showed growth only between 11 and 36 kft, with some slight evaporation below. Analysis of the tephigram in the light of this observation showed that convective instability had been realized between these two levels, and it was even possible to estimate the rate at which the air mass was being lifted.

It should also be pointed out that much of the value of profiles lies in their ability to monitor the evolution of a situation. For instance, a situation of mixed showers and continuous precipitation commonly arises in two ways. In one case, the showers develop within a mass of continuous precipitation, often as a result of the realization of convective instability through continued lifting of a saturated air mass. In the other, the showers themselves generate continuous precipitation, sometimes from a descending plume or anvil. These two processes are immediately distinguished by the sequence of profiles, even though the resulting mixed precipitation patterns may be quite similar.

It is hoped that this brief discussion has given some idea of the potential value of profiles in synoptic meteorology. So far it has only been possible to point out the more obvious qualitative contrasts between profiles of different precipitation patterns. The full potential of profiles will only be realized when the quantitative data they offer is used. There would seem to be some hope of combining the profile data with numerical analyses of the dynamical processes in the atmosphere. Even if the profiles alone do not have much predictive value, a complete knowledge of the state of the atmosphere and its trends is a prerequisite for prediction, and the precipitation pattern is an important component.

5.2 Presentation of Profile Data for Local Use

The McGill University Stormy Weather Group has recently developed techniques to produce radar maps in which the precipitation is displayed

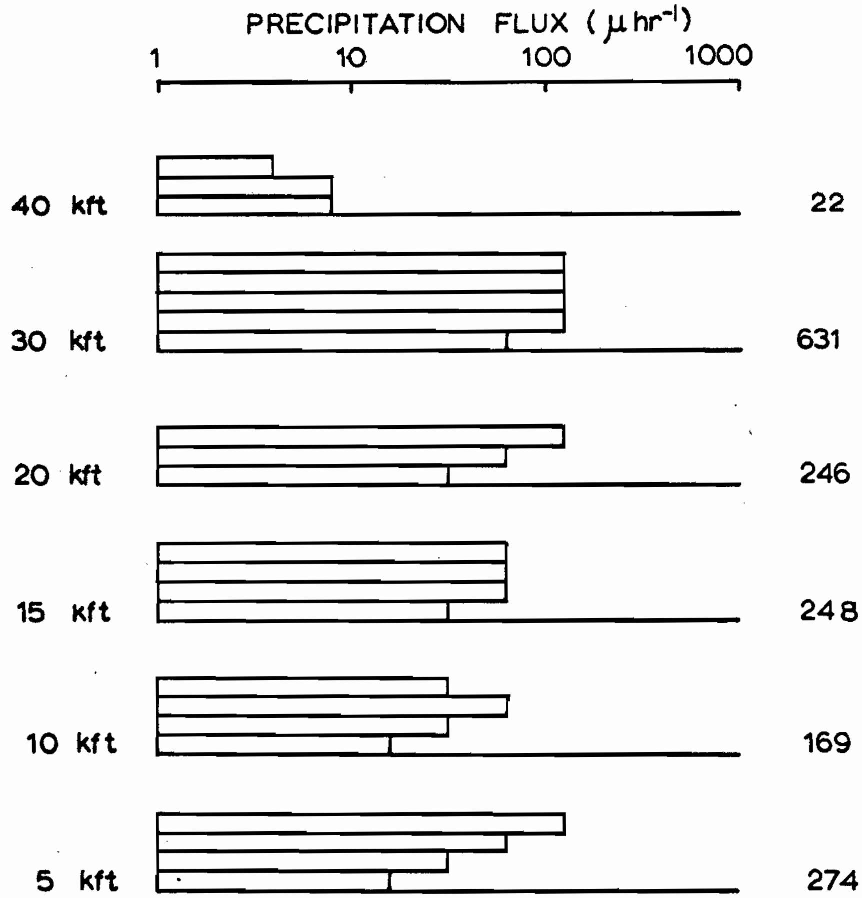

Fig. 5.4. Examples of flux histograms for each of six altitudes, 2 July. Each histogram shows the flux as a function of precipitation intensity, with bars representing mean rainfall rates of 0.4, 1.6, 6.4, 25, 100, 400, and 1600 mm hr^{-1} from bottom to top.

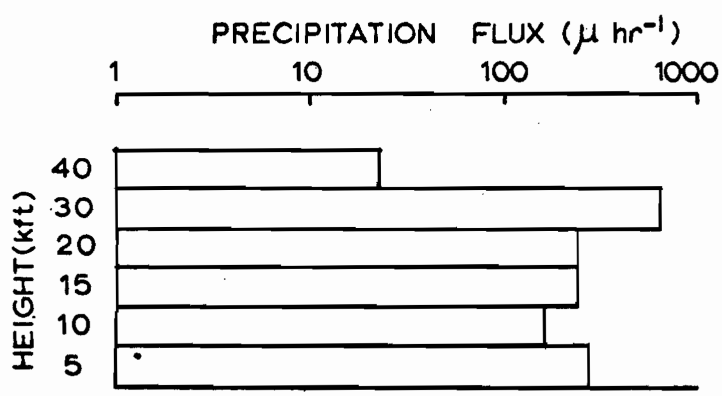

Fig. 5.5. Histogram of the total flux as a function of height. Data taken from the example of Fig. 5.4.

in shades of grey (Wein, 1964). In the particular equipment used at McGill the boundaries between shades represent rainfall rates of 0.2, 0.8, 3.2, 12.5, 50, 200 and 800 mm hr^{-1} (attenuation-corrected values). Important byproducts of the process by which these maps are produced are the areas of the precipitation represented by each shade, and these are the basic data from which profiles are obtained. In the further development of the McGill techniques, Canadian Aviation Electronics (C.A.E.) of Montreal have produced equipment to record and display these profile data (Ballantyne, 1964). The grey shade CAPPI maps are produced on a facsimile record, and immediately following each picture is an analysis of the precipitation in the form of a histogram showing the flux of precipitation arising from each shade. Examples of these histograms are shown in Fig. 5.4.

The scales best suited for displaying profile data can only be arrived at after considerable compromise. For example, flux is most readily interpreted on a linear scale but the wide range of possible values necessitates a logarithmic scale in practice. The histograms of Fig. 5.4 have a logarithmic scale extending over a range of 10^3. The flux has been expressed in the usual way as the average rainfall rate that would result if it were distributed over the entire sampling area, and the most convenient units here are 10^{-3} mm hr^{-1}, or μ hr^{-1}. Each set of bars shows the flux contributed by each intensity of precipitation at the height indicated, with the bottom bar of each set representing the lowest mean rainfall rate of 0.4 mm hr^{-1}. C.A.E. have actually used digital recording techniques, and the fluxes in Fig. 5.4 have been plotted digitally at intervals of a factor 2.0.

The area of each intensity is readily obtained from the flux by dividing by the appropriate mean rainfall rate. The reason that flux has been chosen for display rather than area is partly that it is a slightly more useful quantity and partly for reasons of display. Significant values of flux are observed to range over rather less than three decades, whereas the corresponding areas range over more than four decades, a point that will be returned to later in the next section. Meanwhile it may be noted that one consequence of this is that, for a given number of available display digits, the flux can be displayed with greater resolution than the area.

The histograms of Fig. 5.4 show the distribution of flux with intensity. Although they have not been studied in this work, it is reasonable to expect that a close study of the exact forms of the distributions would reveal that they can provide useful information about the nature of the precipitation processes. The present study has emphasized the significance of the overall pattern of precipitation in the vertical. It is a fairly simple matter to study this from the data of Fig. 5.4. The total flux at each height is readily obtained as the sum of the individual fluxes, and these have been written at the right of the corresponding histograms. The totals can themselves be displayed in a histogram, and this has been done in Fig. 5.5. C.A.E. have not yet fully developed the computing facilities of their equipment, but the digital form of the data of Fig. 5.4 makes them especially amenable to further computing. It would thus be a fairly simple matter to derive and display the total flux profile of Fig. 5.5. Information about the distribution of flux with intensity could be included in Fig. 5.5 by dividing each bar into portions representing the contributions from several intensity intervals and displaying the portions in grey shades.

Other histograms, such as area and rate of growth as functions of height, might also be produced. However, the exact form and number of the profile displays have yet to be determined, and this can only properly be done on the basis of a period of operation in a forecast office. It would also be possible to display the data as arrays of digits, but again this possibility requires careful evaluation. At the moment, the histogram displays which follow the radar maps on the facsimile record do seem to be the form most likely to satisfy local needs.

5.3 Coding of Profile Data

The presentation of profile data for local use has just been discussed in some detail, but in many ways they are potentially more useful on the synoptic scale. The local user can inspect the original radar maps, and the profiles are really only a way of summarizing these maps. It is true that the profiles may point out characteristics of the precipitation that might otherwise go unnoticed, but they certainly cannot stand alone. On the other hand, it is the essential characteristics of the precipitation rather than its detailed configuration that do interest the synoptic meteorologist, and profiles are likely to meet most of his needs.

The great advantage of a summary of the precipitation in the form of profiles is that it can be expressed with relatively few data, and so will be economical of teletype transmission time. Some effort has been devoted to devising the most economical code for transmission of profile data, and Table 5.1 shows the result. The areas of significance in profiles range from about 0.005% to 100% (1 mi^2 to 20,000 mi^2), or almost a factor 2^{15}. However, the requirements for any single intensity of precipitation are considerably less than this. For instance, small areas of light precipitation are insignificant and large areas of heavy precipitation do not

TABLE 5.1

CODE FOR PROFILE DATA

Area (%)		Precipitation Rates (mm hr^{-1})						
Interval		0.2 0.8	0.8 3.2	3.2 12.5	12.5 50	50 200	200 800	800
	Mean	0.4	1.6	6.4	25	100	400	-
		(1)	(2)	(3)	(4)	(5)	(6)	(7)
100-50	71	9						
50-25	35	8	9					
25-12.5	18	7	8	9				
12.5-6.2	8.9	6	7	8	9			
6.2-3.2	4.4	5	6	7	8	9		
3.2-1.6	2.2	4	5	6	7	8	9	
1.6-0.8	1.1	3	4	5	6	7	8	9
0.8-0.4	.55	2	3	4	5	6	7	8
0.4-0.2	.28	1	2	3	4	5	6	7
0.2-0.1	.14		1	2	3	4	5	6
0.1-.05	.071			1	2	3	4	5
.05-.025	.035				1	2	3	4
.025-.012	.018					1	2	3
.012-.006	.009						1	2
.006-.003	.004							1

occur. Therefore a reasonable economy is to provide coding for a smaller range whose limits change from intensity to intensity. Table 5.1 is based on a binary scale, and thus the area intervals are each a factor 2, and the precipitation rate intervals are each a factor 4. The coding range for each intensity is a factor 2^9 in area, and it is shifted down by a factor 2 in going from one intensity to the next higher. Thus the range is from 0.2 to 100% for 0.4 mm hr^{-1} (McGill grey-shade intensity 1), from 0.1 to 50% for intensity 2 and so on.

A set of seven digits, one for each of the intensities, is sufficient for the data of a single CAPPI map. If the data are transmitted in order of increasing precipitation intensity, the set can be terminated with the

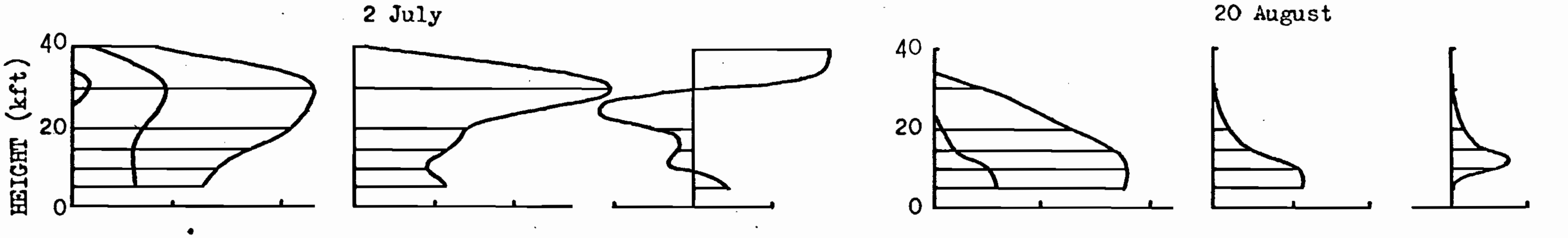

INTENSITY (2 July)

		1	2	3	4	5	6	7
H	40	4	3	1				
E	30	7	7	6	5	4		
I	20	6	6	6				
G	15	6	6	5	4			
H	10	5	5	5	3			
T	5	5	5	5	5			

INTENSITY (20 August)

		1	2	3	4	5	6	7
H	40							
E	30	3	1					
I	20	5	4	1				
G	15	6	5	2	1			
H	10	6	7	5	2			
T	5	6	6	5	2			

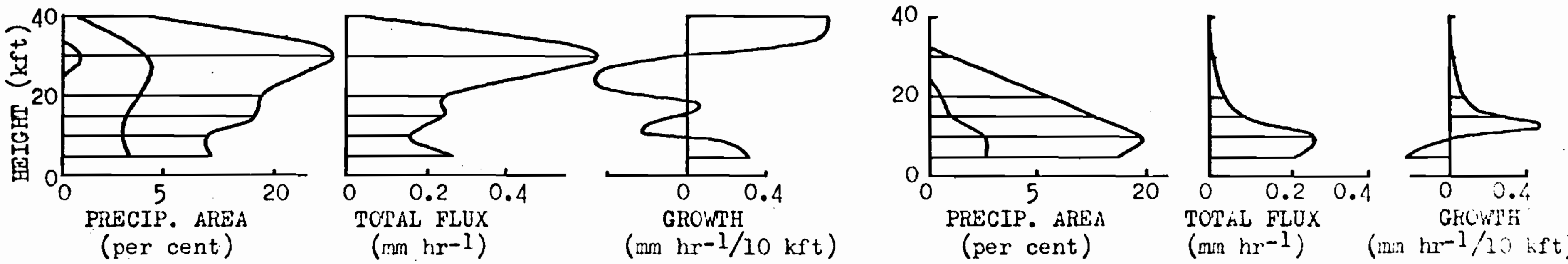

Fig. 5.6. Coding of Profile Data for Shower Situations. Above, original profiles; at middle, coded arrays (from Table 5.1); below, profiles from decoded data.

13 August

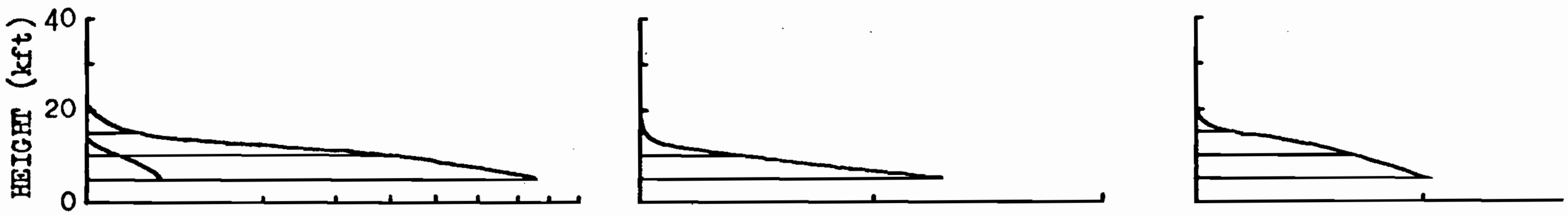

INTENSITY

		1	2	3	4	5	6	7
H	40							
E	30							
I	20	1						
G	15	3						
H	10	7	7	4				
T	5	8	8	5	5			

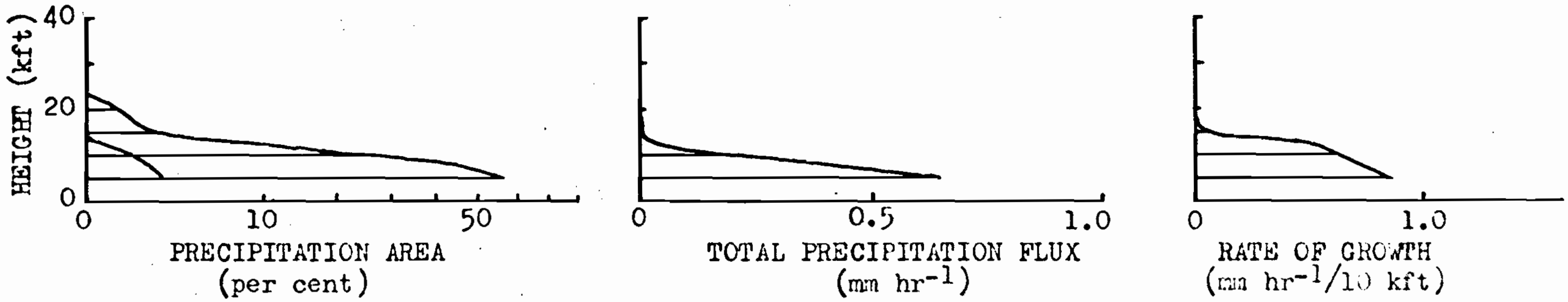

Fig. 5.7. Coding of Profile Data for Continuous Rain Situation. Above, original profiles; at middle, coded arrays (from Table 5.1); below, profiles from decoded data.

first zero. Similarly if data are transmitted for successively higher heights the sequence can be terminated at the first height with no precipitation. The complete profile data for the six heights used in this work require a maximum of about 30 digits for shower situations and a maximum of 15 for continuous rain. A few examples of coding appear in Figs. 5.6 and 5.7. The data of the profiles at the top of each figure have been arranged in arrays, each row representing the data of one height in the form of the areas of successively increasing intensities. It is notable that the shape of the array alone gives a reasonable picture of the general pattern of the profiles. At the bottom of each figure, profiles have been recovered by decoding the arrays. The coding process was based on intervals of area of a factor 2, so individual values in the recovered profiles may be in error by up to a factor $\sqrt{2}$. Although there are irregularities of this order, the decoded profiles show all the main features of the originals without serious distortion. The rate of growth profile is the most affected but even there the main features are preserved. It is possible that the distortions of coding would somewhat reduce the value of profiles to the local user, but there is almost certainly no significant loss on the synoptic scale.

The binary basis of the coding proposed here offers considerable advantages in computing. For example, it is quite easy to derive arrays of area or flux from the coded arrays in Figs. 5.6 and 5.7. Without going into detail, if the digits representing the intensities are added to each number in the column they head, then the result is an array of flux expressed in powers of 2. If they are subtracted then the array is of area in powers of 2. The computing facilities required for these operations would be most modest.

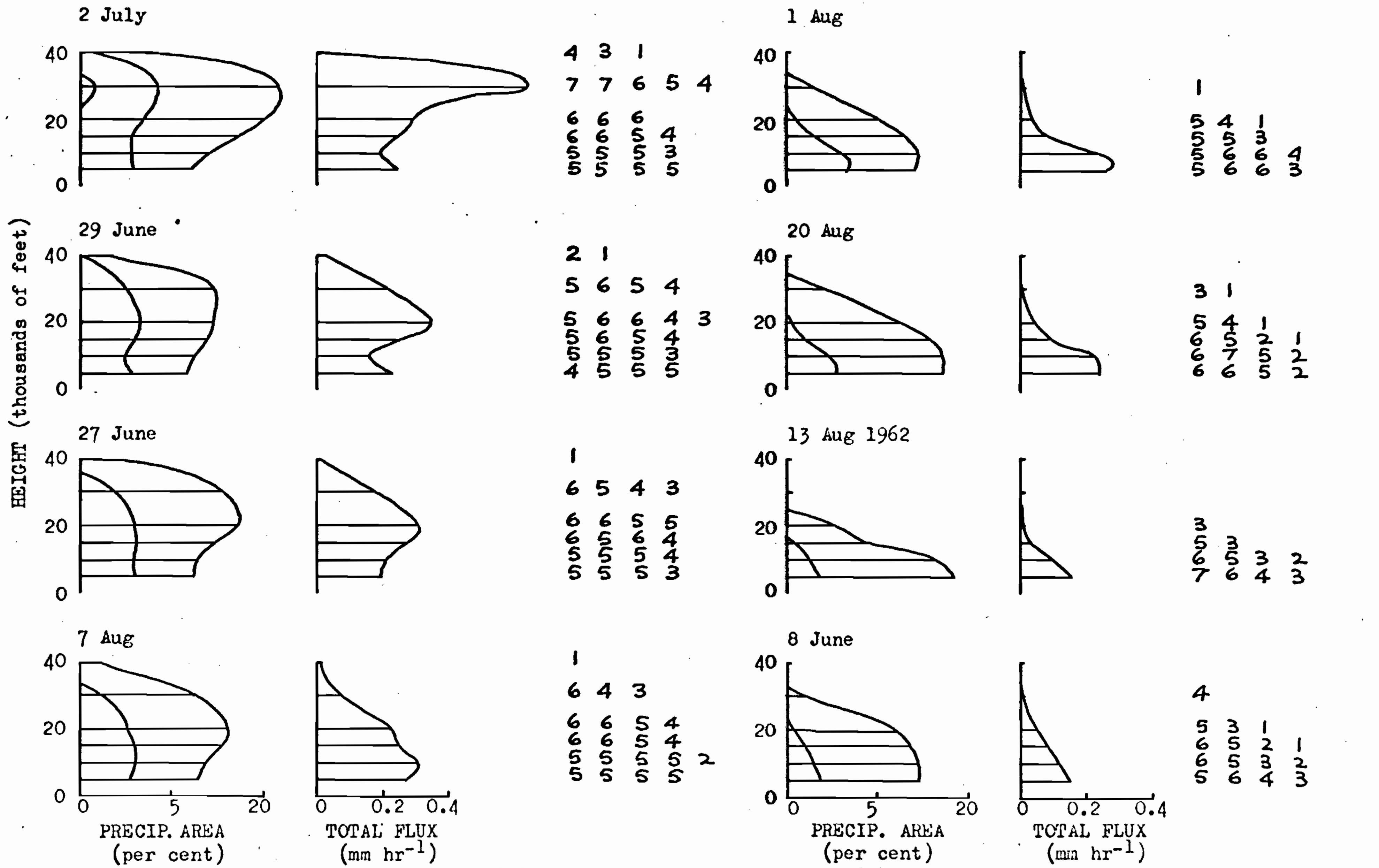

Fig. 5.8. Examples of Coded Arrays of Profile Data, mainly shower situations.

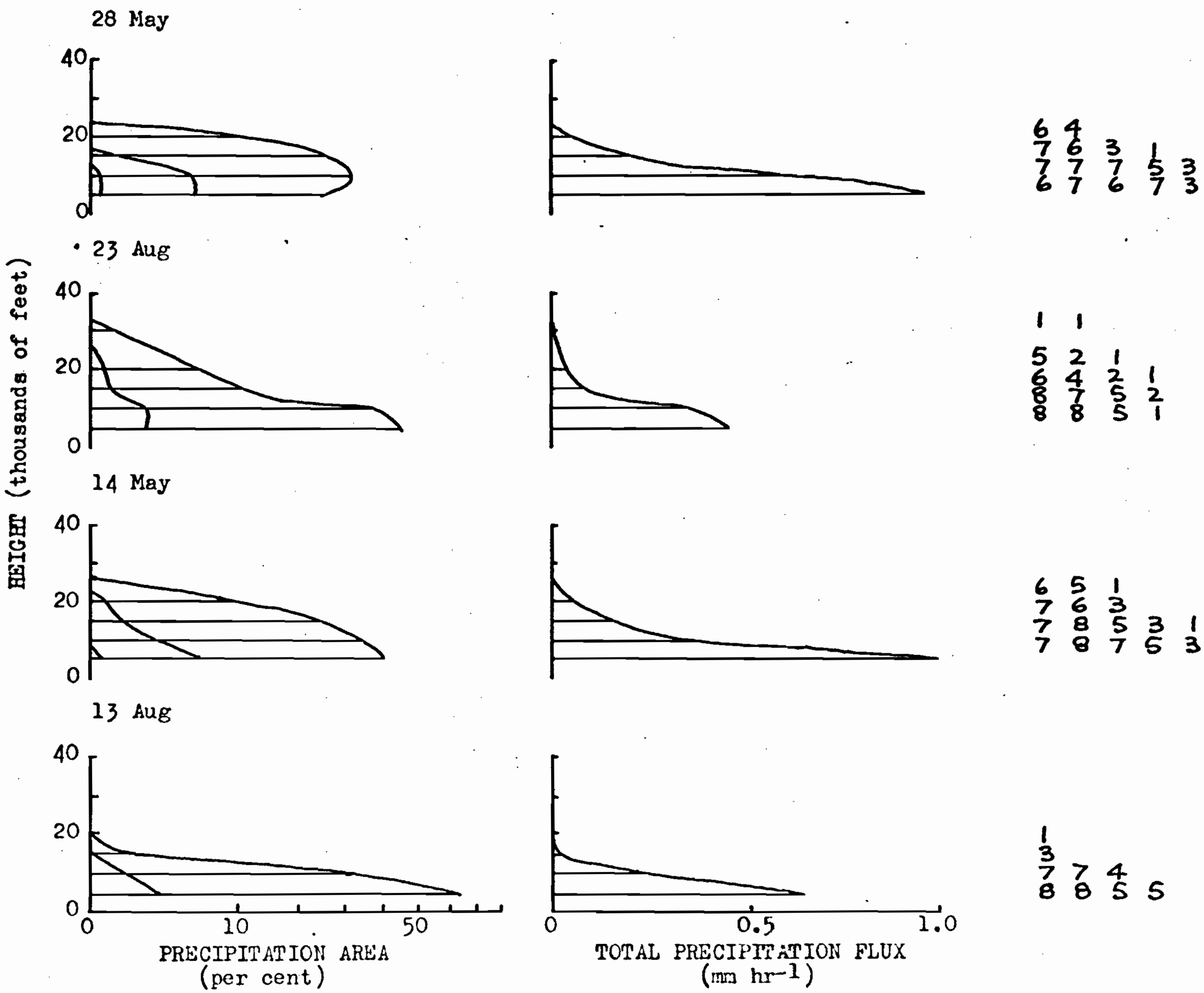

Fig. 5.9. Examples of Coded Arrays of Profile Data, mainly continuous rain.

5.4 Presentation of Data for Synoptic Use

Perhaps the great value of radar on the synoptic scale lies in its ability to probe every cubic mile of the atmosphere within range every few minutes. This may be contrasted with the regular network of synoptic stations which only monitors events at the surface over less than 1% of the total area every hour or so. Not only can radar detect precipitation the moment it has formed, but as this work has shown its pattern in the vertical can provide important information about the processes which produced it. Because of its complete and immediate coverage radar can certainly play an important part on the synoptic scale. However, the fact that radar probes every cubic mile every few minutes does not mean that the synoptic forecaster should be provided with all the data so collected. Apart from the problems of transmission of such a vast amount of data, they would hardly be appreciated anyway. What is appropriate is the frequent provision of brief and easily-digested summaries, and profiles are one way of doing this.

There are many possible ways in which profile data can be displayed on a synoptic scale. The ideal is one which can give the essential features at a glance, and then give the details on close inspection. One form of display with this dual capability is the array of digits into which the profiles were coded in the last section (Figs. 5.6 and 5.7). It was noted at the time that there was a resemblance between the shape of the array and the corresponding flux profile. The resemblance is further brought out in a series of examples shown in Figs. 5.8 and 5.9. The profiles of the situations originally presented in Figs. 5.1 and 5.3 have been coded into arrays, and the arrays are placed after the relevant area and flux profiles. As before, there is one row of digits for each height, and the digits in a row indicate the areas of precipitation of each of the McGill grey-shade intensities.

Looking at the first example of Fig. 5.8, every one of the digits at 30 kft equals or exceeds the corresponding digits at any other height. Thus the array immediately shows that there are maxima in area and flux at 30 kft. In practice, the positions or magnitudes of the last digits provide a good indication of a maximum in flux. Although the greatest intensity may not itself contribute significantly to the flux, the greater it is the greater the total flux is likely to be. Hence, the heights of the flux maxima in three of the four examples at the left of Fig. 5.8. are indicated by the only digit in the fifth place, that is the only precipitation of intensity five. In the other case (27 June) the height of the maximum is the height with the greatest amount of intensity four. Also in practice, a good indication of the total area of precipitation is given by the first digit. This is because the area of intensity one almost always forms more than one-half of the total area, and the proportion that it does form is usually quite similar at all heights. As an example, on 2 July, the first digit increases from 5 at 5 kft to 7 at 30 kft, and this indicates a factor 4 increase in the area of intensity one. The total area increased by a factor 3.3.

Thus, the presentation of profile data in a coded array permits one to determine the main features of a situation from a glance at the first and last digits of each row. This would probably be quite sufficient for most synoptic purposes. However, the complete array does provide all the data needed for the extensive analysis of a particular situation, even down to the drawing of area, flux and rate of growth profiles for each precipitation intensity. Further, one even foresees the possibility of incorporating the profile data into numerical weather prediction techniques. It is quite likely that the array of digits would be a suitable form in which to present the data for computation. It can be seen that the coded array is a most versatile form for the display of profile data.

The modest data transmission involved in the suggested code has already been emphasized. Almost every shower situation can be coded in 30 digits or less, and continuous rain situations require a maximum of 20. Normal teletype equipment can transmit 500 digits per minute, so that 2 minutes would be sufficient to receive the data of 40 radar stations. In this study, profiles have always been drawn for the 20,000-n mi^2 area within range 80 n mi. This area has been found quite convenient, but it is not necessarily the optimum. It would be quite possible to produce profiles for any chosen areas. For instance, a reasonable reduction of the sampling area might be into 5,000-n mi^2 quadrants. However, each subdivision of the sampling area will naturally increase the requirements for data transmission, so that the final choice is a matter for careful consideration.

Experienced forecasters can appreciate the main features of a synoptic situation from a glance at the teletype record of the station reports, especially if they are only looking for recent changes in a situation they have worked with closely for the last few hours. In the same way the radar reports could probably be fairly readily digested by a glance at the sequence of arrays of profile digits on a teletype chart. However, it might be preferable to transfer the arrays to a map, and this could quite easily be done.

It may be mentioned that other possible methods of displaying the data were tried such as the histograms described in section 5.2, and decoded values of the total area and flux. Although histograms can be readily appreciated at a glance, they cannot conveniently include all the detail of the array. None of the other methods had any significant advantage over the array.

It is hoped that the research reported in Chapters 3 and 4 has convincingly demonstrated the value of precipitation profiles in studying the processes of atmospheric convection. Eventually they may be expected to take a place in operational meteorology, and it has been the purpose of this chapter to establish their practicability. Naturally, several of the more detailed recommendations implied in this chapter will need more study to support them. Considerable operational experience will be needed before the full value of profiles can be realized, and as this experience is acquired the most suitable display techniques will evolve. It is rather exciting that the equipment built by C.A.E. is almost ready to run under operational conditions. It is not often that equipment is available to display operationally data whose potential has only just been realized. The routine operation of this equipment will undoubtedly uncover various facets of profile data that have not yet been appreciated.

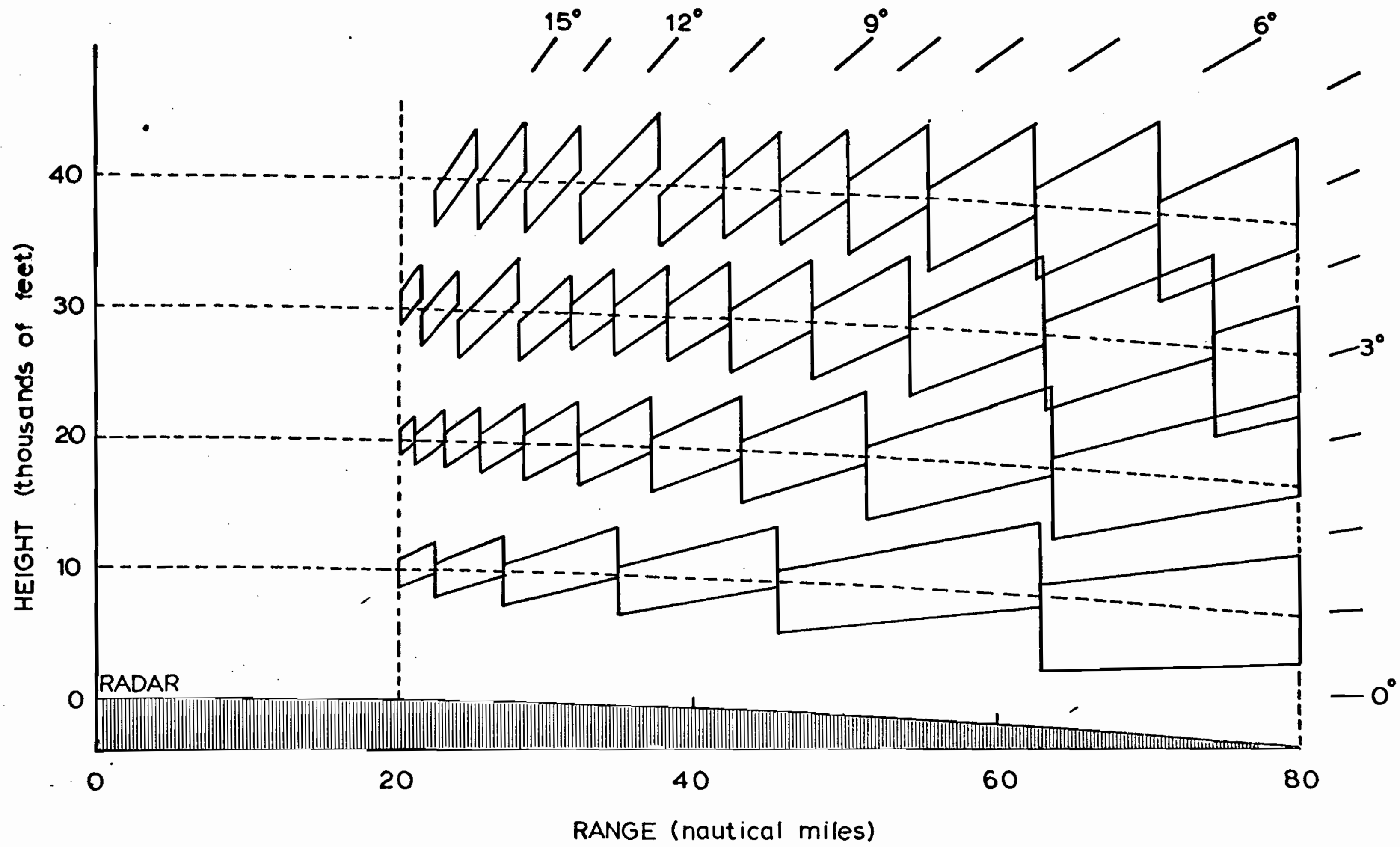

Fig. 6.1 Range intervals used to compose McGill CAPPI maps.

6. TECHNIQUE

6.1 The McGill Weather Radar

The Stormy Weather Group of McGill University has developed, and for several years operated, a highly automatic weather-radar system (Marshall and Gunn, 1961). Each picture from this radar is a map of the precipitation pattern at a constant altitude, in which precipitation intensity is displayed in shades of grey. To produce such pictures the CPS-9 radar operated at Montreal Airport has been modified in several ways.

To produce constant-altitude pictures, the one-degree beam rotates uniformly in azimuth, each successive rotation at a higher angle of elevation. On a PPI display, gating circuits select annular rings from the various angles of elevation. These fit together to produce a Constant Altitude PPI Display (CAPPI) at a selected height. The elevation angles and range intervals used to construct CAPPI maps at several heights are shown in Fig. 6.1. The CAPPI map is synthesized on film by accumulating the various annular rings in a single photograph of the display. Each display progresses through a sequence of heights, usually 5, 10, 15, 20, 30 and 40 thousand feet, completing such a sequence every 22.5 minutes.

To produce maps in grey shades, the radar signal from the precipitation passes through a logarithmic amplifier, and then an exponential amplifier, to the cathode ray display tube. Contrast and brightness controls between the amplifiers are adjusted so that a chosen range of input signals from precipitation just fits the available brightness range of the cathode ray tube. The input range equivalent to rainfall rates from 0.1 to 400 mm hr^{-1} has been chosen, so that 0.1 mm hr^{-1} is displayed at the darkest level and 400 mm hr^{-1} at the brightest. Fig. 6.2 is an

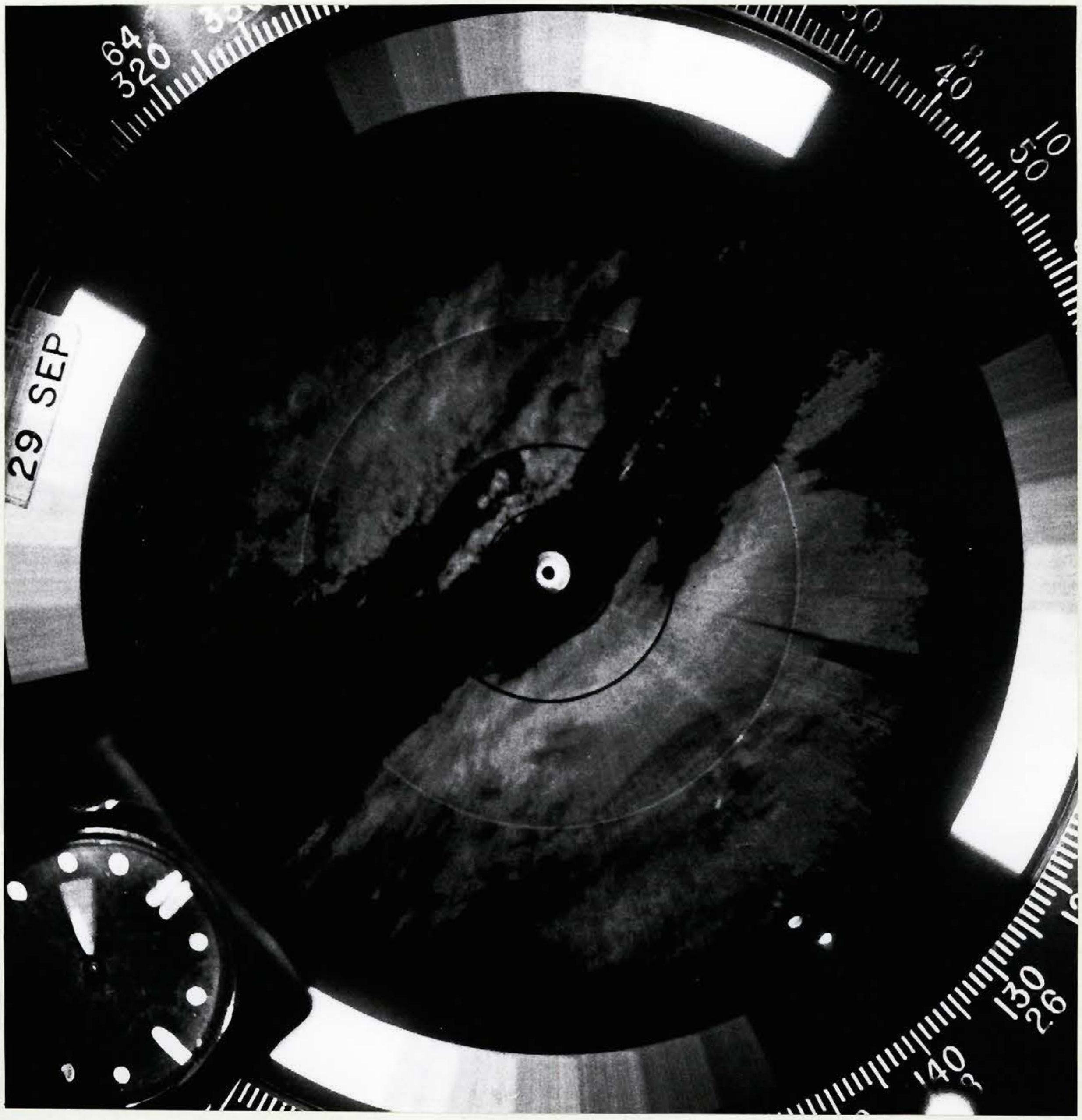

Fig. 6.2. McGill Grey Scale CAPPI map. 5 kft, 0950 EST 29 September 1963
Montreal at centre, range 120 n mi.
Grey shade boundaries at 0.1, 0.4, 1.6, 6.4, 25, 100, 400 mm hr^{-1} (no attenuation correction)

example of a grey-scale CAPPI map.

The exponential amplifier has been designed with stepped response, so that the output signals have seven discrete levels. Thus the map shown in Fig. 6.2 is actually composed of seven discrete grey shades. Successive shades above background represent steps of a factor 4.0 in rainfall rate, and so denote intervals with thresholds 0.1, 0.4, 1.6, 6.4, 25, 100, and 400 mm hr^{-1}. The use of discrete steps is apparent in the peripheral test pattern, which accompanies each picture. It is less apparent in the precipitation pattern because of the fluctuating nature of radar returns from precipitation. Consecutive returns from a given target vary in intensity and, since the writing lines on the display overlap, these varying intensities are averaged. Thus the stepped amplifier is ineffective in giving sharp boundaries betweeen the grey shades.

The CAPPI maps are corrected for range effects. For cases in which the precipitation fills the cross-section of the radar beam, the received signal power varies inversely as the square of the range. An electronic circuit provides good compensation for this effect from 20 to 80 n mi range. Another correction is made for an effect which arises from the polar coordinates of the display. The picture is made up of radial writing lines which converge toward the centre. Thus for radar signals of a given intensity, the brightness is inversely proportional to the range. To compensate for this, the display tube is fitted with a photographic half-tone mask in which density increases from a low value at the edge to a high value at the centre.

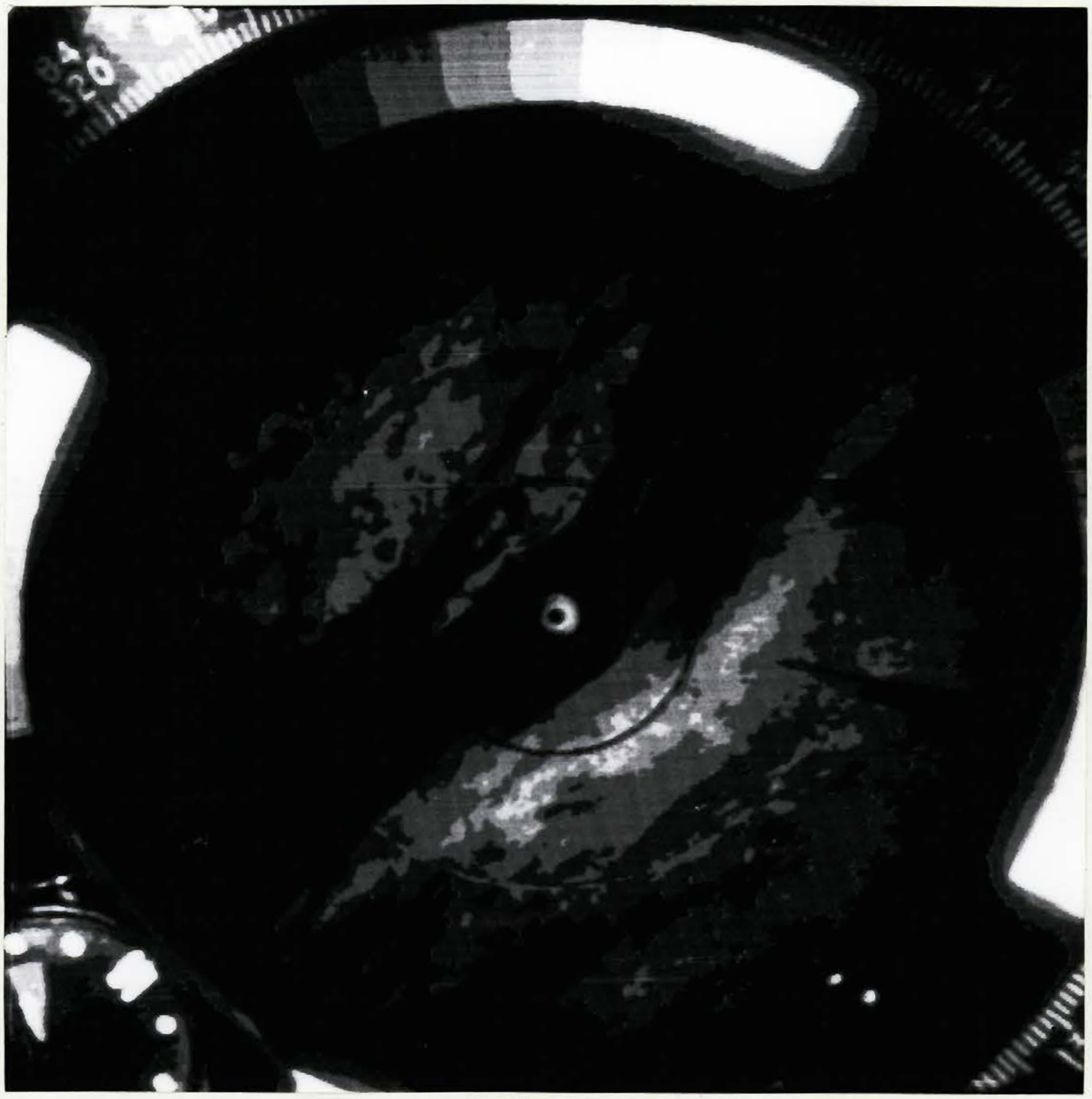

Fig. 6.3. Grey Scale CAPPI map after scanning and thresholding. Same map as in Fig. 6.2.

Although precipitation rates are displayed quantitatively in the grey-scale map of Fig. 6.2, it is quite tedious to measure them. Sharp boundaries between the grey shades greatly facilitate measurements, and these have been achieved in Fig. 6.3. This picture has been produced from the negative of the original CAPPI picture by equipment recently developed at McGill (Wein, 1964)

In this equipment the negative is first scanned by the bright spot of a scanning tube imaged onto the negative. It sweeps from side to side, covering the negative line by line, from top to bottom. Light is transmitted through the negative, depending on its density, and collected in a photomultiplier tube. The output signal of this tube, which thus depends on negative density, passes through an amplifier with stepped response to the display. The picture on the display is written line by line, in discrete grey shades, as the negative is scanned. The equipment is adjusted to give boundaries at the same rainfall rates as in the original picture.

Fig. 6.3 is a photograph of a cathode ray tube display, but the equipment also produces a paper facsimile record. In fact the facsimile record is an operational product of the McGill radar. To meet the operational requirement, negatives of the CAPPI maps are rapidly developed in an automatic processor before scanning. The whole system is automatic and facsimile records can be supplied to any number of users.

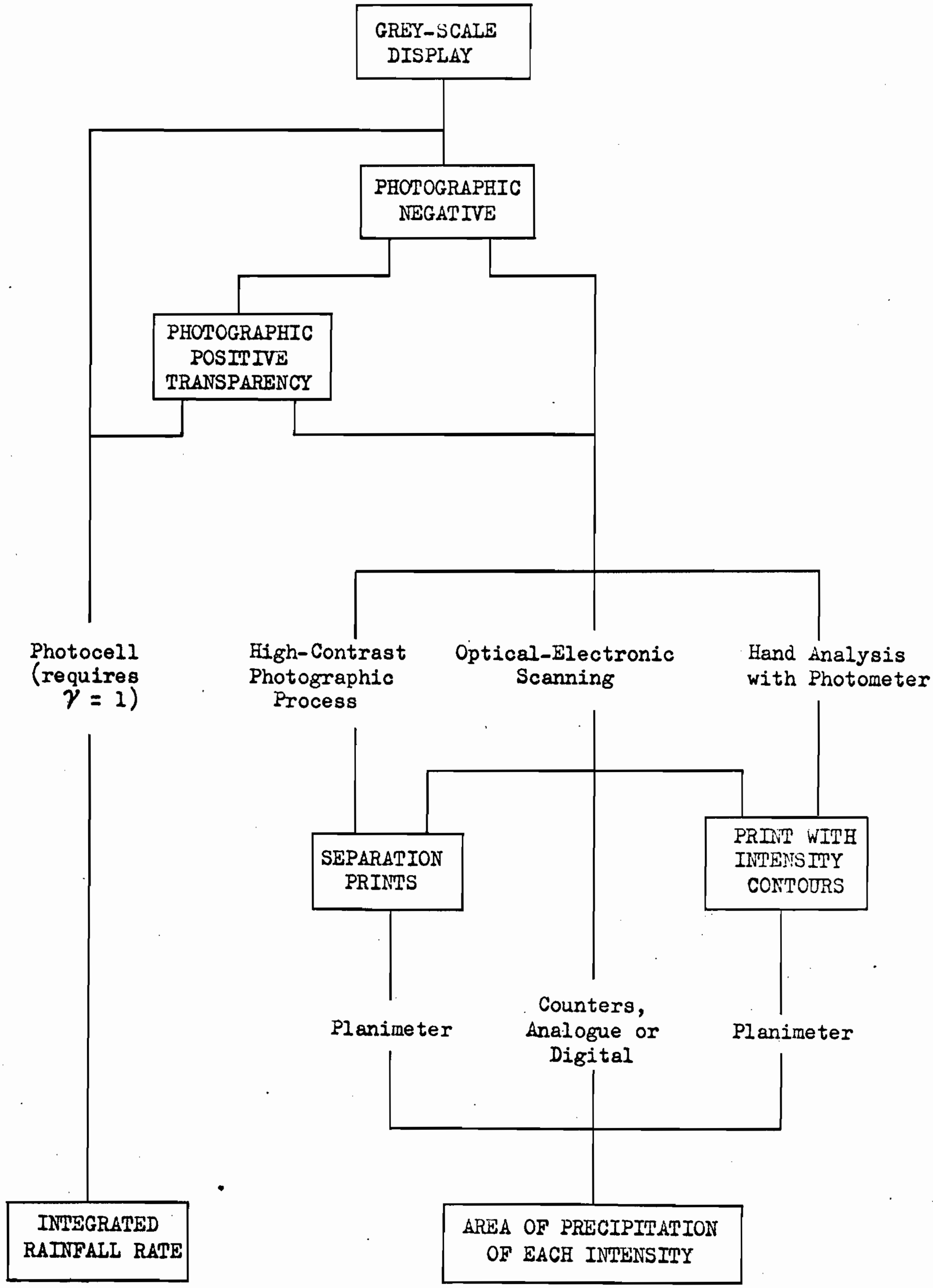

Fig. 6.4. Methods of analysis of grey-scale maps.

6.2 Precipitation Area from Grey-Scale Display

The precipitation map in Fig. 6.3, with its sharp contours, is ideal for quantitative analysis such as measuring areas of various intensities. Unfortunately, the scanning equipment which produced it was developed only recently, and was not available for the present research. The basic grey-scale maps of the kind shown in Fig. 6.2 have been produced for several years and were available. Therefore some work was done toward developing a technique for analyzing these maps. In this section some of the techniques studied are discussed, together with other possible methods of analysis. Fig. 6.4 is a summary of the various methods.

(a) Direct Photo-cell Integration

In most of the methods the analysis starts from the photographic negative of the grey-scale map. However, there is one useful quantity which could be derived directly from the grey-scale display: the integrated rainfall over an area. The method, first suggested by Professor Marshall, is discussed in some detail by Legg (1960).

The radar is adjusted so that the light coming from the PPI display tube is proportional to the rate of rainfall. This light is received by a photo-cell (specifically, a photo-multiplier tube) placed in front of the display. The resulting signals, which are proportional to rainfall rate, are then integrated electronically over a period of time to give the total rainfall. The rainfall may be measured over any given area by masking the display.

There is a possible development of this method of particular interest in the study of rainfall as a function of height. In this case an RHI display tube is masked to display signals from a given height while the radar antenna rotates in azimuth at a series of elevation angles. The

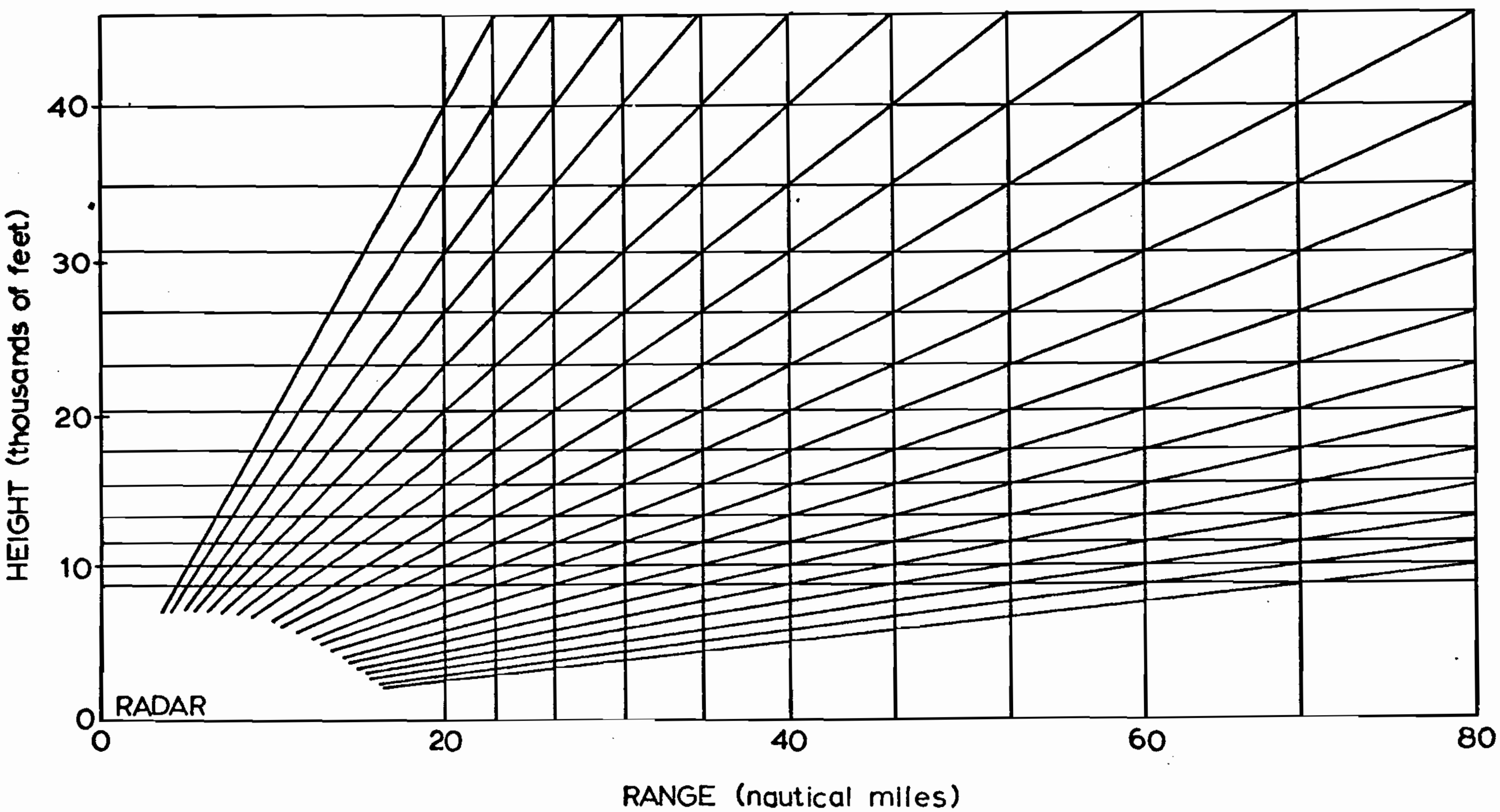

Fig. 6.5. Radar scan for composition of CAPPI maps in geometric progression.

signals are received by the photo-cell, whose output is integrated to give the total rainfall at the given height. Further, with suitable masking, several photo-cells can simultaneously record the signals at each of several distinct heights. This development would appear to have real merit: perhaps the most important single parameter, the total rainfall, is recorded as a function of height, from a single display, with a single spiral radar scan.

There is one form of spiral scan which is particularly attractive here. It is shown in Fig. 6.5, which may be looked upon as a picture of the RHI display. The radar traces arising from the origin neatly intersect the grid of range and height lines. Since both range lines and height lines are in geometric progression this is called a g.p. scan. There are two attractive features of the scan: first, in any given height layer there are exactly the same number of traces at all ranges and second, the height layers are contiguous. Thus masking the display to integrate the rainfall in various layers is simply done by installing partitions at the bounding heights. Further, since the layers are contiguous, the rainfall is measured as a continuous function of height.

It should be noted that photo-cell integration of a photographic transparency of the grey-scale display is also possible. The transparency in this case is a positive in which the transmissivity is proportional to the rainfall rate. Light is projected through the transparency, and the total amount transmitted is a measure of the average rainfall rate. If the display has been adjusted so that brightness is proportional to rainfall rate, and the transparency is the product of several scans, then photo-cell integration yields the total rainfall over the period of scanning.

Fig. 6.6

CAPPI maps at 4 kft
1120 EST 17 Feb 1961
Montreal at centre,
range 123 n mi.

Threshold rainfall rates
from top to bottom
1 - 0.1 mm hr^{-1}
2 - 0.4 mm hr^{-1}
3 - 1.6 mm hr^{-1}
4 - 6.4 mm hr^{-1}
(not attenuation-corrected)

(b) Photometric Analysis

The simplest method of analyzing the grey-scale maps is to use a photometer on the projected image of a transparency. To minimize the effects of lens flare and stray light a positive contact transparency was used. Since the spot which traces the grey-scale map is about one mile in diameter, the projection was at a scale on which the photometer element was also one mile in diameter. After determining the brightness of each grey shade from the peripheral test pattern, contours of intensity were traced out on the paper screen. The screen was then removed for further analysis.

This simple method of analysis, the first attempted in the present research, was found to be tedious and time-consuming. The analysis of a single map often took several hours. It was abandoned in favour of a more sophisticated approach.

(c) High Contrast Process

Various high contrast processes were tried in the attempt to reveal the contours in the grey-scale maps. Most of them were directed towards producing separation prints, such as those shown in Fig. 6.6. These are very high contrast pictures in which the boundary between black and white is set at any chosen rainfall rate. This threshold rainfall rate is indicated by the position of the threshold in the peripheral test pattern. The technique of producing separation prints is analogous to the common technique of reducing the receiver gain in successive radar scans. The prints in Fig. 6.6 were made photographically, and are negative prints from an intermediate positive transparency. Negative prints, with dark precipitation on a white background, are more readily analyzed than positives. In a positive print, ability to distinguish dark grey from a black background depends a great deal on the surface character, and on the level and conditions of illumination. These factors do not interfere as seriously with analysis of the negative print.

The grey shades on the original negative are at intervals of about 0.1 in density, and these became 0.3 in the high contrast positive transparency. The high contrast photographic paper, on which the final prints were made from this positive, just accepts a range of 0.6 in density, or two shades of grey. The exposure is first chosen to reveal precipitation of all shades, and is then reduced to eliminate shades successively, beginning with the lowest one.

The main disadvantage with this technique is the difficulty of controlling the high contrast photographic processes. It is difficult to place the threshold in the final print entirely by choice: a certain amount of trial and error is usually necessary. Once they are obtained the prints are easy to analyze. However, since the complete analysis of a single grey-scale map often takes an hour or more, the method was only used on a limited scale.

Another high contrast process that was tried was facsimile reproduction. The facsimile unit used was a small desk model in which a paper print is scanned on a rotating drum, the facsimile being burned into the recording paper. Positive prints with intervals of about 0.15 in reflection density between grey shades were used. The gain of the facsimile recorder was first set to show precipitation of all shades, and then in successive pictures it was reduced to eliminate shades one by one. The unit had a very well-defined threshold separating what was recorded from what was not, but because of small variations from print to print it was difficult to place it precisely. As in the photographic process, a certain amount of trial and error was necessary. The complete analysis of a single grey-scale map also took an hour or so. The method was used in preference to the photographic method for a preliminary analysis, but was considered too tedious for extensive use.

The third high contrast process that was tried was television. A positive transparency with intervals between grey shades of about 0.3 in density was placed on a diffusely illuminated background in front of the television camera. With the contrast control at maximum, a density difference of about 0.6 in the transparency covered the full range of the display monitor, from the weakest signal to the brightest. As usual, the brightness control was first set to show all precipitation, then reduced to eliminate shades successively, while at each stage the boundary of the precipitation was traced onto a transparent acetate sheet. In contrast to the other processes just discussed, the threshold can be placed easily and immediately at any value. Several grey-scale maps can be analyzed in an hour by television; there is no doubt that it is the best of the high-contrast processes.

(d) Automatic Scanning and Contouring

Now that the scanning equipment described in section 6.1 has been developed at McGill, it is a simple matter to produce the contoured grey-scale maps automatically. In the present research, it is the area of precipitation of each grey shade which is required. This may be measured from the contoured map with a planimeter; or, since a given shade is frequently made up of many relatively small isolated patches, counting the number of squares covered in a grid is often better.

However, to measure areas it is now not even necessary to produce grey-scale maps, for as well as contouring the maps, the scanning equipment can measure the areas. Since the scanning spot covers the map uniformly, the area of a given shade is measured by the total time taken in tracing that shade onto the display. The circuitry of the scanning equipment is such that the area of each shade can be measured separately.

There are several ways of measuring the time taken to trace a given shade. If the signal involved modulates a carrier wave, then a digital counter can be used to count carrier-wave cycles. This is the case with the McGill scanner, and preliminary trials indicate that it works well. There are also two analogue methods of measuring the area. In one, the signal can be used to charge a capacitor, in which case the accumulated charge is a measure of the area. In the other, the signal is used to expose repeatedly a photographic film, and in this case the resulting density measures the area. The capacitor technique has been used successfully in a commercially developed scanner; the film technique has also been developed fairly successfully, by Nitka (1964) at McGill.

These automatic measurements of area have considerable operational significance. In operational form the scanner produces a facsimile paper record, and simultaneously measures the area of each shade. The areas can be recorded immediately the scanning is completed, alongside the facsimile record. This is actually being done in the weather-radar facsimile unit currently under development by Canadian Aviation Electronics in Montreal.

6.3 Precipitation Area from A-Scope Display

It is possible to determine the areas of precipitation of various intensities from an A-scope display as an alternative to the grey-scale display. A method for doing this was developed, because none of the available methods of analyzing the grey-scale display was suitable for

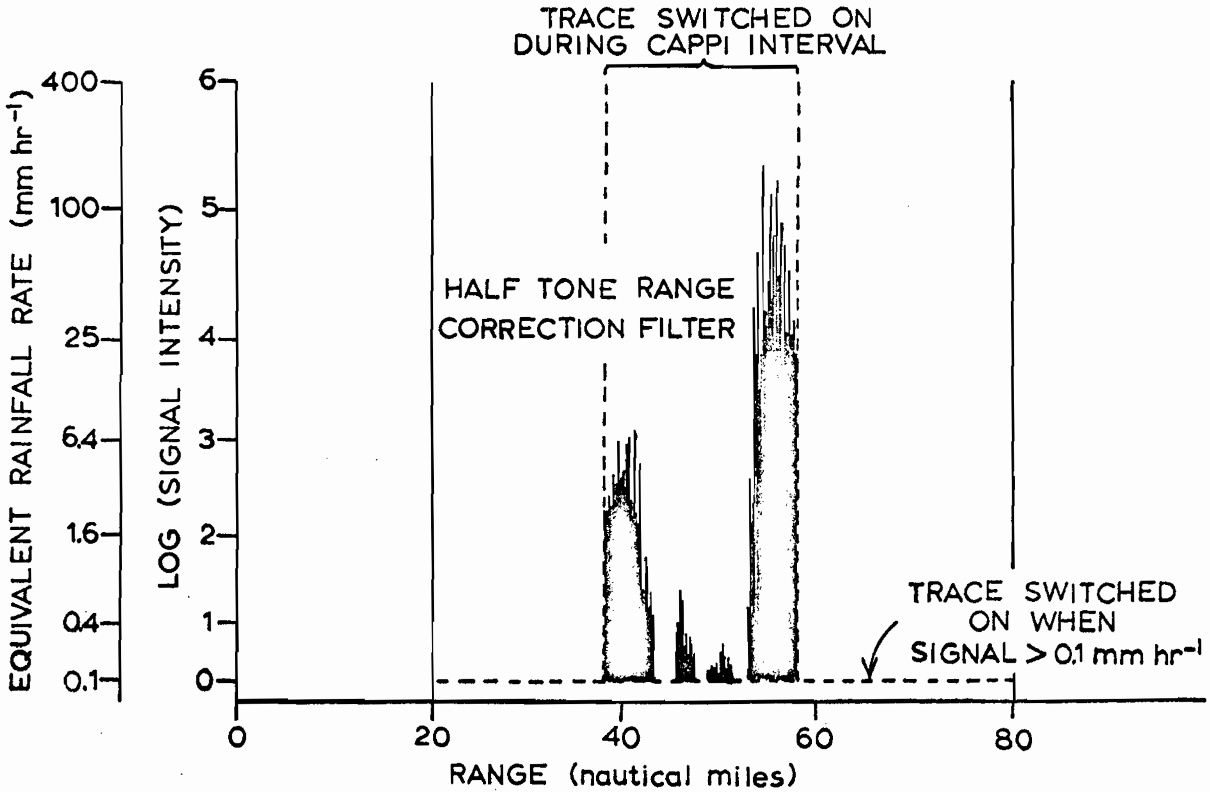

Fig. 6.7. The A-Scope display.

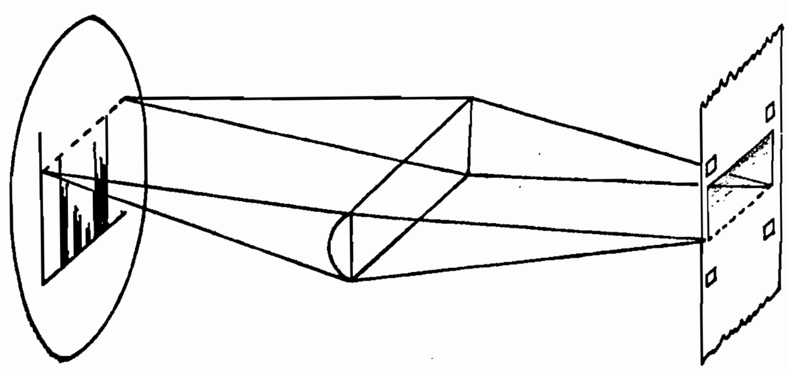

Fig. 6.8. Photography of A-Scope through cylindrical lens.

use on an extensive scale. With the A-scope method described in this section it is possible to analyze a single constant-altitude map in about five minutes. This is about the time it takes to measure the areas on a contoured grey-scale map, apart from the considerable time that was needed to produce the contoured map. Although the method has now been superseded at McGill by the development of automatic scanning equipment, it is nevertheless worth discussing in some detail. The A-scope method can be used with any radar that has a logarithmic receiver and facilities for producing constant-altitude pictures. Moreover its cost is only a fraction of the cost of scanning equipment.

Fig. 6.7 is a picture of the A-scope display. The equipment is operated within the normal programme of the McGill radar in which repeated spiral antenna scans are used to produce CAPPI pictures. Signals from the logarithmic receiver pass through a resistor-capacitor network to the cathode ray oscilloscope display, whose coordinates are log (rainfall rate) against range. The resistor-capacitor network averages the signals with a time constant equivalent to two 1500-metre radar pulse lengths to provide a more meaningful measure of the rainfall rate. This average is the same as that applied to signals in the grey-scale displays. The trace on the display is maintained at constant brightness, and is controlled by switching circuits, for the design and construction of which the author is indebted to Dr M. Wein. The trace is switched on only for the range interval appropriate to the particular constant altitude being synthesized, and only if the signal exceeds a threshold value equivalent to a rainfall rate of 0.1 mm hr^{-1}.

The purpose of the equipment is to integrate or measure the total area of precipitation of a given intensity over the area scanned by the

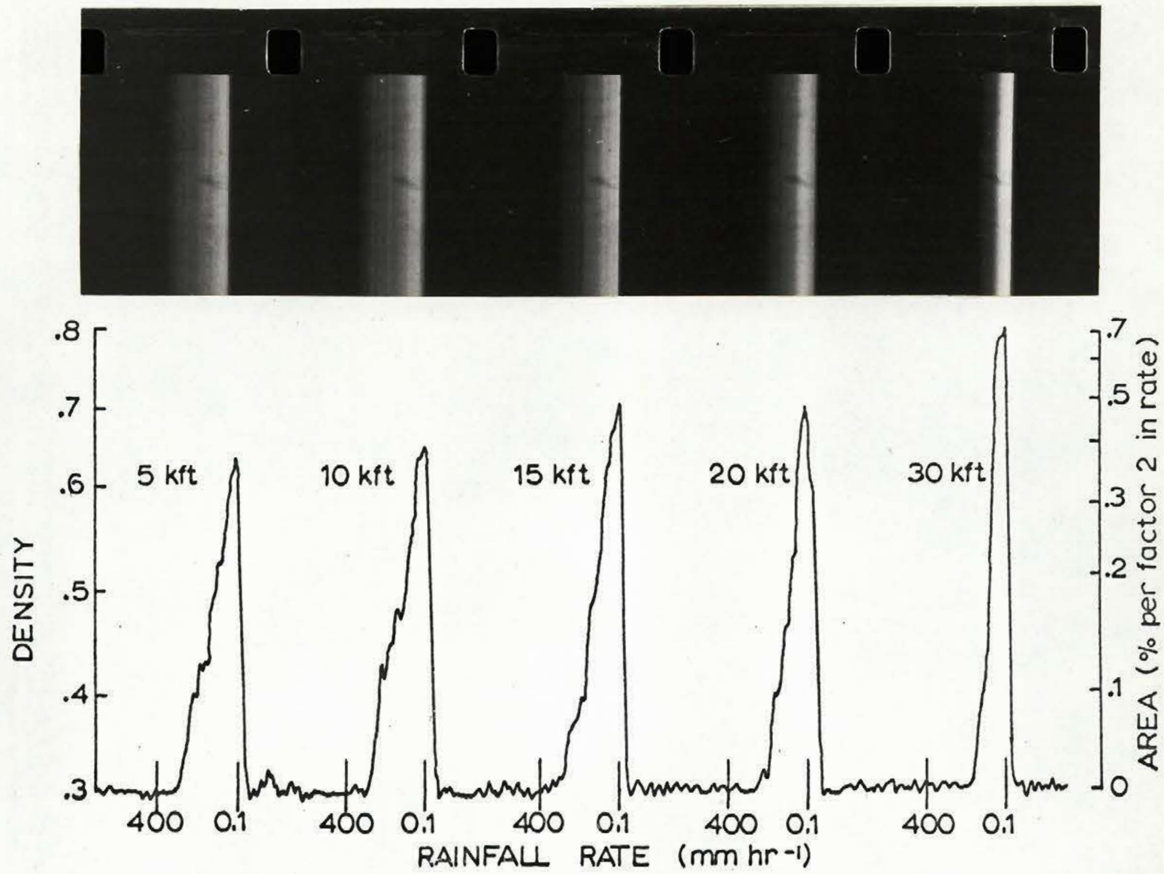

Fig. 6.9. Examples of A-scope film and density record.

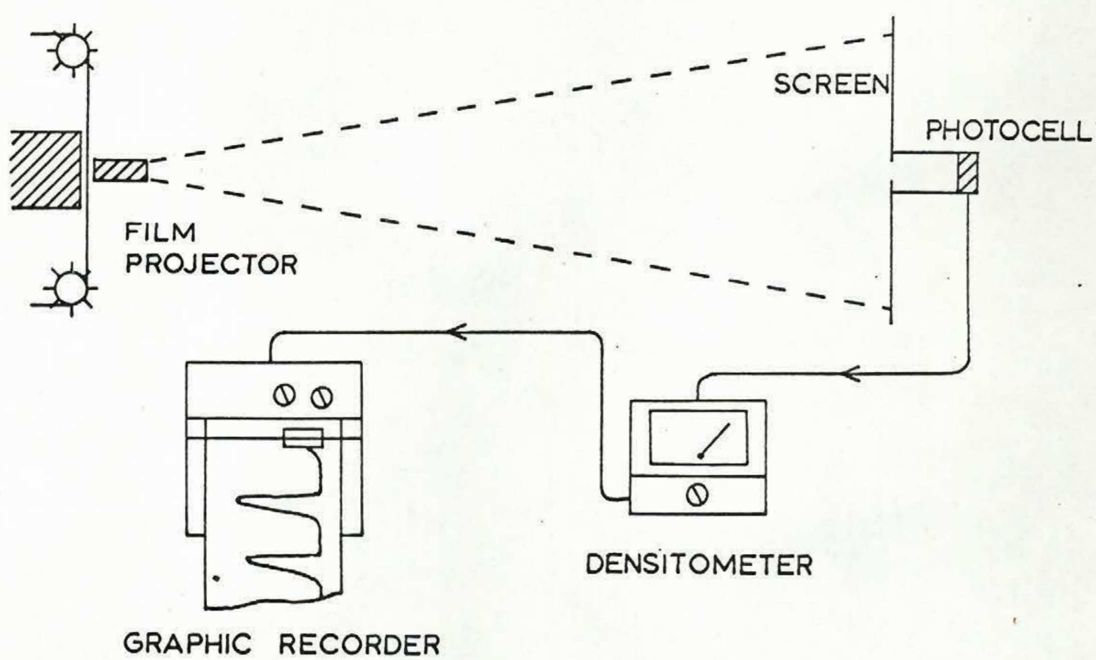

Fig. 6.10. System for automatic densitometry of A-scope films.

radar. To ensure quantitative operation this area of integration is actually restricted to that between 20 and 80 n mi, an area of about 20,000 n mi^2, by masking the display. The first step toward the integration over area is integration over range, and this is followed by integration in azimuth. Integration over range is achieved by photographing the display through a cylindrical lens, a technique suggested by Professor Marshall. The arrangement is shown in Fig. 6.8, and it can be seen that images of signals of the same intensity from different ranges are superimposed on the film. Since the area within the one-degree beam in a small range interval is proportional to the range, the signals must be corrected before being superimposed. This is done by fitting the display tube face with a photographic half-tone mask whose density increases from a low value at range 80 n mi to a high value at 20 n mi.

Integration in azimuth is achieved by accumulating signals from all azimuths in a single photograph. In fact the same frame of film is exposed for the duration of the spiral antenna scan, thus achieving the integration of signals of each intensity, over the entire area scanned, at a given constant altitude. Since the brightness of the trace is constant, density on the film is a measure of area.

Fig. 6.9 shows prints from a sequence of frames on the negative film, together with a plot of the density along some line down the middle of the film. A scale of area has been added to the density plot, and the graph can be read directly to give the distribution of area of precipitation as a function of its intensity. It can be seen that the film record is particularly suited to automatic densitometry, and in fact the density plot shown was produced automatically by the equipment shown in Fig. 6.10. In this densitometer an image of the 16-mm film is projected onto a photocell

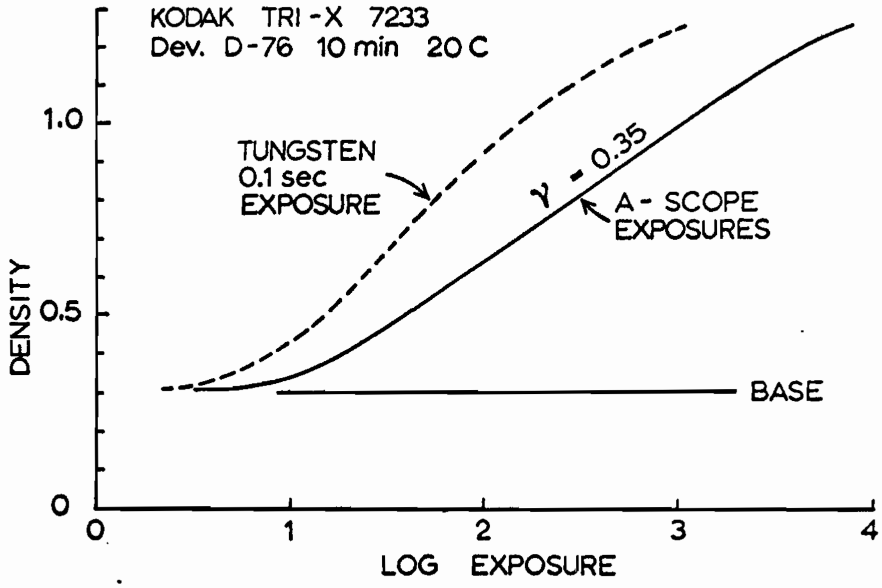

Fig. 6.11. Characteristics of film used in photographing A-scope display.

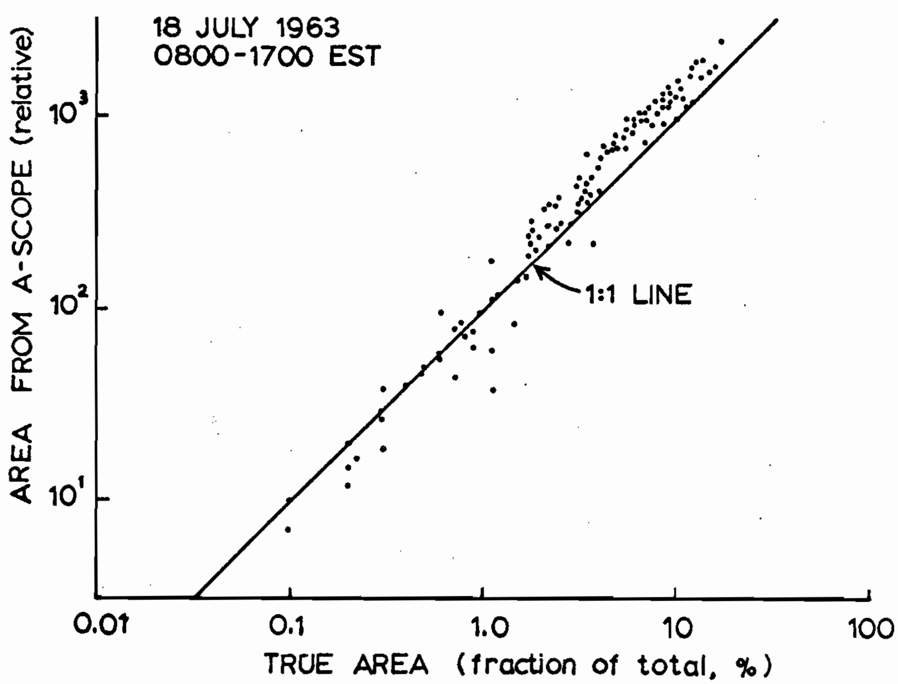

Fig. 6.12. Comparison of total precipitation areas measured from A-scope display with those measured from CAPPI maps.

equipped with a collimator. The film is drawn through the gate of the projector at a rate of one frame per minute, while a meter in circuit with the photocell records density along the film. The meter and photocell are actually components of a commercial photometer. A strip chart recorder placed in parallel with the meter records the density measurements without affecting the operation of the photometer.

The determination of area from density requires a knowledge of the film characteristics. Since the trace on the display is constant in brightness, exposure time is proportional to area of precipitation, and it is the relationship between film density and exposure that is required. It is important to establish this relationship under conditions as nearly as possible resembling the conditions of operation. For example, the film characteristics published by the manufacturer are normally for single daylight exposures of the order of hundredths of a second, while in the present work the film is exposed to an oscilloscope trace, perhaps with hundreds of exposures, each measured in microseconds. Thus a test was devised in which mountains took the place of precipitation as radar targets. The mountains were repeatedly scanned with the antenna rotating at 0° angle of elevation, while a series of exposures was made, successively for the duration of 1, 2, 4, 8 and 16 rotations. The film was then developed and measured in the automatic densitometer. In each picture there is the same relative distribution of area of echo with intensity, but the areas increase throughout the series by successive factors of two. Thus, if the density is measured in each picture at a point corresponding to a given intensity of echo, the series of densities corresponds to a series of areas in the ratios 1:2:4:8:16, and a graph of density as a function of area can be drawn. The areas in this graph are relative, and no attempt was made to determine them absolutely at this stage. The graph was extended by measuring a series of densities for each echo intensity, and then matching the various series on the graph. It was further extended by repeating the exposures with various levels of oscilloscope trace brightness. Fig. 6.11 shows the characteristic plot that was finally obtained, and it can be seen that it extended over a range of almost 40 db in relative exposure, or area. For comparison, the normal film characteristic for identical development is also plotted in the figure. Although the relative positions of the two curves were not determined, as shown, they probably match most closely at low levels of exposure, with densities from oscilloscope exposures falling well below the normal characteristic at higher levels.

The film characteristic thus measured was used to add the scale of relative area to the density record of Fig. 6.9. To determine the units of this scale absolutely the density plot from a series of pictures of precipitation was analyzed. In each picture areas were measured at intervals of a factor 2.0 in rainfall rate directly in terms of the units of the relative scale. These areas were added to obtain the total area of precipitation with intensity exceeding 0.1 mm hr^{-1}. The total areas obtained in this way were plotted against the true areas measured from corresponding CAPPI maps, Fig. 6.12. The near proportionality of the two sets of areas can be seen from the tendency of the points to lie parallel to the 1:1 line, and the constant of proportionality is readily obtained. When the scale of areas on the density plot is multiplied by this constant it becomes an absolute scale, and the area of any given intensity can be measured immediately.

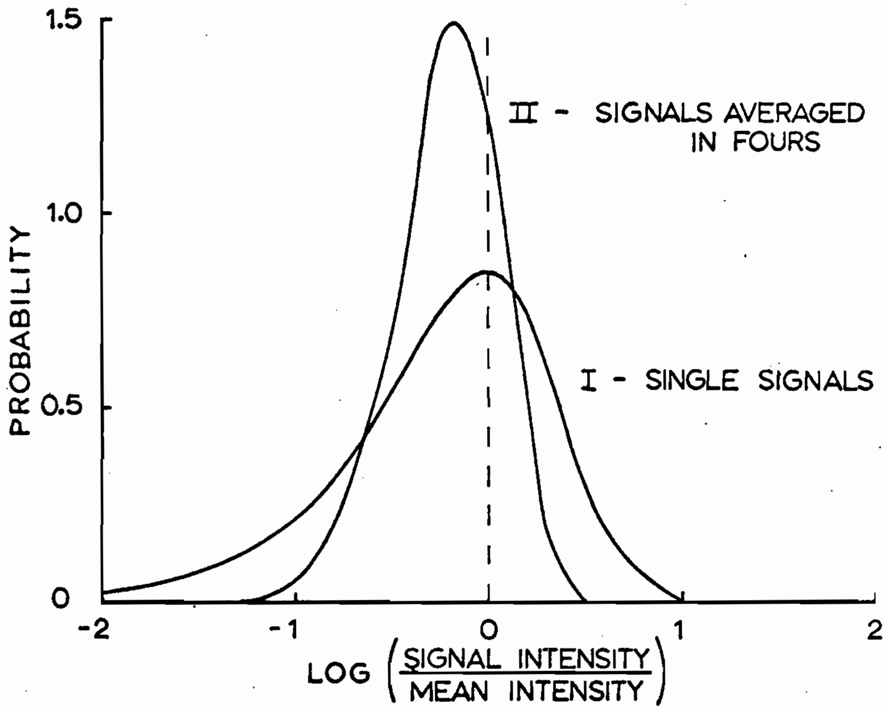

Fig. 6.13. The probability distribution of the fluctuating radar signals from precipitation.

6.4 Evaluation of A-Scope Technique for Measuring Area

In evaluating the present technique of measuring precipitation areas the nature of the radar signal from precipitation and its display on the oscilloscope must first be considered. The radar echo from a randomly distributed array of precipitation particles fluctuates in intensity about a mean value which can be related to the intensity of precipitation. Marshall and Hitschfeld (1953) and Wallace (1953) have studied these fluctuating signals theoretically and have determined the probability distributions which they satisfy. In Fig. 6.13, curve I has been taken from Marshall and Hitschfeld to show the distribution of independent signals as a function of log (signal intensity). As far as the present technique is concerned, in which signals are displayed on an A-scope and superimposed in range and azimuth on photographic film, the curve may be looked upon as the distribution on the film of many signals from precipitation of a given intensity. The maximum density of signals occurs at the mean intensity, but the distribution is broad with 90% occurring over an 18 db range. The distribution can be narrowed by averaging groups of independent signals before display, and curve II, for example, shows the effect for groups of four. Here 90% of the signals are contained in the considerably smaller range of 10 db. Averaging has also lowered the whole distribution slightly, with a shift in the maximum of almost 2 db. Signals in the present equipment are actually averaged continuously in range by means of a resistor-capacitor network whose time constant is equivalent to two radar pulse lengths. Wallace (1953) has shown that continuous averaging is slightly more effective than averaging the same number of completely independent signals. The present operation is probably equivalent to averaging groups of somewhere between three and four independent signals, and curve II has been taken to represent the situation.

One point of some significance to be noted with regard to the distributions of Fig. 6.13 is that the mean log (signal intensity) is less than the log (mean signal intensity). This is why averaging groups of independent values of log (signal intensity) lowers the distribution as well as narrowing it, and for large groups it becomes a narrow distribution with the peak about 2.5 db below the mean signal intensity. One consequence is that, if one were to calculate the precipitation flux from the record of an A-scope in which large groups of signals were averaged before display, it would be lower than the true value by the equivalent of 2.5 db, or a factor 1.4 in rainfall rate. Rather surprisingly, perhaps, the flux calculated from a record in which no averaging has been done is correct. In the present equipment, a numerical calculation based on curve II of Fig. 6.13 showed that averaging in groups of four leads to a value of the flux 1.2 db less than the true value, or a factor 1.2 in rainfall rate. In view of other greater uncertainties in this study, no correction was applied for this error.

Fig. 6.13 is also useful in estimating at what intervals of signal intensity areas should be measured on the A-scope record. Precipitation of a certain constant intensity gives an A-scope record like curve II. The precipitation area is given by the area under this curve, and may be approximated by measuring ordinate values on the curve at a limited number of points. A series of trials was made to find the least number of points that would give satisfactory accuracy. For measurements at 10 db intervals the measured area was in error by up to a factor 1.9, at 5 db intervals by 1.02. Precipitation fluxes were also calculated from these

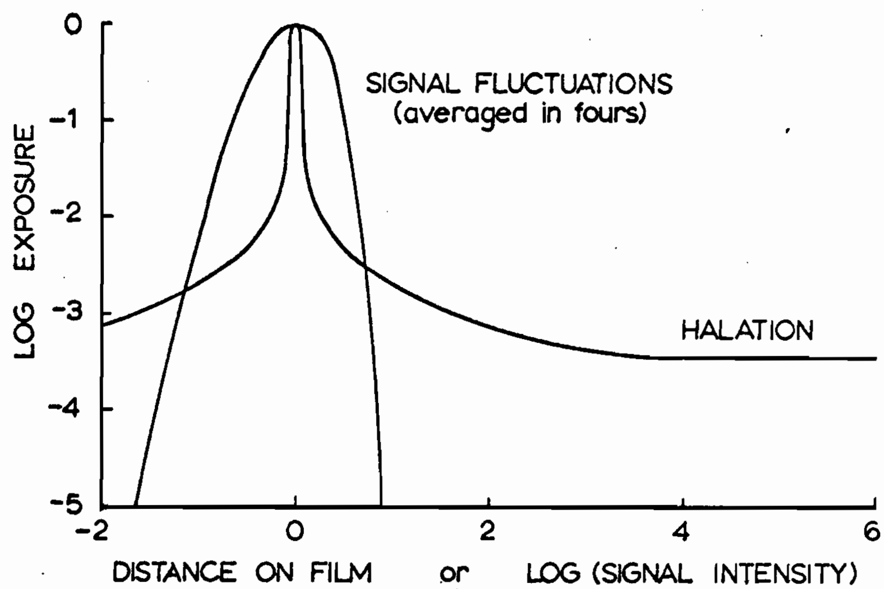

Fig. 6.14. The effects of signal fluctuations and halation on the A-scope display.

series of measurements, and for measurements at 10 db intervals the flux was in error by up to a factor 3.0 in rainfall rate, at 5 db intervals by 1.06 (apart from the consistent factor 1.2 discussed in the last paragraph). The errors arising from measurements at 5 db intervals are thus negligible, and this was the interval used in the present study.

Although the A-scope signal intensity scale is accurately transcribed onto the density record (Fig. 6.9), there is a problem in locating the 5 db points at which to measure areas. An overlay was prepared with the correct intensity scale, but it was difficult to align its origin with the threshold intensity. The threshold is not as well defined as might be hoped, and can be consistently located only to within about ± 2 db (a factor 1.3 in rainfall rate). This margin of error is somewhat greater than those discussed in the preceding paragraph, and is in fact the overall limit to the accuracy of the present measurements of signal intensity.

There is another phenomenon somewhat similar to the fluctuating signal in its effect on the A-scope display. Surrounding the small oscilloscope spot, and associated with it, is a large faint circular region or halo. The spot and its halo are imaged by the cylindrical lens into a fine bright line within a broad parallel band of halation. Measurements of the halation effect were made photographically, and the results are shown in Fig. 6.14 as a plot of log (exposure) against distance on the film perpendicular to the line image. Whereas on the oscilloscope the brightness of the halo is about 60 db less than the brightness of the spot, in the image the difference is reduced to about 35 db. The scale of distance in Fig. 6.14 is also a scale of log (signal intensity) and it is against this latter scale that the effects of halation should be judged.

To enable a comparison between the effect of halation and that of fluctuations in the radar signal, curve II of Fig. 6.13 has been replotted in Fig. 6.14. The most important difference to note is that while the effect of signal fluctuations decreases quickly with distance, halation is never more than 35 db below its maximum value. An immediate consequence of this is that it is halation which determines the dynamic range of the display. This is perhaps best seen by looking at a specific example, and in the following table the measurements from which Fig. 6.14 was drawn have been used to show the effect of halation in the recording of 20,000 mi^2 (full radar coverage) of precipitation of rate 0.1 mm hr^{-1}.

Rainfall rate (mm hr^{-1})	0.1	0.4	1.6	6.4	25	100	400
Area (mi^2)	20,000	40	15	8	6	6	6
Relative flux	2000	16	24	50	150	600	2400

Because of halation, small areas are inevitably recorded at all other rainfall rates, including 6 mi^2 of 400 mm hr^{-1}, and only with several times this area could one afford to neglect the contribution from halation. Thus, the overall range of the display is limited by halation to about 30 db, or 35 db if one is prepared to correct for halation. Perhaps the most serious aspect of halation is found in relation to the calculation of precipitation flux. The fluxes that would result from the small areas arising from halation also appear in the table. Since 6 mi^2 of 400 mm hr^{-1} actually yields more precipitation than 20,000 mi^2 of 0.1 mm hr^{-1}, it is evident that extreme care is needed in measurements at high rainfall rates.

One precaution taken to minimize the effect of halation was to switch the trace off whenever the signal fell below a threshold equivalent to a rainfall rate of 0.1 mm hr^{-1}. This limits the halation effect to an amount proportional to the total precipitation area, while without the switch the film would be constantly exposed to halation for the full 20,000 mi^2 radar coverage. It should also be noted that halation is a property of the display, not the signal, and it is important to use the most open signal intensity scale possible. Despite these precautions, halation is always present to some extent, although it is least serious on occasions with small precipitation area. In practice, the values appearing in the above table were used qualitatively to determine whether halation effects were significant and, if they were, appropriate corrections were made.

The overall accuracy of the A-scope display in measuring precipitation areas is perhaps best judged by returning to Fig. 6.11 and 6.12. Fig. 6.11 shows the relationship between density and exposure (or area) for the film as it was used in this study. By using this relationship with a relative scale of area, areas were measured from the A-scope record, and plotted in Fig. 6.12 against the corresponding true areas measured from CAPPI maps. From this plot a factor was determined with which the relative A-scope areas were converted into true areas. Fig. 6.12 actually contains measurements made on every available picture throughout a period of thundershowers. The areas on the CAPPI maps were measured by superimposing a grid and counting the number of squares covered with precipitation. Although it is the result of a single radar test, the characteristic relationship of Fig. 6.11, with slope (or γ) 0.35, was used for calculating all A-scope areas. This is convenient, but has the disadvantage that inevitable small differences in processing and film batches lead to slightly different characteristics. If the characteristic of a particular record is the same as that of Fig. 6.11, then the calculated A-scope areas will be proportional to the true areas, and the points in Fig. 6.12 will tend to lie along a line of slope 1.0. In the example, the points are best fitted by a line of slope 1.1, and this suggests that the film actually had a characteristic with $\gamma = 1.1 \times 0.35$. This is a fairly extreme deviation from the normal $\gamma = 0.35$. If the best line of slope 1.0 is chosen to fit the points the larger areas will tend to be in error by + 1 db, and the smaller areas by - 1 db. Thus calculations of areas based on a standard film characteristic may be subject to consistent errors of up to ± 1 db on account of variations from this characteristic.

Another source of error lies in the measurement of densities on the film. The performance of the densitometer varied slightly with projector lamp voltage and temperature. A consistent deviation of performance from standard would produce effects precisely similar to those arising from variations in film characteristic, and could equally well account for the deviation of the points in Fig. 6.12 from proportionality. However, the densitometer performance was not as consistent as the film characteristic, and variations could occur over periods of several pictures. Thus the errors in area arising from this source would show up in Fig. 6.12 as scatter about the line of best fit. Their magnitude was rather less than the ± 1 db arising from variations in film characteristic.

Two further sources of error to which the A-scope areas are subject are also random in nature, although they may show trends. They are variation in oscilloscope trace brightness and imperfection in the half tone range correction filter. The brightness of the trace was continuously monitored by means of a photocell, generally being maintained within ± 1 db of a standard value. This range of ± 1 db comprised $\pm \frac{1}{2}$ db in short term fluctuations over periods of minutes superimposed on a similar $\pm \frac{1}{2}$ db drift over hours. In the case of the range correction filter, it was difficult to produce the necessary half tone mask with precisely the required density distribution. The best that could be achieved was again within ± 1 db of the desired values. In this case the error is a function of range, and the overall error generally varies steadily according to the distribution of precipitation with range. Both the errors arising from imperfections of the filter and those arising from variations of trace brightness are similar in nature and may be combined. In sum the effective brightness of the trace will be subject to random variations of about $\pm\frac{1}{2}$ db within the period of a single picture with further variations of up to $\pm 1\frac{1}{2}$ db over a period of several pictures. The measured areas will be in error by the same factor. In a given picture, the measured areas can generally be corrected for these errors by multiplying them all by a constant factor.

All of these random variations in densitometry and trace brightness combine to produce the scatter of the points in Fig. 6.12. In agreement with the preceding discussion of errors, 90% of the data lie within a factor 1.4 (± 1.5 db) of the line of slope 1.1, although there are errors of up to a factor 2. Also, as might be expected, the scatter over shorter periods tends to be less than the scatter over the nine-hour period of Fig. 6.12. Nevertheless, the areas calculated directly from the A-scope record were insufficiently precise for the present study, and a way of achieving greater precision was sought.

An obvious technique was adopted, in which the areas in each picture are multiplied by a correction factor to make the total area equal to the area measured in a corresponding CAPPI map. That is, the A-scope is in effect used to determine the proportions of precipitation of each intensity, and the CAPPI maps are used to convert these proportions into areas. This technique satisfactorily eliminates errors arising from the varying trace brightness and imperfect range filter, and considerably reduces the errors arising from varying film characteristics and densitometry. In fact, since the relative proportions of precipitation of each intensity and the areas from CAPPI maps are each accurate to a factor 1.1, the overall limit to the accuracy of the area measurements is a factor 1.2. This accuracy should be compared with the corresponding accuracy in the intensity measurements of a factor 1.3 in rainfall rate.

Altogether, the A-scope display is capable of measuring the flux of precipitation accurate to within a factor 1.4. More precisely, the probable error in flux measurements is estimated as a factor 1.2, which is equivalent to 1.2 db in signal intensity.

REFERENCES

aufm Kampe, H.J. and H.K. Weickmann, 1957, Meteor. Res. Reviews, 3(18), 182-225.

Austin, P.M., 1963, Proc. Tenth Weather Radar Conf., Amer. Meteor. Soc., Boston, 247-254.

Ballantyne, E., 1964, Proc. 1964 World Conf. on Radio Meteor., Amer. Meteor. Soc., Boston.

Battan, L.J., 1953a, J. Meteor., 10, 311-324.

Battan, L.J., 1953b, Bull. Amer. Meteor. Soc., 34, 227-228.

Battan, L.J., 1959, Radar Meteorology, Univ. of Chicago Press.

Boucher, R.J., 1958, Proc. Seventh Weather Radar Conf., Amer. Meteor. Soc., Boston, H8-H17.

Boucher, R.J., 1959, J. Meteor., 16, 312-326.

Bowen, E.G., 1950, Austr. J. Sci. Res. A3, 193-213.

Browning, K.A. and F.H. Ludlam, 1962, Quart. J.R. Meteor. Soc., 88, 117-135.

Byers, H.R. and R.R. Braham, 1949, The Thunderstorm, Washington, D.C., U.S. Govt. Printing Office, 287 pp.

Byers, H.R. and R.D. Coons, 1947, J. Meteor., 3, 78-84.

Donaldson, R.J., 1958, J. Meteor., 15, 44-50.

Donaldson, R.J., 1959, J. Meteor., 16, 281-287.

Donaldson, R.J., 1961a, Proc. Ninth Weather Radar Conf., Amer. Meteor. Soc., Boston, 165-174.

Donaldson, R.J., 1961b, J. Meteor., 18, 292-305.

East, T.W.R., 1957, Quart. J.R. Meteor. Soc., 83, 61-76.

East, T.W.R., and B.V. Dore, 1957, Proc. Sixth Weather Radar Conf., Amer. Meteor. Soc., Boston, 325-330.

Foster, D.S. and F.C. Bates, 1956, Bull. Amer. Meteor. Soc., 37, 135-141.

Gunn, K.L.S. and T.W.R. East, 1954, Quart. J.R. Meteor. Soc., 80, 522-545.

Gunn, K.L.S. and J.S. Marshall, 1958, J. Meteor., 15, 452-461.

Hamilton, P.M. and J.S. Marshall, 1961, Sci. Rep. MW-32, McGill University (Contract AF-19(604)-2065, AFCRL-TN-60-658) 65 pp.

Hitschfeld, W and K.L.S. Gunn, 1958, Proc. Seventh Weather Radar Conf., Amer. Meteor. Soc., Boston, A10-16

Kessler, E., 1961, J. Meteor., 18, 510-525.

Kessler, E., E.A. Newburg and G. Arnason, 1964, Report No. 5 on Contract DA 36-039 SC 89099, between USAERDL and Travelers Research Center, Inc.

Langille, R.C. and K.L.S. Gunn, 1948, J. Meteor., 5, 301-304.

Langleben, M.P. 1956, J. Meteor., 13, 554-560.

Legg, T.H., 1960, Sci. Rep. MW-31, McGill University.

Ludlam, F.H., 1963, Meteor. Monographs, 5, (27), 1-30.

Marshall, J.S., 1961, Nubila, 4 (2), 59-62.

Marshall, J.S., and K.L.S. Gunn, 1961, Beit. zur Phys. der Atmos., 34, 69-80.

Marshall, J.S., and W. Hitschfeld, 1953, Canadian Jour. of Phys., 31, 962-994.

Marshall, J.S., R.C. Langille and W. McK. Palmer, 1947, J. Meteor., 4, 186-192.

Marshall, J.S. and W.McK. Palmer, 1948, J. Meteor. 5, 165-166.

Maynard, R.H., 1945, J. Meteor., 2, 214-226.

Nitka, G., 1964, M.Sc. Thesis, McGill University.

Runnels, R.C., R.A.Clark and V.E. Moyer, 1963a, Proc. Tenth Weather Radar Conf., Amer. Meteor. Soc., Boston, 98-103.

Runnels, R.C., R.A. Clark and V.E. Moyer, 1963b, Sci. Rep. 63-31T, Dept. of Ocean. and Meteor., Texas A&M University.

Ryde, J.W., 1946, Meteorological Factors in Radio Wave Propagation, (London, Physical Soc., 1946), 169-188.

Wallace, P.R., 1953, Canadian Jour. of Phys., 31, 995-1009.

Wein, M., 1964, Ph.D. Thesis, McGill University.

Wexler, R., 1959, Allied Research Associates, Sci. Rep. No. 3, under ACRC Contract No. AF 19(604)-5204.